QC
1
.U56
vol. 64C
no.1

THE UNIVERSITY OF MICHIGAN
MAR 1 1960
LIBRARY

Volume 64C
Number 1
Jan.–Mar. 1960

Journal of Research

of the

NATIONAL BUREAU OF STANDARDS

C. ENGINEERING AND INSTRUMENTATION

Journal of Research

of the

National Bureau of Standards

C. Engineering and Instrumentation

JAN.–MAR. • 1960

VOLUME • 64C

NUMBER • 1

Editor: W. A. Wildhack

Associate Editors: G. F. Montgomery, R. B. Jacobs

Publication dates: Feb. 15, Apr. 15, Aug. 15, Nov. 15, 1960

JOURNAL OF RESEARCH

The National Bureau of Standards Journal of Research reports research and development in the fields of activity shown at right. Also included from time to time are survey articles and compilations of information on topics closely related to the Bureau's scientific and technical program.

The Journal is published in four separate sections as follows:

A. Physics and Chemistry

Contains papers of interest primarily to scientists working in these fields. Issued six times a year. Annual subscription: domestic, $4.00; foreign, $4.75.

B. Mathematics and Mathematical Physics

Presents studies and compilations designed mainly for the mathematician and the theoretical physicist. Issued quarterly. Annual subscription: domestic, $2.25; foreign, $2.75.

C. Engineering and Instrumentation

Reports research and development results of interest chiefly to the engineer and the applied scientist. Issued quarterly. Annual subscription: domestic, $2.25; foreign, $2.75.

D. Radio Propagation

Reports work in radio propagation physics and upper atmospheric research. Issued six times a year. Annual subscription: domestic, $4.00; foreign, $4.75.

U.S. DEPARTMENT OF COMMERCE
Frederick H. Mueller, Secretary

NATIONAL BUREAU OF STANDARDS
A. V. Astin, Director

Functions and Activities

The functions of the National Bureau of Standards are set forth in the Act of Congress, March 3, 1901, as amended. These include the development and maintenance of the national standards of measurement and the provision of means and methods for making measurements consistent with these standards; the determination of physical constants and properties of materials; the development of methods and instruments for testing materials, devices, and structures; advisory services to government agencies on scientific and technical problems; invention and development of devices to serve special needs of the Government; and the development of standard practices, codes, and specifications. The work includes basic and applied research, development, engineering, instrumentation, testing, evaluation, calibration services, and various consultation and information services. The Bureau also serves as the Federal technical research center in a number of specialized fields. The scope of activities of the National Bureau of Standards is suggested in the following listing of the divisions and sections engaged in technical work.

Washington, D.C

Electricity and Electronics. Resistance and Reactance. Electron Devices. Electrical Instruments. Magnetic Measurements. Dielectrics. Engineering Electronics. Electronic Instrumentation. Electrochemistry.

Optics and Metrology. Photometry and Colorimetry. Optical Instruments. Photographic Technology. Length. Engineering Metrology.

Heat. Temperature Physics. Thermodynamics. Cryogenic Physics. Rheology. Engine Fuels. Free Radicals Research.

Atomic and Radiation Physics. Spectroscopy. Radiometry. Mass Spectrometry. Solid State Physics. Electron Physics. Atomic Physics. Neutron Physics. Radiation Theory. Radioactivity. X-ray. High Energy Radiation. Nucleonic Instrumentation. Radiological Equipment.

Chemistry. Organic Coatings. Surface Chemistry. Organic Chemistry. Analytical Chemistry. Inorganic Chemistry. Electrodeposition. Molecular Structure and Properties of Gases. Physical Chemistry. Thermochemistry. Spectrochemistry. Pure Substances.

Mechanics. Sound. Mechanical Instruments. Fluid Mechanics. Engineering Mechanics. Mass and Scale. Capacity, Density, and Fluid Meters. Combustion Controls.

Organic and Fibrous Materials. Rubber. Textiles. Paper. Leather. Testing and Specifications. Polymer Structure. Plastics. Dental Research.

Metallurgy. Thermal Metallurgy. Chemical Metallurgy. Mechanical Metallurgy. Corrosion. Metal Physics.

Mineral Products. Engineering Ceramics. Glass. Refractories. Enameled Metals. Concreting Materials. Constitution and Microstructure.

Building Technology. Structural Engineering. Fire Protection. Air Conditioning, Heating, and Refrigeration. Floor, Roof, and Wall Coverings. Codes and Safety Standards. Heat Transfer.

Applied Mathematics. Numerical Analysis. Computation. Statistical Engineering. Mathematical Physics.

Data Processing Systems. SEAC Engineering Group. Components and Techniques. Digital Circuitry. Digital Systems. Analog Systems. Applications Engineering.

• Office of Basic Instrumentation. • Office of Weights and Measures

Boulder, Colorado

Cryogenic Engineering. Cryogenic Equipment. Cryogenic Processes. Properties of Materials. Gas Liquefaction.

Radio Propagation Physics. Upper Atmosphere Research. Ionosphere Research. Regular Prediction Services. Sun-Earth Relationships. VHF Research. Radio Warning Services. Airglow and Aurora. Radio Astronomy and Arctic Propagation.

Radio Propagation Engineering. Data Reduction Instrumentation. Radio Noise. Tropospheric Measurements. Tropospheric Analysis. Propagation-Terrain Effects. Radio-Meteorology. Lower Atmosphere Physics.

Radio Standards. High-Frequency Electrical Standards. Radio Broadcast Service. Radio and Microwave Materials. Electronic Calibration Center. Microwave Circuit Standards.

Radio Communication and Systems. Low Frequency and Very Low Frequency Research. High Frequency and Very High Frequency Research. Modulation Systems. Antenna Research. Navigation Systems. Systems Analysis. Field Operations.

Order all publications from the Superintendent of Documents
U.S. Government Printing Office, Washington 25, D.C.

Use of funds for printing this publication approved by the Director of the Bureau of the Budget (June 24, 1958).

JOURNAL OF RESEARCH of the National Bureau of Standards—C. Engineering and Instrumentation
Vol. 64C, No. 1, January–March 1960

DEPOSITED BY THE
UNITED STATES OF AMERICA

Power Loss and Operating Temperature of Tires[1]

R. D. Stiehler, M. N. Steel, G. G. Richey, J. Mandel, and R. H. Hobbs

(June 19, 1959)

The power loss of pneumatic tires was measured under steady-state conditions by means of two dynamometers, one of which measured the total power input and the other power output. A steel wheel was used to measure the power loss in the equipment and in windage. The power required to flex the tire (input power minus output power minus equipment and windage losses), was not affected by the tractive effort (output power). The coefficient of rolling resistance, a dimensionless quantity, was calculated by means of the equation: $R=(P/SL)$, where P is power loss of tire, S is speed, and L is load. This coefficient increased at an increasing rate with the slip angle (angle between plane of tire and direction of travel) and was approximately doubled at an angle of 2 degrees.

The change in R with speed varied and appeared to depend on construction of the tire. Both nylon and steel wire truck tires exhibited a decrease in R with speed, rayon truck tires showed either no change or a linear increase in R with speed, and for passenger car tires R increased at an increasing rate with speed, particularly for a rayon tire. R increased with load for all but the steel wire tire. The change in R with inflation pressure was studied only for rayon truck tires. R increased linearly with the reciprocal of the pressure but the rate was dependent on the speed and load conditions.

The type of rubber had a pronounced effect on R and combinations of natural and styrene-butadiene rubber caused R to be larger than expected from the values of R for tires made from a single rubber. Varying the type of carbon black in the treads of truck tires had no effect on R, but SAF black in passenger car tires caused R to be larger than that when HAF black was used. Because of constructional differences, no conclusions on effect of cord could be drawn. However, R for a steel wire truck tire was the lowest observed, and the values for rayon tires were lower than those for nylon tires except at high speeds.

The temperature rise of the air in the inner tube was found to be related to the power loss by the relation: $\Delta T/P=G+H/(SL)^{0.8}$ where G and H are parameters dependent on the thermal resistance of the rubber compounds and of the interface between tire and air or roadway, respectively. The ratio $\Delta T/P$ remained essentially unchanged by changes in inflation pressure and did not appear to be affected by the type of cord.

1. Introduction

Work is required to flex a tire as it rotates. This work is converted into heat which increases the temperature until the rate of heat dissipation equals the rate of heat generation or power loss in a tire. In large tire sizes, the resulting high operating temperature is a serious problem. It shortens the life of a tire and is the principal deficiency of synthetic rubber for use in these tires. Even natural rubber is far from an ideal rubber in this respect.

The importance of power loss and its effect on operating temperature has long been realized. However, a survey of the rubber literature reveals few systematic studies published on this subject since the early work of Holt and Wormeley [1][2] in 1922 and 1923. The paper by Billingsley et al. [2] in 1942 and that by Evans [3] in 1948 are perhaps the most comprehensive of those published in the last 20 years. The importance of this problem in the Government Synthetic Rubber Program led to a resumption of work on power loss of tires at the National Bureau of Standards in 1948 after a lapse of over 20 years. This paper summarizes the work of the past 10 years on the measurement of power loss and the resultant operating temperature in pneumatic tires.

2. Equipment

The basic method of Holt and Wormeley [1] was used in these studies. Since the equipment used by them was no longer available, new equipment was constructed which differed in some respects from that used in the early work.

The arrangement of the equipment is shown schematically in figure 1. Dynamometer A having a capacity of 60 hp at 250 rpm is connected to a standard smooth-face steel drum (D), 1/300 mile in circumference and 14 in. in width. This dynamometer is operated as a generator and provides the desired tractive effort.

Dynamometer B has a capacity of 40 hp at 250 rpm and is operated as a motor in measuring the power loss of truck and bus tires. It is connected through universal joints to one axle of a truck rear wheel assembly on which the tire (T) is mounted. The rear axle housing is suspended from the ceiling by means of two rods approximately 20-ft long; the tire and wheel assembly are supported like a ballistic

[1] This paper was presented at the International Rubber Conference, Washington, D.C., Nov. 8 through 13, 1959.
[2] Figures in brackets indicate the literature references at the end of this paper.

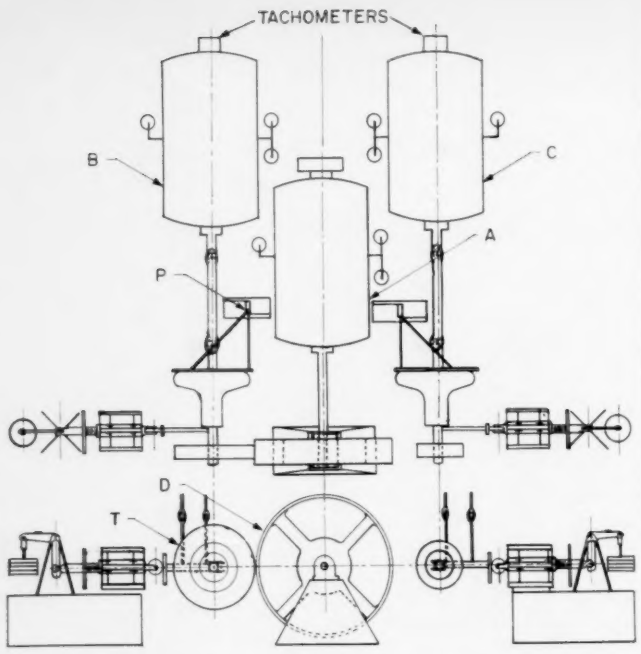

FIGURE 1. *Schematic arrangement of equipment for measuring power loss of tires.*

(A) Absorption dynamometer connected to steel drum, D; (B) Dynamometer used for driving truck tire, T; (C) Dynamometer used for driving passenger car tire; (P) Ball and socket pivot used for alining the plane of tire with the plane of the drum.

pendulum. The assembly is pivoted in a ball and socket joint located in the vertical plane tangent to the steel drum (point P in fig. 1). The pivot point can be adjusted vertically which rotates the plane of the tire and permits its alinement with the plane of the steel drum. The pivot also prevents axial motion of the tire. Adjustments are provided for keeping the axes of rotation for tire and steel drum parallel during test under any load. Radial motion in the horizontal plane is restrained by the load applied to the tire. The load is applied by means of weights acting through a lever arm so that the load on the tire is approximately four times the applied load. This loading system is almost free of friction, being under 10 lb or less than 1 percent of the applied load. (NOTE: Initially the load was applied to the axle housing through a conventional leaf spring. The friction and power loss in the spring made it necessary to revert to an unsprung load.)

Dynamometer C has a capacity of 20 hp at 700 rpm and is operated as a motor in measuring the power loss of passenger car tires. The arrangement is the same as that described for truck tires. Either dynamometer B or C, but not both, is used in conjunction with dynamometer A in any one test. Each dynamometer is instrumented to permit measurement of speed within 0.1 rpm or 0.2 percent at the slowest speed and of torque on the armature shaft within 0.1 lb-ft or 1 percent of the difference between input and output torques.

The tire and steel drum are enclosed in a housing. The temperature of the air within the housing is controlled at 100° ±5° F. The temperature of the air contained within the tire is measured by means of a copper-constantan thermocouple which extends beyond the valve stem into the tire approximately 0.7 the distance between the rim and crown of the tire. The thermocouple is connected to a recorder through a compensating circuit and copper slip-rings as described by Richey, Hobbs, and Stiehler [4]. The valve stem is connected through a rotating joint to a precision pressure gage for measuring the inflation pressure.

3. Calibration of Equipment

A calibrated pressure gage accurate to within 0.1 lb/in.^{2} was used to measure the pressure within the tire. The copper-constantan thermocouples were calibrated using a benzoic acid cell [5] and found to be within 1° F of the correct temperature. The power loss in the bearings, in windage, and in other parts of the equipment was determined by means of a steel tire assembly constructed in the following manner:

An annular steel ring about 40 in. in outside diameter and 1 in. in thickness was mounted on a 20-in. tire rim. Wood blocks were fastened to the sides of the steel ring. A 9.00–20 tire was split and fastened to the rim and wood blocks so that the completed assembly appeared like a tire mounted on a rim with a center steel rib extending about ⅛ in. above the tire. This assembly was mounted in place of the truck tire and the circumference of the steel ring was machined true. A similar assembly was constructed for determining power loss in the equipment when testing passenger car tires.

The power loss of each system was measured with these steel tires at a combination of speeds and loads ranging from 10 to 60 mph and 600 to 5,000 lb. It was found that the equipment power loss could be expressed as a polynominal function of speed and load in accordance with the following equation, where P represents power loss, S speed, and L load:

$$P=aS+bS^2+cS^3+dLS \qquad (1)$$

Using dynamometers A and B, the best values for the parameters a, b, c, and d, derived by the method of least squares from a total of 40 measurements, are as follows:

$$a=96.4$$
$$b=\ 4.26$$
$$c=\ 0.0644$$
$$d=\ .0288$$

when power loss is expressed in feet-pounds per minute, speed in miles per hour, and load in pounds.

4. Procedure

Since the power loss of a new tire decreases rapidly during the first few hours of running and then changes

at a much slower rate, the tires were preconditioned by running them for at least 16 hr at 45 mph under 80 to 100 percent of maximum rated load.

After preconditioning, the load, speed, and inflation pressure were adjusted to the desired values for test; the axle of the rotating tire was made parallel to the axle of the steel drum; and the tire was run until the temperature of the contained air remained constant within 1° F for at least 10 min. Readings were then taken of the torque on the dynamometers, their speed, and the inflation pressure. The readings were repeated about 5 min later. The temperature of the ambient air and of the contained air were recorded. This procedure was repeated for the next combination of load, speed, and inflation conditions.

The sequence of measuring the various combinations of load, speed, and inflation was varied in accordance with a statistical design in order to eliminate systematic bias.

The measured values of power loss were corrected for power loss in the equipment and windage as determined from eq (1). For convenience in comparing tires, the dimensionless quantity—hereinafter called coefficient of rolling resistance or R—was derived from the corrected power loss by the following equation:

$$R=\frac{P}{88SL} \tag{2}$$

where P is power loss in feet-pounds per minute, S is speed in miles per hour, and L is load in pounds.

5. Tractive Effort

A few measurements were made on the effect of tractive effort on power loss. The results for a tire made from natural rubber (NR) and one made from styrene-butadiene rubber (SBR) are given in table 1. Over the range of tractive effort studied, there is no evidence of any change in power loss. Measurements on tires used in the treadwear study by Mandel, Steel, and Stiehler [6] also indicate no change in power loss with tractive effort. These results are not in accord with those of Billingsley et al. [2] and Holt and Wormeley [1]. No explanation for the difference in results is apparent.

The creep was determined in these experiments by means of the equation

$$C=(l-2\pi r)/l,$$

where l is the distance the tire travels in one revolution and r is the measured rolling radius. The creep remained constant with increasing tractive effort. It was positive and amounted to about 2 percent, being slightly greater at 50 mph than at 20 mph.

Since it was easier to adjust the speed with some tractive effort on the tire, all subsequent measurements were made with a constant tractive torque of 52.5 lb-ft (630 lb-in.), corresponding to 0.5 and 2.5 hp at speeds of 10 and 50 mph, respectively.

6. Slip Angle

The power loss of the tires in table 1 was also measured at several angles, ranging from 0° to 2° between the plane of the tire and the plane of the steel drum. The coefficients of rolling resistance measured at each condition of test are given in table 2. Since the values for the two speeds are practically identical, their averages are plotted in figure 2 as a function of the slip angle. The results in table 2 and figure 2 show that the increase in rolling resistance is not dependent on the speed and is practically the same for the two types of rubber.

TABLE 1. *Effect of tractive effort on power loss 9.00–20, 10 ply tires; load 4,000 lb; inflation pressure 90 lbs/in.² gage; ambient temperature 100° F*

Tractive torque [a]	Power loss in horsepower			
	NR tire		SBR tire	
lb-in.	*20 mph*	*50 mph*	*20 mph*	*50 mph*
315	1.33	3.29	2.08	5.08
630	1.34	3.29	2.07	5.13
945	1.32	3.28	2.10	5.11
1,260	1.32	3.23	2.07	5.09
1,575	1.33	3.26	2.08	5.13
1,890		3.24		5.15
2,205		3.28		5.17

[a] On output dynamometer.

TABLE 2. *Effect of slip angle on rolling resistance 9.00–20, 10 ply tires; load 4,000 lb; inflation pressure 90 lbs/in.² gage; ambient temperature 100° F*

Slip angle	Rolling resistance			
	R for NR tire		R for SBR tire	
min	*20 mph*	*50 mph*	*20 mph*	*50 mph*
0	0.00623	0.00623	0.00938	0.00958
12	.00630	.00632	.00968	.00970
24	.00666	.00675	.01007	.01012
36	.00709	.00722	.01073	.01058
48	.00780	.00783	.01114	.01133
60	.00807	.00840	.01211	.01214
72	.00910	.00920	.01302	.01314
84	.01002	.01026	.01397	.01399
96	.01095	.01072	.01488	.01502
108	.01269	.01309	.01623	.01634
120	.01421	.01438	.01776	.01819

As the slip angle increases from 0° to 2°, the rolling resistance and power loss approximately doubles. At the same time, there is only a slight increase in the temperature of the air contained within the inner tube. These results lead to the conclusion that the increase in power loss with slip angle is dissipated at the interface between tire tread and steel drum. There is a large increase in temperature at the interface as manifested by the amount of liquified rubber appearing on the drum. The heat generated at the interface is dissipated mainly through the drum so that the temperature of the air within the tire is only slightly affected. Since the increase in rolling resistance is practically the same for the two types of tires, their coefficients of friction against steel must be alike or nearly so.

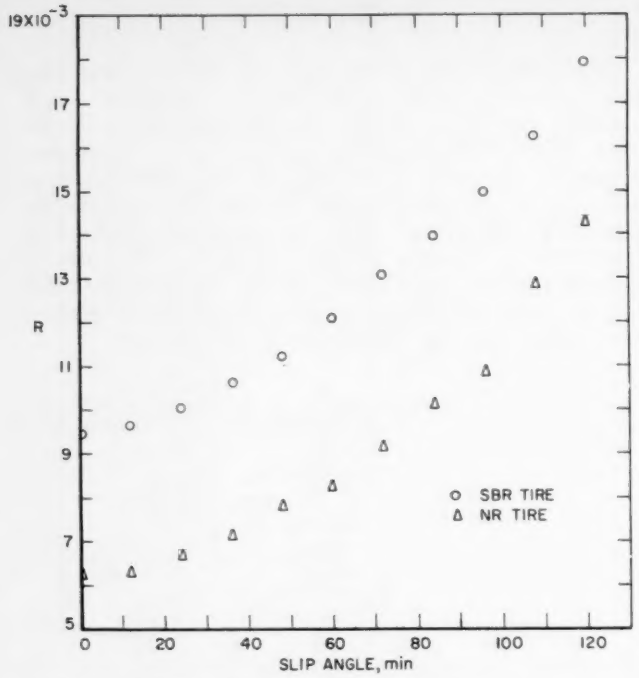

FIGURE 2. *Effect of slip angle on coefficient of rolling resistance, R, for 9.00–20, 10-ply truck tire.*

7. Speed and Load

Information on the effect of speed and load was obtained from two comprehensive experiments, denoted in the following discussion as experiments A and B. Experiment A employed 9.00–20, 10-ply tires and experiment B employed 10.00–20, 12-ply tires.

Experiment A

(9.00–20, 10-Ply Tires)

This study was made on the following four experimental tires involving different combinations of two types of rubber in the tread and in the carcass.

Tire construction	Tread	Carcass
1	NR	NR
2	NR	SBR
3	SBR	NR
4	SBR	SBR

Two tires of each construction were tested. In each run the inflation pressure of the tire was set initially at 90 psi at a temperature of 100° F. No further pressure adjustment was made during the run. The experiment was carried out in two parts. First each tire was run at speeds of 5, 10, 20, 30, 40, and 50 mph under constant loads of 1,000 and 4,000 lb. Then, the speed was held constant at each of two levels, 10 and 50 mph, while the tire was run under loads of 500, 1,000, 2,000, 3,000, 4,000, and 5,000 lb.

The mean values of the coefficients of rolling resistance are listed in table 3 for duplicate tires of each construction. The standard deviation for experimental error, determined from the differences between the results obtained on duplicate tires tested under the same conditions, is 0.00038 for these data. Thus, the uncertainty in the values given in table 3 is in the second significant figure. However, for purposes of statistical analysis three significant figures are retained.

Using this estimate as a standard of reference, several mathematical formulas were tried to express the coefficient of rolling resistance as a function of speed and load. It was found that the following relation fitted the data within experimental error:

$$R = R_0 + B(S) + C(L) + D(SL). \qquad (3)$$

TABLE 3. *Experiment A: Coefficients of rolling resistance for experimental tires*

	R at load 1,000 lb				*R* at load 4,000 lbs			
Speed	Tire 1	Tire 2	Tire 3	Tire 4	Tire 1	Tire 2	Tire 3	Tire 4
mph								
5	0.00356	0.00506	0.00656	0.00694	0.00551	0.00750	0.00814	0.00844
10	.00371	.00525	.00645	.00739	.00517	.00765	.00821	.00874
20	.00446	.00615	.00660	.00780	.00499	.00788	.00806	.00904
30	.00435	.00596	.00712	.00810	.00544	.00776	.00799	.00862
40	.00439	.00596	.00795	.00821	.00562	.00772	.00791	.00870
50	.00472	.00668	.00750	.00802	.00596	.00788	.00855	.00908

	R at speed 10 mph				*R* at speed 50 mph			
Load	Tire 1	Tire 2	Tire 3	Tire 4	Tire 1	Tire 2	Tire 3	Tire 4
lb								
510	0.00345	0.00529	0.00604	0.00675	0.00514	0.00641	0.00788	0.00802
1,000	.00371	.00525	.00645	.00739	.00472	.00668	.00750	.00802
2,000	.00431	.00656	.00750	.00788	.00514	.00754	.00739	.00844
3,000	.00502	.00712	.00814	.00851	.00529	.00731	.00806	.00859
4,000	.00517	.00765	.00821	.00874	.00596	.00788	.00855	.00908
5,000	.00622	.00874	.00840	.01035	-------	-------	-------	-------

In this equation, S represents speed in miles per hour, and L, load in pounds. The constants R_0, B, C, and D were derived from the data by the method of least squares. Values for B, C, and D, given in table 4, are nearly alike for the four tire constructions.

A statistical analysis shows that the differences are not significant on the basis of the evidence provided by the experiment. Of course, more comprehensive data might reveal significant differences for these parameters, but it is unlikely that the differences would be of practical importance. For these reasons, it is assumed that the value of each coefficient in eq (3) has the same value for each construction. The best statistical estimates of B, C, and D based on this assumption are listed in the last line of table 4. As expected, the parameter R_0 varies with the construction. This parameter is discussed in section 10.

It may be inferred from eq (3), and from the constancy of B, C, and D for all four constructions that the quantity $R-R_0$ depends only on speed and load. Consequently, when $R-R_0$ is plotted against either speed or load, the points should follow the same curve for all four constructions. Figures 3 and 4 are plots of the average of $R-R_0$ versus speed and load, respectively. The straight lines represent

TABLE 4. *Experiment A: Parameters in eq 3*

Tire construction	B	C	D
1	30.8×10^{-6}	0.559×10^{-6}	-0.00421×10^{-6}
2	38.4	.835	−.00878
3	32.0	.579	−.00570
4	26.4	.607	−.00613
All[a]	33.8	0.642	0.00708

[a]Best statistical estimate on assumption of single values for B, C, and D.

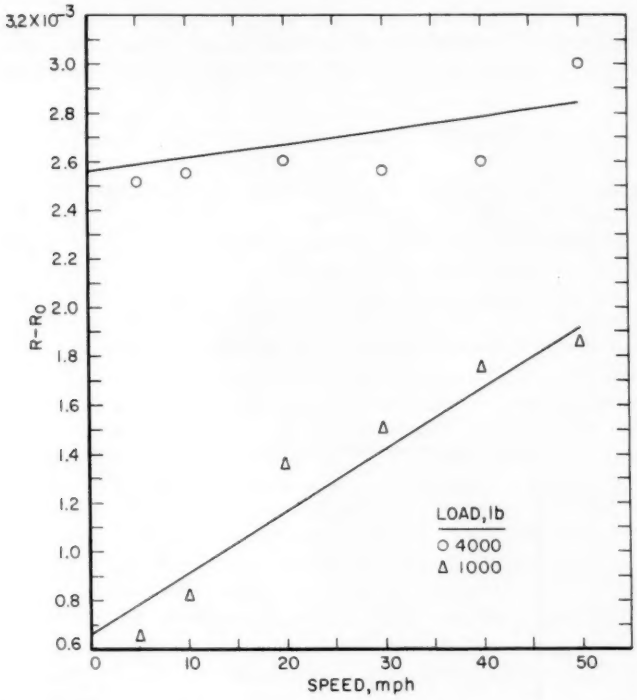

FIGURE 3. *Increase in coefficient of rolling resistance, $R-R_o$' with speed for 9.00–20, 10-ply truck tire (experiment A).*

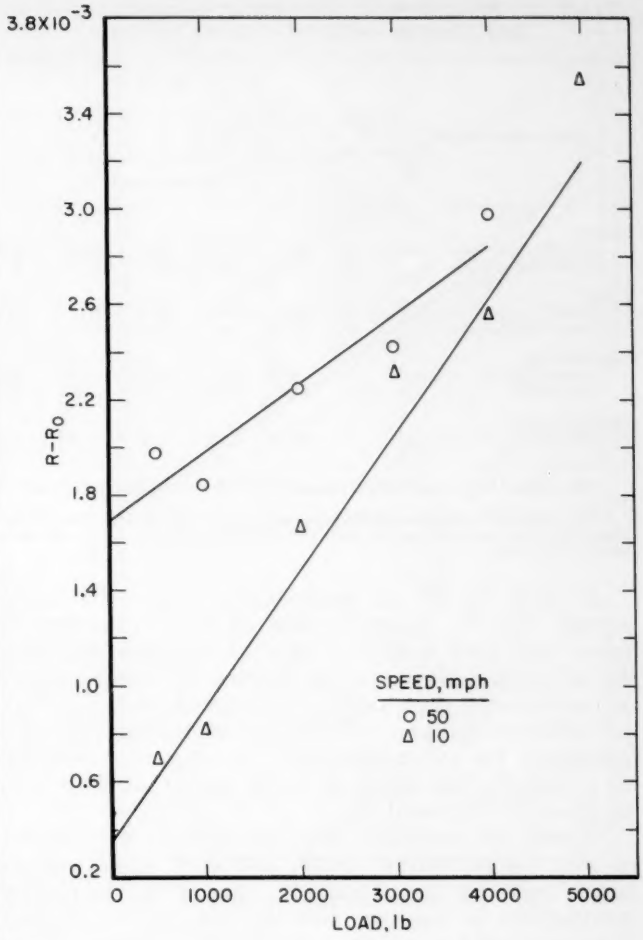

FIGURE 4. *Increase in coefficient of rolling resistance, $R-R_o$, with load for 9.00–20, 10-ply truck tires (experiment A).*

eq (3), using the values for all constructions in table 4. In general, the effects of speed and load given by eq (3) are in satisfactory agreement with the experimental results. The difference in the slopes of the two lines in each graph is related to the last term in eq (3), containing the product of speed and load, with a negative coefficient.

Experiment B

(10.00–20, 12-ply tires)

In this experiment, one tire from each of five commercial brands was run at five different speeds and five different loads. The pressure was held constant at 105 psi at running temperature. The speeds were 10, 20, 30, 40, and 50 mph; the loads were 1,000, 2,000, 3,000, 4,000, and 5,000 lb. Thus, 25 speed-load combinations were run on each of 5 tires. In order to eliminate possible biases due to time and order of running, a graeco-latin square design was used with respect to the factors tire, speed, load, and order.

To test the adequacy of eq (3) for the representation of the data yielded by experiment B, an analysis of variance was made for the data corresponding to each tire. The results are summarized in table 5. The "linear" part of the speed mean square corresponds to the term $B(S)$ in eq (3); the "linear" part of the load mean square corresponds to the term $C(L)$; and the "linear×linear" part of the speed× load interaction corresponds to the $D(SL)$ term.

In table 5, practically all nonlinear terms are of the order of magnitude of experimental error, the variance of which is 7.0×10^{-8}. This value corresponds to a standard deviation of the coefficient of rolling resistance of 0.00026. This value is smaller than the one in experiment A. The difference may be due to the fact that the standard deviation in experiment A includes the variability between duplicate tires, whereas this estimate reflects only experimental error.

It can be inferred from table 5 that the data of experiment B are adequately represented by the following equation:

$$R=R_o+B(S)+C(L). \quad (4)$$

TABLE 5. *Experiment B: Analysis of variance of speed and load effects on coefficient of rolling resistance*

Source of variation	Degrees of freedom	Brand 1	Brand 2	Brand 3	Brand 4	Brand 5
		Mean squares[a]				
Speed:						
Linear	1	131.2	6.5	39.8	43.9	54.3
Nonlinear	3	8.4	12.7	14.1	1.7	9.6
Load:						
Linear	1	228.4	648.0	352.4	141.2	370.5
Nonlinear	3	20.7	9.3	11.8	22.5	7.6
Speed×load:						
Linear×linear	1	9.7	21.7	31.2	1.4	5.6
Nonlinear	15	12.7	13.1	10.7	5.2	6.8
Nonlinear terms:						
Pooled[b]	21	13.2	12.5	11.3	7.2	7.3

[a] The analysis was carried out on rolling resistance values, after multiplication by 10^4.

[b] The variance of experimental error, obtained independently from a comparison of replicate measurements on the same tire, was found equal to 7.0, in the units used in this table.

A term in SL is unnecessary, since the mean square for the linear portion of the interaction of speed and load is of the order of experimental error for all tires. Moreover, in the case of brand 2, there is no evidence that variation in speed has any effect on rolling resistance. Table 6 gives the least squares estimates for the parameters R_0, B, and C for the five brands; the value B being made equal to zero in the case of brand 2.

It may be concluded from the data in experiment A that the parameters B, C, and D in eq (3) are, at most, only slightly affected by changes in the rubber compounds in the tire, but the data in experiment B show that the parameters B and C in eq (4) are appreciably influenced by other changes in construction.

TABLE 6. *Experiment B: Parameters in equation (4) for five brands of tires*

Brand of tire	B	C	R_0
1	16.2×10^{-6}	0.214×10^{-6}	3.824×10^{-3}
2	0	.360	3.315
3	8.9	.266	4.655
4	9.4	.168	4.127
5	10.4	.272	4.008

8. Inflation Pressure

Measurements of power loss were made at several inflation pressures using tires 1 and 4 of experiment A and brands 1, 2, 3, and 4 of experiment B. Five combinations of speed and load were used in the study with tires 1 and 4. The rolling resistances given in table 7 were obtained. An analysis indicated that for each speed-load condition R is essentially linearly related to the reciprocal of the pressure. The intercepts and slopes given in table 7 for each speed-load condition were calculated by the method of least squares. The agreement of these parameters with the data was good, as can be seen in figure 5. However, they indicated a large

TABLE 7. *Effect of inflation pressure on rolling resistance 9.00–20, 10-ply tires; ambient temperature 100° F*

Speed, mph		20	50	35	20	50
Load, lb		1,000	1,000	2,500	4,000	4,000
Pressure (p) 1,000/p		R for NR Tire				
lb/in.²						
120	8.3	5.72	5.14	4.84	5.34	5.40
105	9.5	5.81	5.40	4.89	5.58	5.58
90	11.1	6.00	5.59	5.53	6.09	6.15
75	13.3	6.00	5.96	5.98	6.91	6.91
60	16.7	6.19	6.49	6.62	7.90	7.88
Intercept (A)[a]		5.32	3.84	2.92	2.64	2.75
Slope (B)[a]		53	159	225	316	308
		R for SBR Tire				
120	8.3	9.28	7.87	7.47	7.90	9.66
105	9.5	9.34	8.01	7.87	8.70	10.05
90	11.1	9.86	8.62	8.50	9.42	10.69
75	13.3	10.35	10.05	9.30	10.23	11.97
60	16.7	10.63	9.81	10.64	11.71	13.40
Intercept (A)[a]		7.82	5.64	4.28	4.39	5.72
Slope (B)[a]		176	274	380	441	461

NOTE: All values are rolling resistance multiplied by 1,000.

[a] Calculated by least squares to fit linear regression: $R=A+B/p$.

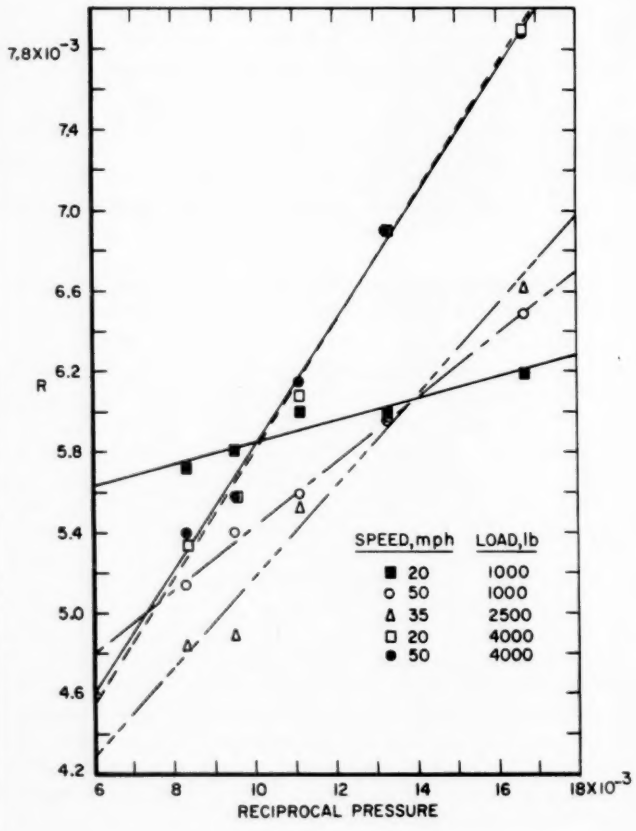

FIGURE 5. *Effect of inflation pressure on coefficient of rolling resistance, R, for NR 9.00–20, 10-ply truck tire.*

The reciprocal of the gage pressure in lb/in.² is used for the abscissa.

interaction with speed and load which could not be resolved with the limited data available.

The results obtained with brands 1, 2, 3, and 4 of experiment B confirmed the linear relationship between R and the reciprocal of the inflation pressure. However, the large interaction with speed and load complicated the analysis of the data obtained with a $4\times4\times4$ graeco-latin square design.

Nevertheless, it appears that the effect of pressure on R is practically independent of the speed at normal rated loads but markedly dependent on speed at low loads. On the other hand, the effect of pressure on R increases with the load at all speeds, the rate of increase being more pronounced at low speeds.

9. Variation Among Brands

The variation among brands was determined from experiment B and two other experiments conducted at a speed of 45 mph. In one of these experiments, 6 brands of 9.00–20, 10-ply tires were studied and in the other, 5 brands of 11.00–20, 12-ply tires.

Figure 6 represents eq (4) for the five brands included in experiment B at a fixed load of 5,000 lb, and figure 7 represents the same equation at a fixed speed of 50 mph. It is seen that distinct differences exist between some of the brands. The effect of speed on rolling resistance is far smaller than the effect of load. In view of the linearity of eq (4), the slopes of the lines drawn in figure 6 are independent of load. Thus, if a load other than 5,000 lb were selected, the straight line corresponding to each brand in figure 6 would be shifted parallel to itself, but the amount of the shift would vary from brand to brand. A similar conclusion holds for figure 7. It is apparent from these two figures

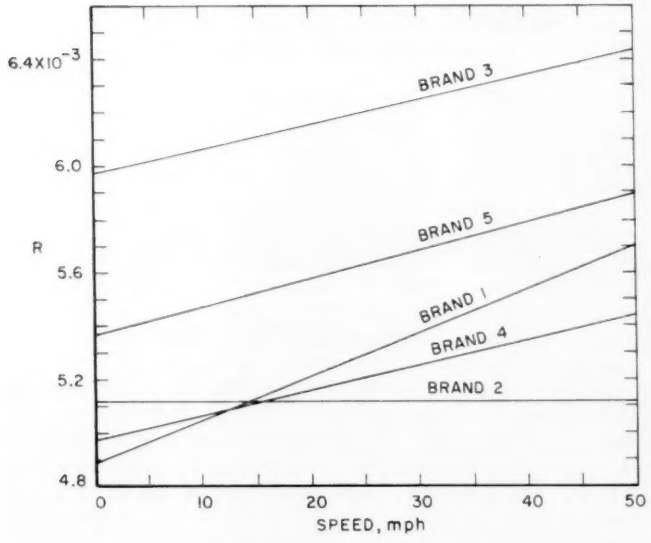

FIGURE 6. *Effect of speed on coefficient of rolling resistance, R, for five different commercial brands of 10.00–20, 12-ply truck tires (experiment B).*

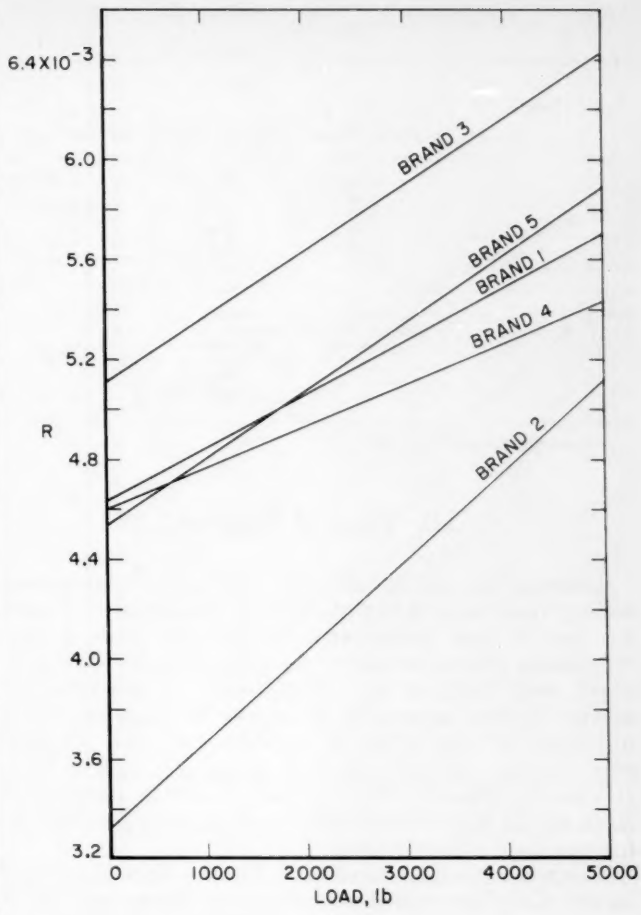

FIGURE 7. *Effect of load on coefficient of rolling resistance, R, for five different commercial brands of 10.00–20, 12-ply truck tires (Experiment B).*

that the relative coefficients of rolling resistance or power losses for various brands of tires are dependent on the speed and load at which the comparison is made.

A comparison of the results obtained in experiment B with those obtained in the experiments at 45 mph is given in table 8. The values for experiment B are interpolated from eq (4) at a speed of 45 mph and a load of 4,000 lb. All values in the table were corrected for power loss in equipment and windage. It is seen that the three sets, representing three different sizes, show considerable consistency in the ranking of the brands with respect to power loss. The consistency is remarkable since the various sizes were produced at different times over a period of several years. Since the tires were not produced concurrently, definite conclusions cannot be drawn about the effect of size of the tire on power loss. However, it appears that the coefficients of rolling resistance should be approximately the same for different sizes at the same speed and under loads appropriate for the tire size.

TABLE 8. *Coefficients of rolling resistance for several brands and sizes*

Brand	Size of tire		
	9.00–20, 10 ply	10.00–20, 12 ply [a]	11.00–20, 12 ply
1	6.03×10^{-3}	5.41×10^{-3}	5.88×10^{-3}
2	5.54	4.76	
3	6.99	6.12	9.26
4	5.54	5.22	6.18
5	6.51	5.56	6.80
6	6.51		9.36
Speed	45 mph	45 mph	45 mph
Load	3,450 lb	4,000 lb	4,500 lb
Inflation	65 psig at 100° F	105 psig at running temperature	70 psig at 100° F

[a] Values calculated from eq (4).

10. Type of Rubber

Information on the influence of type of rubber on rolling resistance was provided by experiment A and by power loss measurements on the tires whose treadwear characteristics were reported by Mandel, Steel, and Stiehler [6]. Experiment A described in section 7 was primarily designed to determine the influence of the type of rubber and the relative contribution of carcass and tread to power loss. It was mentioned in that section that the parameter R_0 in eq (3) was the only one that varied significantly for the four constructions.

Table 9 lists the values of R_0 for the tires in experiment A. The standard error of these values is 0.13×10^{-3}. Accordingly, the differences in R_0 have only a small uncertainty due to error of measurement.

The difference in R_0 values for tires 1 and 3 is 2.7×10^{-3} and that for tires 2 and 4 is 1.38×10^{-3}. Similarly, the difference for tires 1 and 2 is 2.04×10^{-3} and that for tires 3 and 4 is only 0.72×10^{-3}. Thus, it is apparent that the contributions of the rubber in tread and carcass to power loss are not additive. Instead, there is a pronounced interaction between tread and carcass which causes the power loss to be greater than anticipated when SBR is present in either. Although quantitative conclusions concerning the relative contribution of tread and carcass are not possible, the data indicate that the greater power loss is in the tread. Considering only power loss, it appears advantageous to make 100 percent natural and synthetic rubber tires from the available rubber rather than to use one rubber in the carcass and the other in the tread.

Results of the tire constructions whose treadwear characteristics were reported by Mandel, Steel, and Stiehler [6] are given in table 10. These tires had natural rubber carcasses and differed only in the composition of the tread. In view of the interaction between tread and carcass, comparisons of these tires are only qualitative indices of the effect of rubber on power loss. Recognizing this limitation, the results show the pronounced increase in power loss when synthetic rubber is present.

TABLE 9. *Effect of rubber in carcass and tread on rolling resistance*

Tire construction	Rubber		R_0
	Tread	Carcass	
1	NR	NR	2.84×10^{-3}
2	NR	SBR	4.88
3	SBR	NR	5.54
4	SBR	SBR	6.26

TABLE 10. *Effect of rubber and carbon black on coefficient of rolling resistance*[a]

Carbon black [f]		Type of rubber				
Type	Loading[b]	NR	X-485 GR-S[c]	GR-S-10[d]	GR-S[c]	Average
(a) HAF	50	9.15	8.96	11.66	11.02	10.20
(b) Channel	46	7.50	9.45	10.01	10.84	9.45
(c) HAF	50	8.78	9.60	10.76	11.14	10.07
(d) VFF	50	8.21	10.35	10.35	10.91	9.96
(e) HAF	50	9.22	10.01	9.64	10.65	9.88
(f) Acetylene	50	8.62	10.09	10.76	11.14	10.15
(g) RF	50	8.02	9.56	11.29	11.25	10.03
Average		8.50	9.72	10.64	10.99	

[a] Speed: 45 mph; load: 3,450 lb; inflation pressure: 65 psig at 100° F; 9.00-20, 10-ply truck tires. Values in the body of the table are rolling resistance multiplied by 1,000.
[b] Parts by weight per 100 parts rubber.
[c] SBR-1500 type.
[d] SBR-1002.
[e] SBR-1000.
[f] HAF=high abrasion furnace; VFF=very fine furnace; RF=reinforcing furnace.

Measurements were also made comparing polybutadiene and X–578 GR–S (similar to SBR 1500) in 7.00–15 passenger car tires. The results given in table 11 show that the rolling resistance for polybutadiene tires is appreciably lower than that for X–578 GR–S.

TABLE 11. *Effect of rubber and black on R in passenger car tires*

Rubber	Carbon black [a]	Coefficient of rolling resistance [b]
Polybutadiene	HAF	9.03
	SAF	11.89
X-578 GR-S [c]	HAF	10.75
	SAF	13.03

[a] HAF=high abrasion furnace; SAF=super abrasion furnace.
[b] Speed: 60 mph; load: 1,095 lb; inflation pressure: 26 psig at 100° F; 7.00-15, 4-ply passenger car tires. Values are rolling resistance multiplied by 1,000.
[c] SBR-1500 type.

11. Type of Carbon Black

Tables 10 and 11 also present data for ascertaining the influence of type of carbon black on rolling resistance or power loss. A statistical analysis of the data in table 10 indicates that the type of black has little effect. On the other hand, the data in table 11 show that there is a pronounced difference between HAF and SAF blacks in their effect on power loss.

This complicated and confusing situation apparently results from a balancing of the relative effects of black on modulus and resilience. The poor corre-

lation between laboratory tests for resilience or power loss on rubber compounds and tire performance is probably attributable to the same cause. Further systematic investigation is needed in order to devise a reliable laboratory test using small specimens of the compounds present in tires. Nevertheless, it may be concluded from the present study that the effects of black on abrasion resistance and power loss are not correlated. Consequently, it is possible to utilize to the fullest extent any advantage of a particular black with respect to abrasion resistance without necessarily affecting power loss adversely.

12. Type of Cord

The power loss studies reported thus far were made with tires having rayon cords. These tires were made in the late forties and early fifties. In 1958, a few measurements were made with 10.00–20, 12-ply rating commercial heavy duty truck tires having rayon, nylon, and wire cords. These tires were not made by the same manufacturers so that the results include not only the influence of cord, but the influence of rubber compounds and constructional geometry as well. Nevertheless, the study indicated the following pattern for the coefficient of rolling resistance with speed and load:

	Rayon	Nylon	Wire
Increasing speed	Constant	Decrease	Decrease.
Increasing load	Increase	Increase	Constant or decrease.
Rolling resistance		Highest	Lowest.

It is interesting to note that the rolling resistance of the tire having wire cords tended to decrease as the speed and load increased. This behavior may be associated with constructional features of the tire rather than the wire cords. If so, future developments may lead to similar behavior of the tires having textile cords.

Another study was made with 8.00–15, 4-ply passenger car tires having rayon or nylon cords and the same rubber compounds in both. Three tires of each type were tested under a load of 1,385 lb. and at speeds of 25, 40, 55, and 70 mph.

Figure 8 shows the change in coefficient of rolling resistance with speed at inflation pressures of 25- and 30-psi gage. The values of R for rayon tires are 10 to 15 percent lower at 25 mph, but they increase much more rapidly with speed. At 70 mph and higher, they equal or exceed those for nylon tires. In view of the diverse patterns exhibited by rayon truck tires, the sharp increase in R with increasing speed is probably an interaction between the particular geometrical construction used and rayon cords. Other constructions may not show this pattern, but it is likely that improved constructions will be favorable in both rayon and nylon tires. In this connection, it is important to note that the coefficients of rolling resistance for passenger car tires are much greater than those for truck tires.

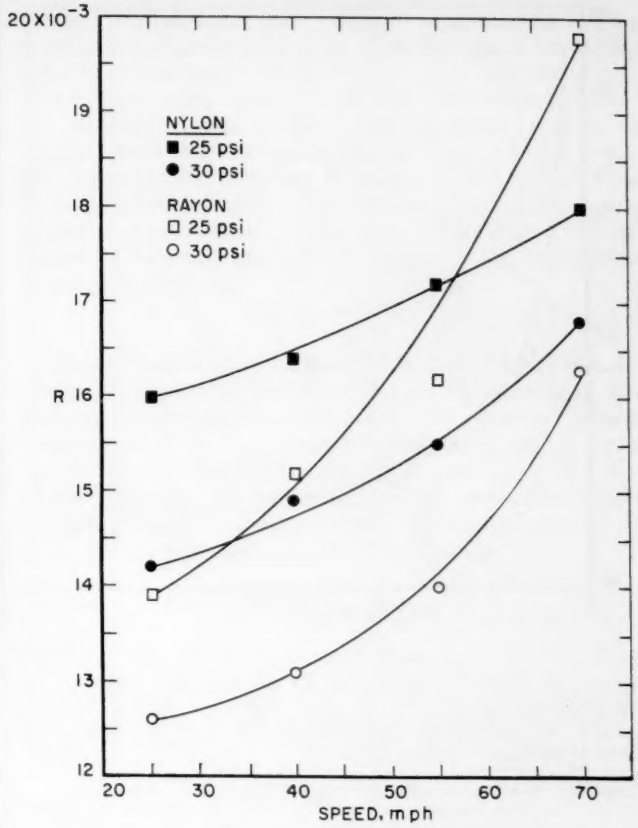

FIGURE 8. *Comparison of rayon and nylon cords in 8.00–15, 4-ply passenger car tires with respect to the coefficient of rolling resistance, R, at various speeds.*

13. Relation Between Power Loss and Temperature of Air Within Tire

In all the experimental work described in this paper, measurements of internal air temperature were made along with the measurements of power loss. Because the rise in temperature is often considered a measure of power loss, a detailed study was made of the relation between temperature rise and power loss. To this effect, the ratio of these two quantities, denoted as $\Delta T/P$, was examined as a function of speed, load, inflation pressure; and tire brand or construction.

An examination of the data showed that, for a given tire, the ratio $\Delta T/P$ was essentially a function of the product of speed and load. For example, a speed of 40 mph at a load of 1,000 lb gave practically the same value for $\Delta T/P$ as a speed of 10 mph at a load of 4,000 lb. No explanation is available for this relationship, but the tires of experiments A and B conform to it. Figure 9 is a typical plot of $\Delta T/P$ versus the speed$\times$load product, where $\Delta T/P$ is expressed in Fahrenheit degrees per horsepower and SL is expressed in mile-pounds per hour. The curves are statistically fitted in accordance with the following empirical relationship:

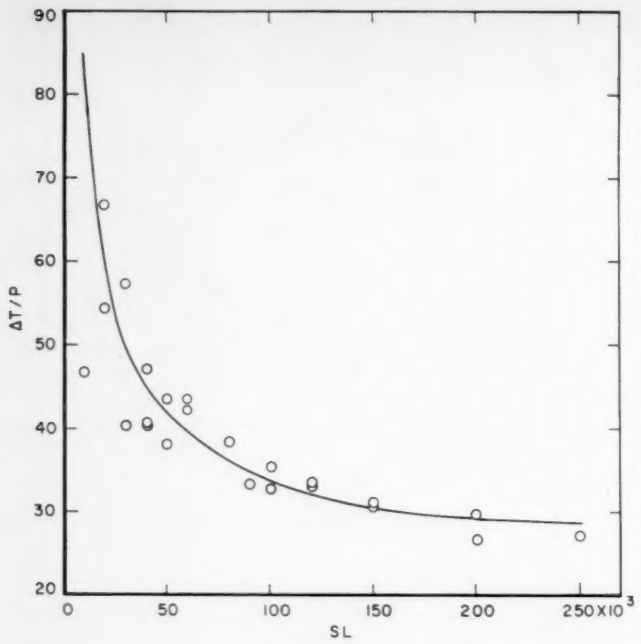

FIGURE 9. *Relationship for brand 1, 10.00–20, 12-ply truck tire between temperature rise of air within tire/unit power loss, $\Delta T/P$ in fahrenheit degrees/horsepower, and the product of speed and load, SL in lb-mi/hr.*

The solid curve represents the equation $\Delta T/P=23.3+100{,}400/(SL)^{0.8}$.

$$\frac{\Delta T}{P}=G+\frac{H}{(SL)^{0.8}}, \qquad (5)$$

where G and H are parameters characteristic of the tire.

The exponent 0.8 for speed is in accord with other equations for heat transfer between solids and gases. In connection with load, there is no prior basis for its use. However, an exponential power of load might be expected from the increase in contact area between tread and roadway with increase in load. The curves derived from this equation represent the experimental points well. A statistical analysis confirms this conclusion by showing that departures from the curves are within experimental error.

It is interesting to note that under usual running conditions (e.g., at speed-load products exceeding 100,000) the relation between $\Delta T/P$ and speed or load tends to become constant, approaching a value of approximately 28° F/hp. Thus, unless a sufficiently large range of speed and load values are included in the study of temperature-power loss relationship, it is easy to conclude that the ratio of these two quantities is essentially independent of speed and load.

Table 12 contains the best values for the parameters G and H in eq (5), for the four constructions in experiment A and the five brands in experiment B. It is worth noting that in experiment A, the value of H appears to group the four types of tires into two classes, according to the type of rubber in the tread,

TABLE 12. *Parameters in equation: $\Delta T/P=G+H/(SL)^{0.8}$*

Experiment	Brand or type	G	H
A	1	22.6	132,900
	2	24.6	106,500
	3	22.7	68,600
	4	23.6	72,200
B	1	23.3	100,400
	2	26.6	88,700
	3	23.4	101,300
	4	24.6	83,400
	5	26.1	96,700

whereas the value of G groups them in accordance with the type of rubber in the carcass (see table 9).

The relationship between $\Delta T/P$ and SL for brands 1, 3, and 4 is the same within experimental error. Similarly, the relationship for brands 2 and 5 is the same, and higher than that for the other brands. These parameters are apparently not correlated with power loss. It is suspected that the thermal conductivity of the tread and carcass is responsible for the difference but proof is lacking for this supposition.

This supposition is based on an examination of eq (5). The ratio $\Delta T/P$ is a measure of the thermal resistance of the tire and can be divided into two parts. The term G represents that portion of the thermal resistance which is independent of speed and load; whereas, the term $H/(SL)^{0.8}$ represents that portion which is dependent on speed and load. The internal characteristics of the tire such as the thermal resistance of the rubber and cord should be independent of speed and load and represented by G. The external characteristics such as ambient air film resistance, direct thermal resistance at the drum through the tire tread, etc., should be dependent on speed and load. It is important to note that at values of SL near 25,000 the thermal resistance is about equally affected by both terms of the equation. At higher SL values the term G becomes the predominant one and as the speed and load approach the range of normal operation the term $H/(SL)^{0.8}$ becomes less than 25 percent of the total thermal resistance. Hence, one would expect devices such as ribs, holes, etc., in the tread or shoulder to be of little or no practical value in reducing the thermal resistance of tires whereas reductions in the thermal resistance of the rubber may result in a very significant decrease in the operating temperature of the tire for the same power loss.

Surprisingly, changes in inflation pressure or in the type of cord have little or no effect on the ratio $\Delta T/P$. It is essentially the same for rayon, nylon, and wire cord tires. This observation indicates that the cord does not have an appreciable effect on the thermal resistance of the tire. The limiting factor appears to be the thermal conductivity of the rubber compounds. This conclusion is substantiated by the small effect of slip on the temperature rise of the contained air, ΔT, when power loss, P, is markedly increased as in cornering.

14. Discussion

A comparison of these results with those in the literature indicates qualitative agreement in most instances. There are pronounced quantitative differences which may arise from one or more of the following sources:

1. Power loss of most published data includes windage of the tire.
2. The drum deceleration and road test methods used by some workers do not permit measurements under steady state conditions.
3. Previous studies include a more limited range of load conditions.
4. The flexure and power loss of tires is greater when run on the outside circumference of a steel drum than when run on a flat surface.
5. The design and construction of tires during the past 40 yr has markedly changed.
6. The inherent difficulty and error in making power loss measurements are relatively large.

No attempt is being made to discuss these differences here. Nevertheless, the results indicate the need for further study both on the method of measuring power loss and on the performance characteristics of tires. The need for such measurements is greater today than ever with the many new polymers and cords, unconventional constructions, etc., that are being considered for tire use. Reliable power loss measurements provide a valuable tool for new tire design and development.

15. Conclusions

The effects of speed, load, and inflation pressure on power loss or rolling resistance (R) are intimately connected with the constructional design of the tire. For rayon truck tires, R seems to be linearly related to speed, load, and reciprocal pressure. The type of rubber has a pronounced effect, but two types of rubber in the same tire interact so that the rolling resistances are not additive. On the other hand, the type of black may or may not have an influence. The type of cord influences R, but the effect involves the constructional design. Truck tires appear to have a lower R than passenger car tires. The operating temperature of a tire depends on the power loss, thermal conductivity of the rubber, speed, load, and ambient temperature. The type of cord and the inflation pressure appear to have little effect on thermal resistance.

These studies were supported in part by the Reconstruction Finance Corporation and its successor, the Federal Facilities Corporation. The special tires for experiment A were supplied through the courtesy of the B. F. Goodrich Co. Many members of the National Bureau of Standards staff contributed to various phases of these studies. The assistance of all persons concerned is gratefully appreciated.

16. References

[1] W. L. Holt, P. L. Wormeley, Power losses in automobile tires, Tech. Pap. BS **16,** 451 (1922); Dynamometer tests of automobile tires, ibid. **17,** 559 (1923); Effect of tire resistance on fuel consumption, ibid. **19,** 213 (1925).
[2] W. F. Billingsley, R. D. Evans, W. H. Hulswit, E. A. Roberts, Rolling resistance of pneumatic tires as a factor in car economy, S.A.E. Journal **50,** 37 (1942).
[3] R. D. Evans, Factors affecting the power consumption of pneumatic tires, Proc. 2d Conf. Rubber Technol., p. 438 (London, 1948).
[4] G. G. Richey, R. H. Hobbs, R. D. Stiehler, Temperature studies of the air in a truck tire, Rubber Age **79,** 273 (1956).
[5] F. W. Schwab, E. Wichers, Freezing temperature of benzoic acid as a fixed point in thermometry, J. Research NBS **34,** 333 (1945) RP1647.
[6] J. Mandel, M. N. Steel, R. D. Stiehler, Treadwear of tires, influence of type of rubber and black, Ind. Eng. Chem. **43,** 2901 (1951).

Washington, D.C. (Paper 64C1–18)

JOURNAL OF RESEARCH of the National Bureau of Standards—C. Engineering and Instrumentation
Vol. 64C, No. 1, January–March 1960

Effects of Antioxidants on Asphalt Durability

Burton D. Beitchman*

(October 26, 1959)

The mechanism by which asphalt degrades during weathering can be studied profitably by observing the action of materials which inhibit this degradation.

A number of antioxidants which are believed to function either by their ability to inhibit chain reactions or to decompose peroxides were studied for their effectiveness in retarding weight loss and promoting durability of roofing asphalts. Inhibitors of chain reactions in some cases inhibited weight loss without extending durability. Compounds which decompose peroxides were observed to be capable of extending the durability of an asphalt and also of retarding weight loss. Phenothiazine, which is believed to function primarily as a peroxide decomposer, proved to be the most outstanding of the inhibitors tested.

A study made in one asphalt of the dependence of phenothiazine activity on concentration indicated that a concentration of 2 percent was optimum. In several other asphalts, 2 percent phenothiazine retarded weight loss to varying extents without significantly altering the durability of the asphalt.

Synergistic activity was shown by the use of an inhibiting mixture containing phenothiazine and *N*-phenyl-2-naphthylamine.

The results of this study support the hypothesis of a free radical process being involved to a considerable degree in asphaltic degradation during weathering.

1. Introduction

Asphalt is the material that is used most widely for roofing in the United States; however, little information is available concerning the mechanism of degradation of roofing asphalt during exposure to the weather.

This paper reports a study of the effect of two classes of antioxidants on the durability and weight loss of asphalts used as roof coatings during accelerated weathering. These antioxidants have been shown to be effective in inhibiting air oxidation of hydrocarbons, a reaction which is considered to be a free radical chain process. The mechanism, first proposed by Criegee and coworkers [1][1] and Bolland and Ten Have [2], and also described by Kennerly and Patterson [3] is:

$$\text{Initiation}\begin{cases}\mathrm{ROOH}\rightarrow\mathrm{RO}\cdot+\mathrm{HO}\cdot & (1)\\ \mathrm{RO}\cdot(\mathrm{HO}\cdot,\mathrm{HO_2}\cdot)+\mathrm{RH} \\ \quad\rightarrow\mathrm{ROH}(\mathrm{H_2O},\mathrm{H_2O_2})+\mathrm{R}\cdot & (2)\\ \mathrm{AH}+\mathrm{O_2}\rightarrow\mathrm{A}\cdot+\mathrm{HO_2}\cdot & (3)\end{cases}$$

$$\text{Propagation}\begin{cases}\mathrm{R}\cdot+\mathrm{O_2}\rightarrow\mathrm{RO_2}\cdot & (4)\\ \mathrm{RO_2}\cdot+\mathrm{RH}\rightarrow\mathrm{ROOH}+\mathrm{R}\cdot & (5)\end{cases}$$

$$\text{Termination}\quad 2\mathrm{RO_2}\cdot\rightarrow\mathrm{X} \qquad (6)$$

$$\text{Inhibition}\begin{cases}\mathrm{RO_2}\cdot(\mathrm{RO}\cdot,\ \mathrm{HO}\cdot,\ \mathrm{HO_2}\cdot)+\mathrm{AH}\rightarrow\mathrm{ROOH} \\ \quad(\mathrm{ROH},\mathrm{H_2O},\mathrm{H_2O_2})+\mathrm{A}\cdot & (7)\\ \mathrm{RO_2}\cdot(\mathrm{RO}\cdot,\ \mathrm{HO}\cdot,\ \mathrm{HO_2}\cdot)+\mathrm{A}\cdot\rightarrow\mathrm{Y} & (8)\end{cases}$$

The above equations have been explained by Kennerly and Patterson [3] essentially as follows. Peroxides, which are present or form in the hydrocarbons, initially cleave into free radicals when supplied with energy in the form of heat or ultraviolet light (eq (1)). Alkyl radicals are formed by reaction of these radicals with hydrocarbon molecules (eq (2)). These reactions are termed initiation steps in the oxidation. A chain reaction then ensues in which more molecules of the hydrocarbon react (eqs (4) and (5)). The chain process can terminate with the dimerization of two peroxy radicals to form an inactive product (eq (6)).

One type of antioxidant functions by its ability to intercept radicals which would propagate the chain reaction (eqs (7) and (8)). Other mechanisms have been suggested by which these inhibitors may intercept the propagating radicals [4, 5]. The inhibitor can contribute to initiation (eq (3)) and the rate of this reaction is directly dependent on inhibitor concentration.

The class of antioxidants, referred to as peroxide-decomposers, function by their ability to accelerate decomposition of peroxides into products which would be inactive in initiating or propagating a free radical oxidation. Inhibitors of chain reactions have been found to be superior for low temperature-low concentration applications and have been used for protection of gasoline in storage [3]. Compounds which decompose peroxides have been found to be superior for high temperature-high concentration applications and have been used in automotive lubricating oils, where high temperatures are encountered [3].

Asphalts are a complex mixture, containing hydrocarbons for the most part, and on exposure to natural and accelerated weathering yield a variety of oxidation products. Ultraviolet light produces deteriorating effects during these exposures, and thus it appears reasonable to propose that a free radical process may be one of the principal means by which asphalt degrades. A study of the action

* Present address, Houdry Process Corp., Linwood, Pa.

[1] Figures in brackets indicate the literature references at the end of this paper.

of inhibitors of chain reactions and peroxide-decomposers on durability and weight loss of asphalts during accelerated weathering may indicate whether a free radical process is involved in this degradation.

2. Procedure

Each of the asphalts was melted in a seamless ointment can on a hot plate and stirred periodically until the asphalt was fluid. The inhibitors, which are listed in tables 1 to 5, were added to the asphalt and stirred for several minutes. Exposure specimens were prepared by the hydraulic press method [6]. The asphalts used in this study were selected on the basis of previously determined values [2] for durability in order to include asphalts with a wide range of durability. These asphalts are identified by the symbols *A* to *F*. Four panels of each specimen were prepared except for samples of asphalt *A* and in this case only three panels for each specimen were prepared. The panels of asphalt were exposed in accelerated weathering machines to 51 min of light and 9 min of cold (40° F) water spray and light during every hour of exposure. Panels were weighed periodically to determine weight loss. The method for determining durabilities was that described by Greenfeld [6]. This procedure involves periodic inspection of panels with a high voltage electric probe. The failures in the coating are determined by making a spark photograph of the surface. A 60-square grid is placed over the photograph and when half of the squares show the presence of cracks or holes, the coating is considered to have failed. Durability is defined as the time required to reach this condition. Softening points [3] of uninhibited asphalts in this report ranged from 208° to 224° F and the penetrations [4] at 77° F from 16 to 20.5.

3. Results

A number of compounds which are considered to function as antioxidants by peroxide decomposition or inhibition of chain reactions were tested for their activity in retarding degradation effects in asphalt caused by weathering. The inhibitors of chain reactions used in this study were classified as such on the basis of studies by other investigators [4, 7]. Compounds identified as peroxide decomposers were part of a group discussed by Kennerly and Patterson [3]. The effectiveness of the inhibitors of chain reactions in retarding weight loss and promoting durability is shown in table 1. The durability is measured in terms of average number of hours to failure (col. 4). An arbitrary point has been chosen for comparison of weight losses in the exposed asphalts. The point chosen, 594 hr, is close to the failure points of the least durable asphalts.

Some of the values of percent weight loss at 594 hr were determined by interpolation or extrapolation when weighings were not made at this exact interval. Resorcinol and hydroquinone were observed to

[2] Unpublished data of S. H. Greenfeld and coworkers.
[3] ASTM Method D36-26.
[4] ASTM Method B5-52.

TABLE 1. *Antioxidant activity of inhibitors of chain reactions*

Asphalt	Inhibitor	Softening point	Durability (avg hr to failure)	Avg wt change at 594 hr
		° *F*		%
A	None	219	682	−10.46
A	1% resorcinol	218	725	−9.76
A	1% hydroquinone and 1% resorcinol	214	705	−9.75
A	1% hydroquinone	218	682	−9.39
A	1% diphenylamine	214	705	−8.99
B	None	221	639	−8.45
B	1% resorcinol	219	572	−9.91
B	1% t-butyl phenol	225	616	−8.92
B	1% hydroquinone	213	660	−8.91
B	1% diphenylamine	226	660	−8.26
B	1% *N,N*-diethyl-*p*-phenylenediamine	218	616	−7.83
B	1% *α*-naphthylamine	223	639	−7.57
B	1% *N*-phenyl-2-naphthylamine	216	749	−6.13
B	5% diphenylamine	191	901	−5.67

reduce weight loss to a slight extent in asphalt *A* and on the other hand to promote weight loss in asphalt *B*. *N*-phenyl-2-naphthylamine, *α*-naphthylamine, and *N,N*-diethyl-*p*-phenylenediamine were found to be the best of the antioxidants tested which function by free radical inhibition. The use of 5 percent diphenylamine in comparison to 1 percent of this inhibitor resulted in greater weight loss in the early stages of exposure but in significantly less weight loss in later stages. A slight increase in durability as measured by the crack pattern also resulted when 5 percent diphenylamine was used. These desirable effects, however, were attended by a marked decrease in softening point. The changes in softening point produced by the inhibitors can be obtained from table 1. Curves of weight change as a function of exposure time for asphalts to which have been added compounds which inhibit chain reactions are shown in figures 1, 2, and 3.

The effectiveness of several antioxidants which function as peroxide decomposers is shown in table 2. In order to compare the relative effectiveness of these inhibitors, the same number of moles were used in each case. Phenothiazine was found to

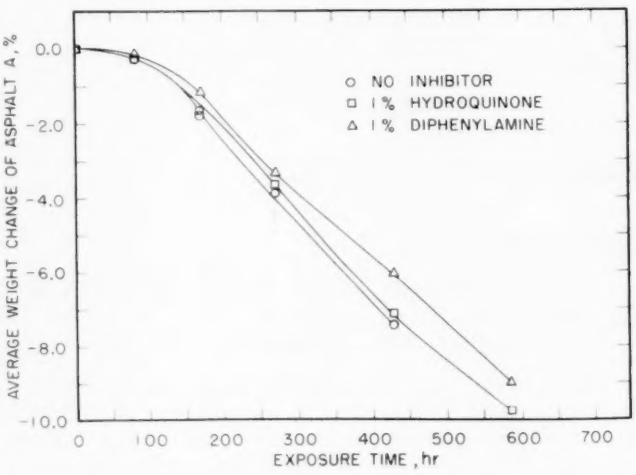

FIGURE 1. *The effect of inhibitors of chain reactions on weight loss of asphalt A.*

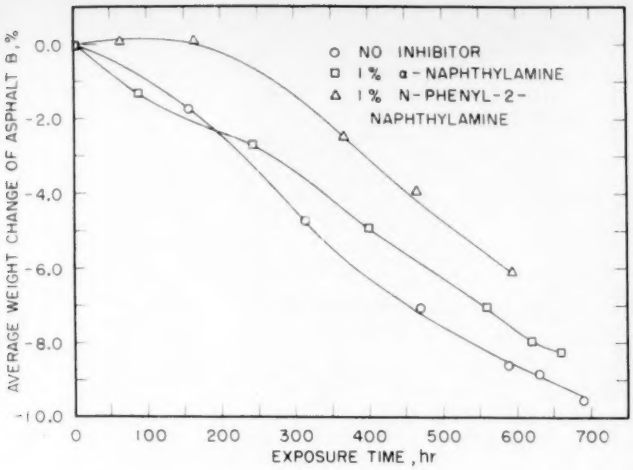

FIGURE 2. *The effect of inhibitors of chain reactions on weight loss of asphalt B.*

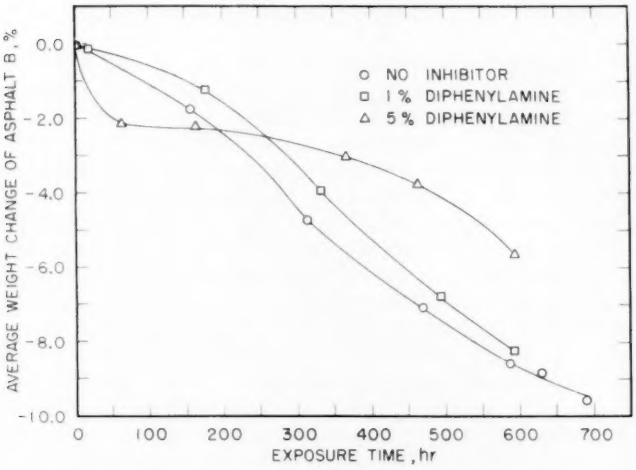

FIGURE 3. *The effects of two concentrations of diphenylamine on the weight loss of asphalt B.*

excel in its ability to retard weight loss and promote durability in asphalt *B*. The use of phenothiazine in asphalt to provide nondusting asphaltic coatings has been patented [8]. Other peroxide decomposers proved capable of extending the durability of the asphalt and retarding weight loss caused by accelerated weathering. Curves demonstrating the effect of two peroxide decomposers on weight loss as a function of time are shown in figure 4.

TABLE 2. *Antioxidant activity of compounds which decompose peroxides*

Asphalt	Inhibitor	Softening point	Durability (avg hr to failure)	Avg wt change at 594 hr
		°F		%
B	2.0% phenothiazine	212	3,180	+0.33
B	1.79% butyl sulfone	218	945	−7.30
B	1.47% butyl sulfide	226	1,142	−7.35
B	1.87% phenyl sulfide	218	1,120	−8.16
B	None	221	638	−8.45

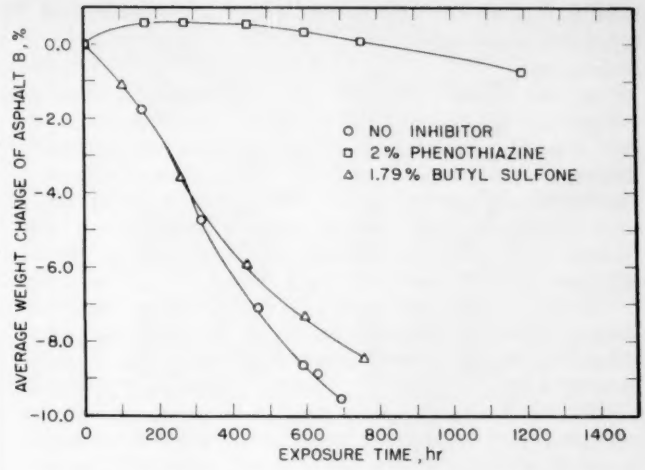

FIGURE 4. *The effect of compounds which decompose peroxides on weight loss of asphalt B.*

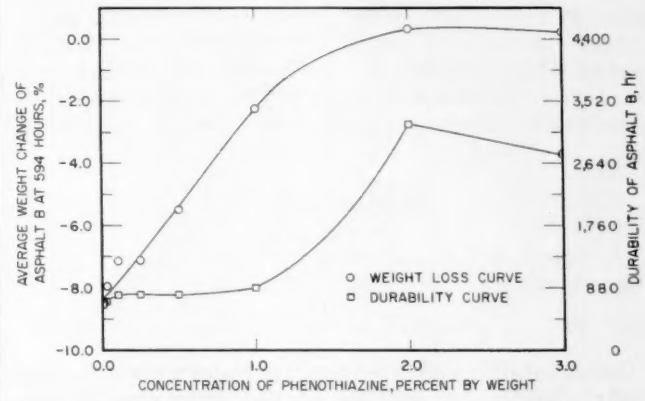

FIGURE 5. *The concentration dependence of phenothiazine activity in asphalt B.*

A study was made of the dependence of phenothiazine activity on concentration of inhibitor used. The activity of the inhibitor in inhibiting weight loss showed an approximately linear dependence up to 1 percent and then reached maximum activity at 2 percent (fig. 5 and table 3). The effect of inhibitor concentration on durability was slight up to 1 percent, but an abrupt increase in durability was observed when a concentration of 2 percent inhibitor was used (fig. 5). The use of 1 percent or more inhibitor produced a decrease in softening point. A concentration of 10 percent inhibitor produced a poor coating material with a low softening point although weight loss inhibition was still quite excellent.

Four other asphalts of varying durabilities were studied to determine the ability of phenothiazine to improve their weathering characteristics (table 4).

TABLE 3. *Concentration dependence of phenothiazine as an antioxidant in asphalt B*

Concentration of phenothiazine	Softening point of inhibited asphalt	Durability (avg hr to failure)	Avg wt change at 594 hr
%	° F		%
0.000	221	639	−8.45
.002	227	616	−7.88
.015	225	682	−7.96
.100	226	770	−7.12
.250	223	692	−7.10
.500	221	692	−5.45
1.000	218	880	−2.23
2.000	212	3,180	+0.323
3.000	210	2,780	+0.221
10.000	181	528	+0.49 [a]

[a] Value of weight loss at 528 hr.

TABLE 4. *Antioxidant activity of phenothiazine in other asphalts*

Asphalt	Concentration of phenothiazine	Durability (avg hr to failure)	Avg wt change at 594 hr
	%		%
C	0.0	1,210	−3.31
C	1.0	1,361	−3.28
C	2.0	1,340	−0.90
D	0.0	1,608	−6.32
D	1.0	1,718	−4.02
E	0.0	815	−6.43
E	1.0	859	−4.29
E	2.0	880	−0.83
F	0.0	1,450	−4.69
F	1.0	1,540	−3.45

The durabilities of these four asphalts were increased only slightly by the use of phenothiazine in concentrations of 1 or 2 percent. Weight-loss inhibition, however, was quite significant when a concentration of 2 percent phenothiazine was used (figs. 6 and 7). A concentration of 1 percent phenothiazine produced some weight loss inhibition in asphalts *D*, *E*, and *F*, but no significant effect in asphalt *C*.

In table 5 the synergistic action of a combination of peroxide decomposer and an inhibitor of chain reactions is shown. The combination of phenothiazine and *N*-phenyl-2-naphthylamine produces a greater increase in durability than would be obtained if the effects of each inhibitor in combination were merely additive. The combination also reduces weight loss to a greater extent than the individual inhibitors during later hours of exposure (fig. 8).

Small percentages of asphaltic fractions from a good weathering asphalt, *C*, were added to a less durable asphalt, *B*, to determine whether good weathering characteristics might be imparted to the latter. The fractions used were the asphaltenes and maltenes which are the pentane-insoluble and pentane-soluble fractions of asphalt, respectively. No significant improvements were observed in weight loss inhibition or durability.

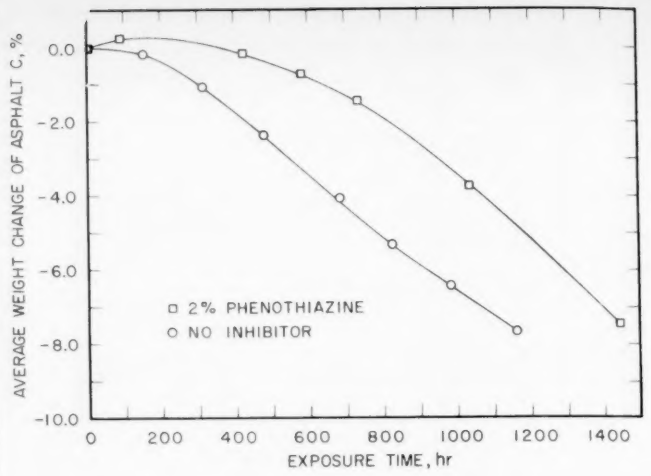

FIGURE 6. *The effect of phenothiazine (2 percent by weight) on weight loss of asphalt C.*

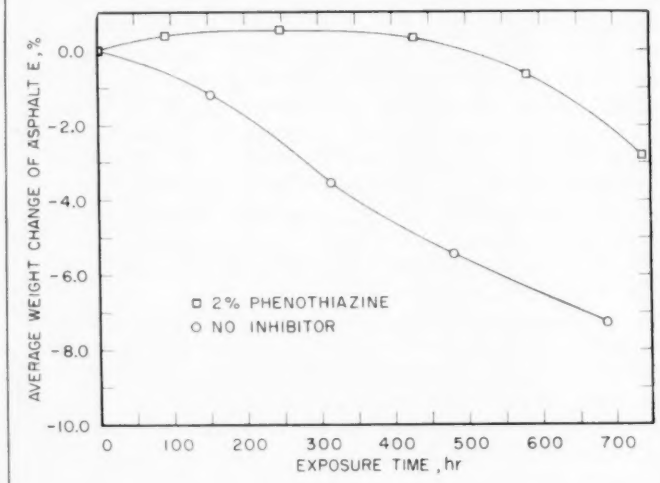

FIGURE 7. *The effect of phenothiazine (2 percent by weight) on weight loss of asphalt E.*

TABLE 5. *Additional antioxidant studies*

Asphalt	Inhibitor	Softening point	Durability (avg hr to failure)	Avg wt change at 594 hr
		° F		%
B	None	221	638	−8.45
B	1% phenothiazine	218	880	−2.23
B	1% *N*-phenyl-2-naphthylamine	216	748	−6.13
B	1% phenothiazine plus 1% *N*-phenyl-2-naphthylamine	212	1,300	−1.89
B	1.34% *C* maltenes	225	705	−7.59
B	3.00% *C* maltenes	221	660	−7.40
B	1.34% *C* asphaltenes	229	638	−7.86
B	3.00% *C* asphaltenes	222	550	−7.80

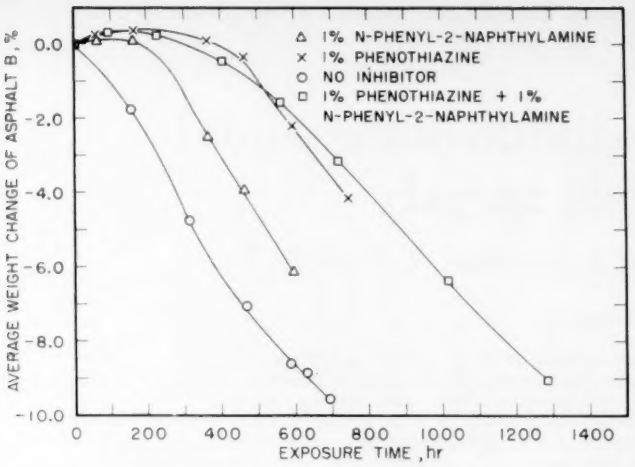

FIGURE 8. *The effect of a combination of an inhibitor of chain reactions and a peroxide decomposer on weight loss of asphalt B.*

4. Discussion of Results and Conclusions

The results of this study strongly support the hypothesis that asphaltic degradation during accelerated weathering involves a free radical oxidation. The similarity in effects produced by natural and accelerated weathering suggests that this process also occurs in natural weathering. Antioxidants which function by peroxide decomposition have been shown capable of extending the durability of asphalts and inhibiting weight loss to varying extents. The antioxidant properties of peroxide decomposers show a marked concentration dependence in mineral oils [1]. This dependence was established in asphalt also in a study made of the dependence of phenothiazine activity on concentration. Phenothiazine, a peroxide decomposer, in concentrations of 2 percent by weight, produced excellent inhibition of weight loss in the several asphalts tested.

Phenothiazine, in concentrations of 2 percent, also extended the durability of one asphalt more than fivefold, but had no great effect on the durabilities of two other asphalts. Inhibitors of chain reactions were shown to be capable of retarding weight loss to varying extents but did not produce significant increases in durability in the asphalts tested. The individual characteristics of the asphalts determine the effectiveness of a particular inhibitor. A similar dependence of additive effectiveness was also observed by Greenfeld [9] in studies of the effects of mineral additives on the durability of coating-grade roofing asphalts.

The reactions producing weight losses in asphalts involve formation of gaseous decomposition products [10] and water-soluble products [11]. If the uninhibited asphalts are examined for weight loss in the early stages of exposure, a slight gain in weight during an induction period may be observed rather than a loss in weight (asphalt *C* in fig. 6). This induction period which is commonly observed in free radical processes can be extended by the use of phenothiazine, considered to be a peroxide decomposer (figs. 6, 7, and 8) and also by the use of 1 percent *N*-phenyl-2-naphthylamine, an inhibitor of chain reactions.

A synergistic effect has been observed when a combination of a peroxide decomposer and an inhibitor of chain reactions was used. This produced a greater increase in durability than would result if the effects of each inhibitor were merely additive. Synergistic effects have also been observed when inhibitors of chain reactions and peroxide decomposers are used in combination for protection of mineral oil [3].

Addition of small percentages of asphaltenes and maltenes of a more durable asphalt to a less durable asphalt produced no increase in durability or inhibition of weight loss. These tests were conducted to determine whether natural antioxidants exist in more durable asphalts. On the basis of these tests alone, one cannot conclude that natural antioxidants are either present or absent since such inhibitors may be present in low concentrations in the original asphalt.

5. References

[1] R. Criegee, H. Pilz, and H. Flygare, Ber. **72,** 1799 (1939).
[2] J. L. Bolland and P. Ten Have, Trans. Faraday Soc. **43,** 201 (1947).
[3] G. W. Kennerly and W. L. Patterson, Jr., Ind. Eng. Chem. **48,** 1917 (1956).
[4] C. J. Pedersen, Ind. Eng. Chem. **48,** 1881 (1956).
[5] G. S. Hammond, C. E. Boozer, C. E. Hamilton, and J. N. Sen, J. Am. Chem. Soc. **77,** 3238 (1955).
[6] S. H. Greenfeld, ASTM Bull. **193,** 50 (1953).
[7] G. S. Hammond, C. E. Boozer, C. E. Hamilton, and J. N. Sen, J. Am. Chem. Soc. **77,** 3240 (1955).
[8] E. W. Mertens (to California Research Corp.), U.S. Pat. 2,797,169 (June 25, 1957).
[9] S. H. Greenfeld, NBS Building Materials and Structures Report 147 (1956).
[10] R. R. Thurston and E. C. Knowles, Ind. Eng. Chem. **33,** 320 (1941).
[11] O. G. Strieter and H. R. Snoke, A modified accelerated weathering test for asphalts and other materials, J. Research NBS **16,** 481 (1936) RP886.

WASHINGTON, D.C. (Paper 64C1–19)

JOURNAL OF RESEARCH of the National Bureau of Standards—C. Engineering and Instrumentation
Vol. 64C, No. 1, January–March 1960

Temperature Stratification in a Nonventing Liquid Helium Dewar[1]

L. E. Scott, R. F. Robbins, D. B. Mann, and B. W. Birmingham

(August 25, 1959)

The presence of a large temperature gradient in Dewars used for transporting helium is undesirable because it may be accompanied by unnecessarily high internal pressures when the contents are sealed. In a study of the problems, such gradients were observed in experiments conducted with a 39.7-liter stainless steel Dewar. A method is shown for calculating the pressure rise in the absence of temperature gradients and the results are compared with the observed pressure rise. In some cases curves representing calculated and observed pressure rise intersect. A possible explanation of this situation is given. The destratifying effect of a concentrated heat input and of copper rods is shown.

1. Introduction

For many applications, a greater economy of transportation can be achieved by shipping helium at moderate pressures at or near the liquid density rather than as a warm compressed gas [1].[2] Savings can be realized even though the end use of the product is in gaseous form. The transportation and storage, however, should be accomplished with no loss of helium to keep total costs minimal. An ideal method is one in which the heat input to the Dewar increases the pressure and temperature of the contents rather than causing loss of helium by evaporation.

Temperature gradients may exist in containers of very small heat flux as a consequence of the low thermal conductivity of helium near its normal boiling point, approximately 6.3×10^{-5} cal/cm ° K sec for the liquid [2] and 5.3×10^{-5} cal/cm ° K sec for the vapor [3]. A layer of warm fluid at the top of the container has no tendency to mix. In addition, warm helium anywhere in the container will tend to rise to the top of the container and increase the temperature gradient. For example, at 3 atm, 5.5° K fluid is over twice as dense as fluid at 6.5° K [4]. The practical significance of a temperature gradient in a self-pressurizing system is the difference in the rate of pressure rise as compared to a system in thermal equilibrium.

The object of the experiment to be described was to verify the existence of temperature gradients in a nonventing Dewar and to determine the approximate magnitude of these gradients by experimental measurements.

2. Theoretical Pressure Rise at Thermal Equilibrium

From the first law of thermodynamics, eq (1), and the definition of enthalpy, eq (2), we have:

$$\Delta U=Q-W \tag{1}$$

$$H=U+pv \tag{2}$$

where

Q=heat added to the system,
U=internal energy function,
H=enthalpy function,
W=work done by the system,
p=pressure,
v=specific volume=$\dfrac{\text{container volume}}{\text{total mass of liquid and vapor.}}$

Since the process is one of constant volume and the external work between the system and its surroundings is zero we have:

$$\Delta U=Q$$

$$\Delta H=Q+v\Delta p$$

or

$$Q=\Delta U=\Delta H-v\Delta p \tag{3}$$

A convenient method of expressing eq (3) is a plot of pressure versus internal energy for various specific volumes [4] as shown in figure 1. This process can be illustrated by following an isochor (line of constant volume) for the horizontal distance corresponding to ΔU or Q.

3. Previous Experiments

Previous experiments conducted by Wilson and Robbins of this laboratory with a 2.3-liter capacity Dewar constructed of high thermal conductivity copper, have given pressure rise results which agree with predicted values obtained from figure 1. The copper construction assured that the contents were in thermal equilibrium. The range of specific volumes covered in the experiments were 7.8 to 13.0 liter/kg. The pressure was allowed to rise to 5 atm.

[1] This work was supported by the Bureau of Aeronautics, Department of the Navy.
[2] Figures in brackets indicate the literature references at the end of this paper.

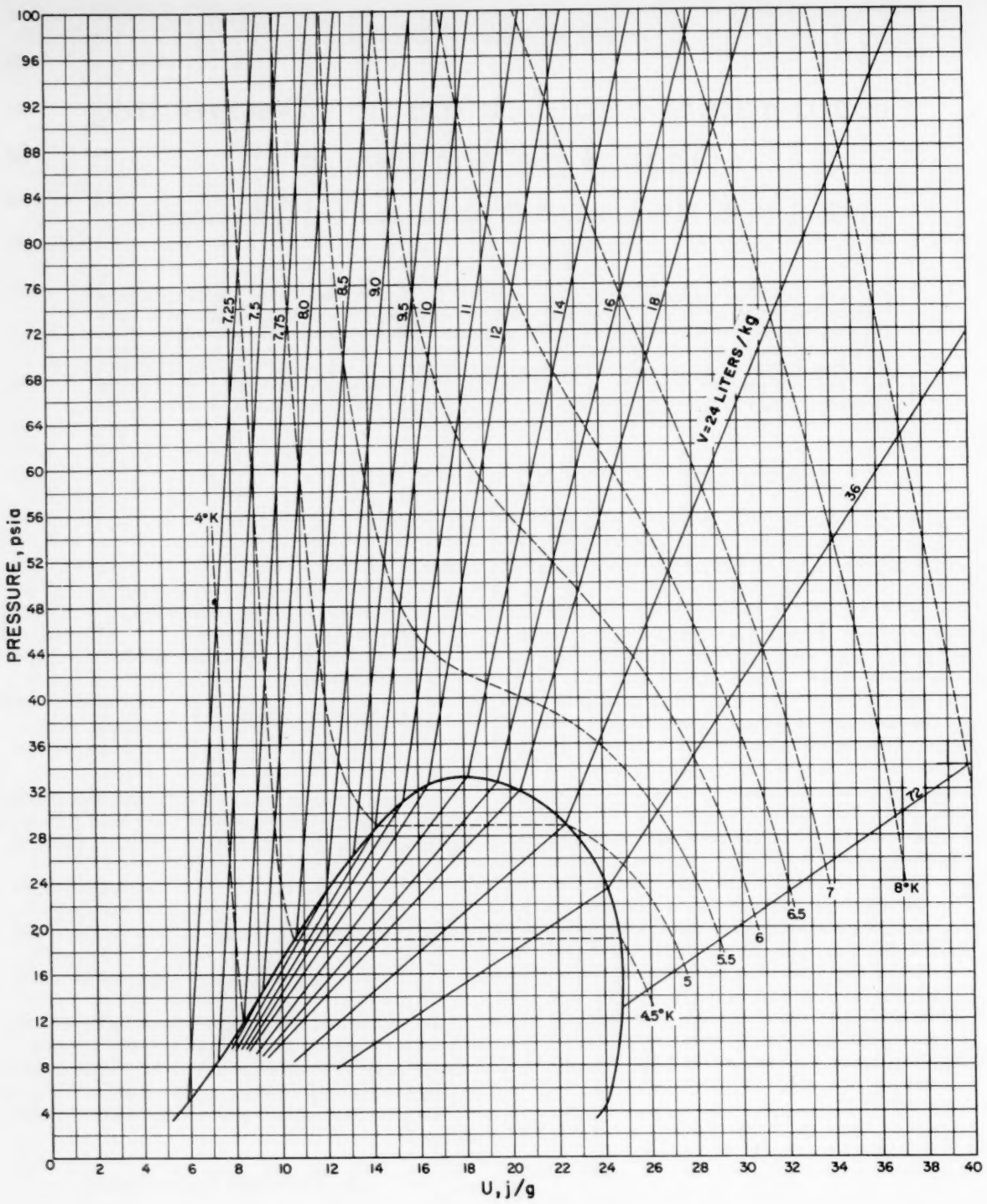

FIGURE 1. *Pressure-internal energy diagram for helium, 0 to 100 psia.*

The Dewar used in these experiments had a fill tube with a temperature gradient from 4° to 76° K. One might erroneously speculate that if a container is filled with liquid helium to a greater level than that corresponding to the critical density, the liquid meniscus might expand into the fill tube. This phenomenon did not occur, undoubtedly as a result of the high compressibility of liquid helium (0.0025g/cm^3/atm at 2.5 atm and 4° K [5]).

It was concluded from the experimental results that the heat input was not affected by a rising liquid meniscus in the Dewar, and that pressure rise as a function of total heat input may be accurately predicted *if the contents are in thermal equilibrium.*

4. Experimental Details

4.1. Description of Apparatus

For the present experiments a Dewar of 39.7-liter capacity (excluding volume in the supporting neck) was constructed from type 304 stainless steel as shown in figure 2. Stainless steel was selected, because of its low thermal conductivity, to reduce vessel wall conduction and thereby minimize effects of the wall on the temperature gradient in the contents. The entire assembly with the exception of the upper 12 in. of supporting tubes was submerged in liquid nitrogen during the measurements. Twelve difference thermocouples (gold plus 2.1 at. percent cobalt versus copper) were installed on the outside of a micarta tube at the vertical centerline and spaced as shown in figure 2. Thermocouple 12 was placed on the sensing bulb of a helium vapor pressure thermometer and was used as the reference for the 11 remaining thermocouples. The thermoelectric emf was measured with a precision Wenner potentiometer. The thermocouples and temperature measuring equipment were capable of an accuracy of better than $\pm 0.1°$ K in the range of absolute temperatures measured. A resistance wire heater was spiraled around the top and bottom hemispheres to allow a known and concentrated heat flux to be applied.

In experiments 4, 5, and 6, four rods of electrolytic-tough-pitch copper 25-in. long having a combined cross-sectional area of 0.258 sq in. were placed vertically in the Dewar to reduce the temperature gradient.

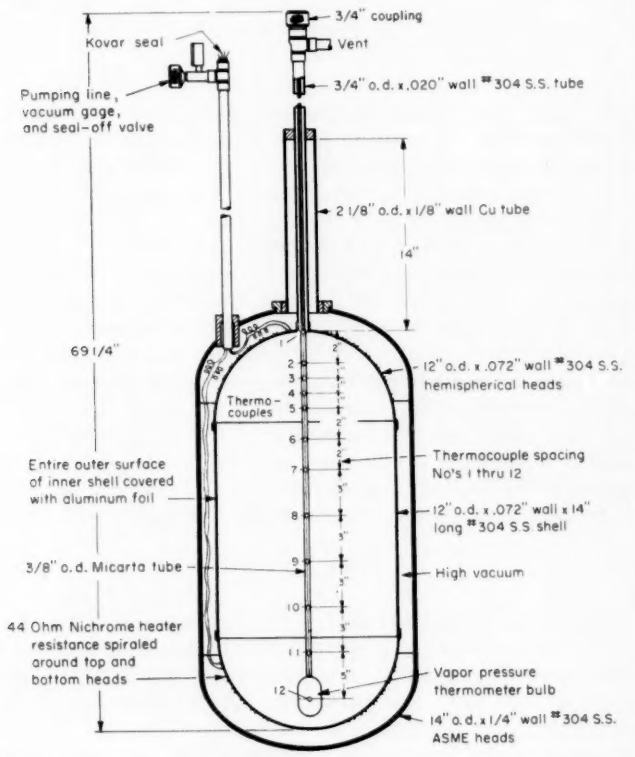
3/4" coupling
Kovar seal
Vent
3/4" o.d. x .020" wall ≋304 S.S. tube
Pumping line, vacuum gage, and seal-off valve
2 1/8" o.d. x 1/8" wall Cu tube
14"
69 1/4"
12" o.d. x .072" wall ≋304 S.S. hemispherical heads
Thermo-couples
Thermocouple spacing No's 1 thru 12
Entire outer surface of inner shell covered with aluminum foil
12" o.d. x .072" wall x 14" long ≋304 S.S. shell
3/8" o.d. Micarta tube
High vacuum
44 Ohm Nichrome heater resistance spiraled around top and bottom heads
Vapor pressure thermometer bulb
14" o.d. x 1/4" wall ≋304 S.S. ASME heads

FIGURE 2. *Dewar schematic showing thermocouple positions.*

4.2. Experimental Procedure

The Dewar was filled to various levels with liquid helium. The liquid level was then measured by means of an electrical resistance probe [6] inserted through the neck. The liquid evaporation rate was measured prior to closing the vent to determine the heat input. A correction was calculated for the increased heat input down the neck in the nonventing condition. The system was then sealed and periodic pressure and temperature readings were obtained.

5. Data and Discussion

Six experiments were performed as shown in table 1. In each experiment, the starting conditions were saturated liquid and vapor at 12.2 psia.

TABLE 1

Experiment No.	Liquid volume	Specific volume	Total heat input	Measured time to 50 psia	Theoretical time to 50 psia	Notes
	% full	*l/kg*	*w*	*hr*	*hr*	
1	99	7.8	0.10	15.4	23.2	
2	82	9.23	.10	27.5	60.8	
3	71	10.5	.54	12.5	13.2	Concentrated heat input at bottom.
4	97.5	7.93	.10	24.6	29.4	Copper rods installed.
5	78	9.65	.10	63.4	65.7	Do.
6	81	9.32	.10	55.6	54.8	Do.

Experiments 1 through 5 were terminated after a pressure buildup to approximately 70 psia. Experiment 6 was continued until the pressure reached 160 psia.

Figure 3 shows absolute temperature as a function of vertical position in the Dewar and Dewar pressure for experiments 1 through 5. Temperature readings, taken after the vapor pressure thermometer reference reached the critical temperature (approx 5.2° K) such as shown for experiments 3 and 5, are less accurate because the absolute value of the reference has been extrapolated for values above 5.2° K. Since the majority of data in experiment 6 is above the critical point, temperature readings are not shown.

In each case, essentially all of the temperature gradient existed in the upper one third of the test Dewar. Those thermocouples not plotted were essentially at the reference temperature throughout the test. Thermocouple No. 1 is probably greatly influenced by the heat transferred down the fill tube and is therefore of questionable value.

Dewar pressure as a function of change in internal energy (ΔU) is shown in figure 4 for all six experiments. The calculated thermal equilibrium pressure versus ΔU is also shown for comparison.

Temperature stratification was quite pronounced in all of the experiments performed without the copper rods (see figs. 3 and 4). Comparison of experiments 1 and 2 indicate an increasing temperature gradient and pressure rise deviation from the calculated thermal equilibrium pressure with in-

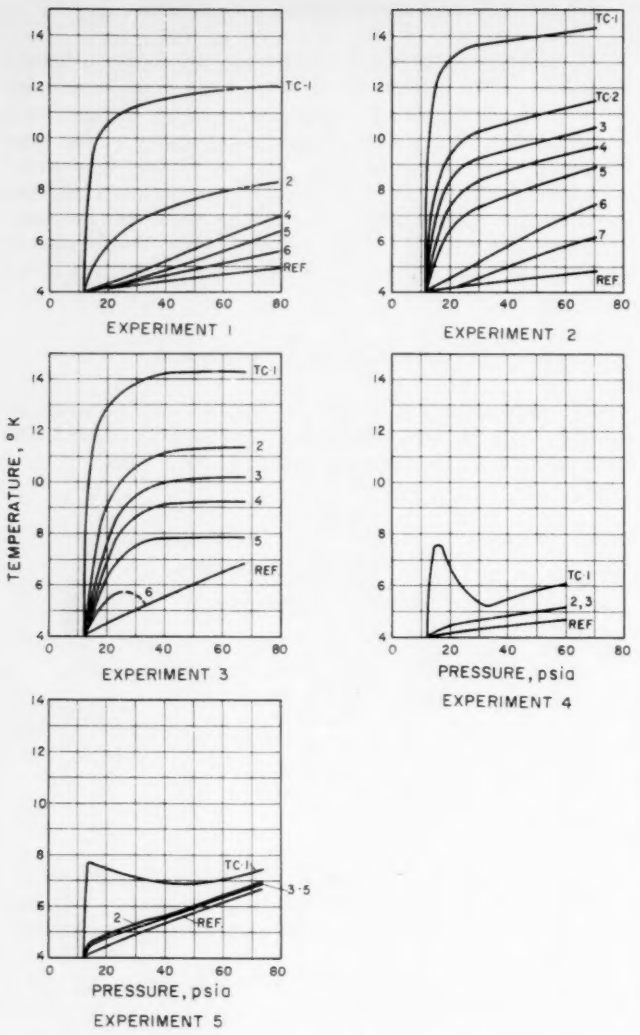

FIGURE 3

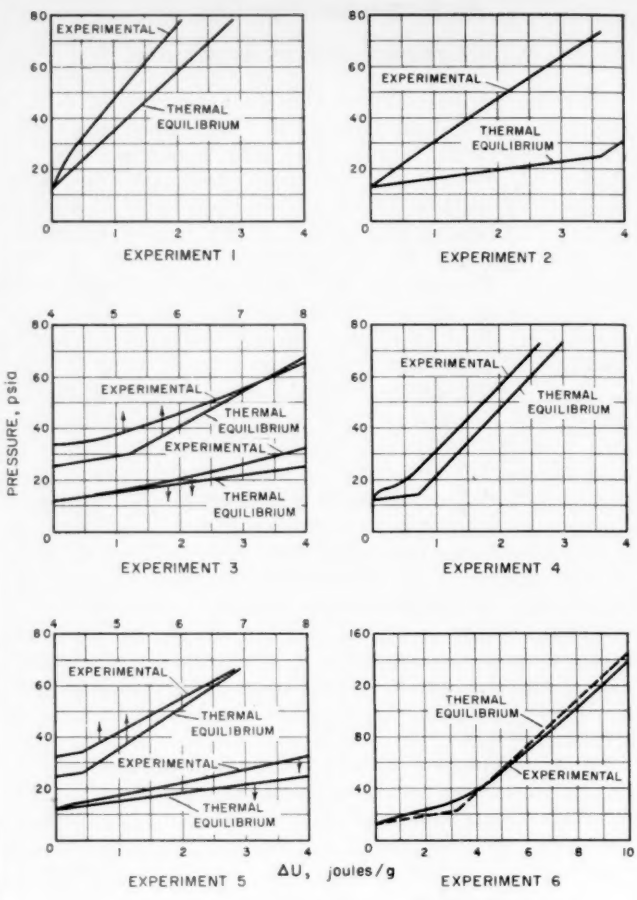

FIGURE 4

creasing specific volumes. Experiment 3 when compared with the trend of experiments 1 and 2 shows that, as would be expected, a concentrated heat input to the bottom of the dewar results in increased convection and therefore reduces the temperature gradient.

The excellent heat conducting characteristic of the copper rods is evidenced by the virtual elimination of temperature gradients in experiments 4 and 5. The experimental pressure rise in experiments 4, 5, and 6 is shown to be in close agreement with the calculated thermal equilibrium curve.

Some of the nonequilibrium pressure rise curves in figure 4 appear to intersect the thermal equilibrium curves. This phenomenon may not be entirely unexpected. As the helium increases in temperature and pressure, the system changes from a two phase gas and liquid system to a single phase fluid. If the single phase fluid was an ideal gas, obeying the ideal gas law, and therefore having a constant specific heat (C_v), it can be shown mathematically that a temperature gradient would not affect the rate of pressure rise in the single phase regime. Thus, it appears that the pressure rise deviation resulting from temperature stratification is possibly a result of the nonideality of the fluid. Consequently, one might speculate that a nonequilibrium pressure rise curve may intersect or become asymptotic to the equilibrium pressure rise curve at some pressure or pressures which would depend upon the magnitude and distribution of the temperature gradient. This speculation is supported by (a) the knowledge that at pressures and temperatures somewhat higher than those investigated, helium tends to obey the ideal gas law, and (b) the behavior of the compressibility factor of helium [4] as shown in figure 5. The compressibility factor Z is defined as PV/nRT. In the constant volume processes under consideration here

$$P=CZT \tag{4}$$

where C is a constant and Z is a function of temperature and pressure. Figure 5 illustrates that at lower pressures Z generally increases with increasing temperature at any one pressure. At higher values of pressure, the situation is reversed; that is, Z decreases with increasing temperature at any one pressure.

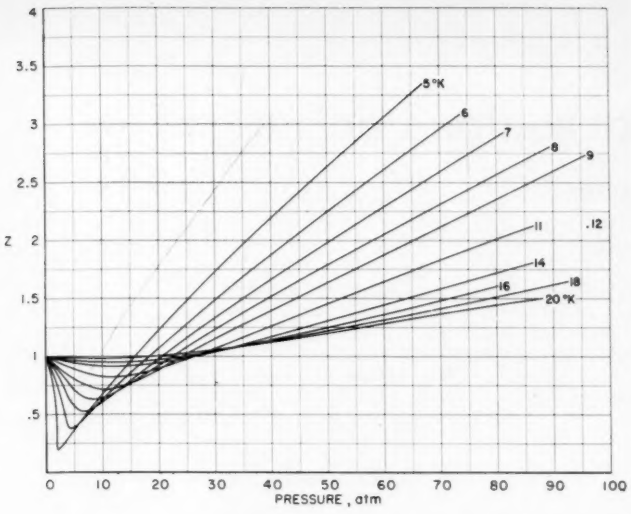

FIGURE 5. *Compressibility factor* **Z** *for helium gas.*

The point of intersection may also depend to a lesser extent upon the variation of (C_v) with temperature and pressure. Even though the necessary thermodynamic data are now available, a suitable method of computation of the nonequilibrium pressure rise that would be expected in a container which will support temperature gradients has not yet been attempted.

6. Conclusion

The presence of a good heat conducting material appears to be the most satisfactory method of eliminating temperature gradients and unnecessarily high pressures as well as allowing a pressure rise prediction to be made with the aid of figure 1. It is to be expected that both geometry and the distribution of heat input will influence the stratification tendencies of a Dewar. The use of high conductivity construction materials such as aluminum and copper will greatly reduce this tendency. Very large Dewars may require additional material to conduct heat into the center of the helium mass.

7. References

[1] R. E. Brown, Economic and other aspects of the distribution of Navy helium in liquid form, Proc. of Cryogenic Eng. Conf., Boulder, Colo. (Aug. 1957).
[2] Grenier, Phys. Rev. **83,** 598 (1951).
[3] Ubbihm, Physica **13,** 629 (1947).
[4] D. B. Mann and R. B. Stewart, Thermodynamic properties of helium at low temperatures and high pressures, NBS Tech. Note 8 (PB151367) (1959).
[5] W. H. Keesom, Helium, p. 236 (Elsevier, New York, N.Y., 1942).
[6] R. B. Scott, Cryogenic engineering, p. 246 (D. Van Nostrand Co., Inc., New York, N.Y., 1959).

BOULDER, COLO. (Paper 64C1–20)

JOURNAL OF RESEARCH of the National Bureau of Standards—C. Engineering and Instrumentation
Vol. 64C, No. 1, January–March 1960

Expansion Engines for Hydrogen Liquefiers[1]

Edmund H. Brown

(October 10, 1959)

Criteria are developed for the practicability of expansion engines and expansion turbines in large hydrogen liquefiers. Some additional data on pertinent properties such as the sonic velocity of normal hydrogen are included. The analysis suggests that use of expansion turbines in hydrogen liquefiers having a production capacity of less than 5,000 liters per hour ordinarily would not be justified. For greater capacities, however, use of modern materials and design should make expansion turbine performance even more favorable than in liquefiers for denser fluids.

1. Introduction

New processes using large quantities of liquid hydrogen require the development of liquefiers of much greater productive capacity than any existing plants. The magnitude of this increase introduces many engineering design problems and shifts emphasis to parameters of lesser importance in laboratory production units.

In particular, only thermodynamic cycles which result in a high overall plant efficiency can be considered. Using the general properties of fluids and the history of the air liquefaction industry as guides, the course of efficient design can be charted with confidence; larger liquefier capacity will require increased use of expansion engines at certain stages of the cycle.

The increasing interest in the use of such expansion devices suggests that the following analysis, originally issued as an informal communication in late 1957, might be of value to a larger audience. A few changes and additions have been introduced to make the ideas current. An excellent introduction to the use of expansion engines and turbines, including both historical commentary and descriptions of machines, has recently been published by Collins and Cannaday [1][2] which also includes analyses of Land [2] and Jekat [3].

The *type* of expansion engine that should be used in a particular liquefaction plant depends, again, on the production capacity. Engines which have been developed sufficiently in other applications to be considered in hydrogen liquefier design include (listed roughly in order of increasing flow capacity): reciprocating expanders; "positive displacement" rotary expanders, especially the Lysholm design; radial flow turbines; and axial flow turbines.

Since liquefaction of hydrogen requires refrigeration over a wide temperature range (20° to 300° K), expansion engines may not be the most desirable means of supplying such refrigeration at all stages of the process. At higher temperatures (200° to 300° K), vapor-cycle units or vapor-cycle cascades using readily available refrigerants would be inexpensive to procure and operate. Precooling to the temperature of liquid nitrogen (65° to 80° K, depending on the vapor pressure maintained) would be advantageous, since liquid nitrogen plants have been extensively developed, can readily be procured, and will operate at relatively low cost.

At the lower end of the liquefier (due to the cooling of the gas to the temperature range 20° to 35° K) the yield of a simple Joule-Thomson expansion process is high. The overall plant yield α^* (=mass rate liquefied/mass rate through the compressor) can be only slightly increased by substituting an expansion engine. At this time, problems in the development of an expander, operating in a range where the fluid condenses, more than offset such possible small gains in production. Thus, the expected operating range of expansion engines for hydrogen liquefaction lies within the region 30° to 80° K. Figure 1 shows the lower stages of a typical one-expander cycle.

The low temperatures at which hydrogen expanders will operate may introduce new problems in the design of power-output devices. Clearly, the adiabatic extraction of power from a gas at some desired refrigeration temperature will be advantageous only if this power is transferred to some

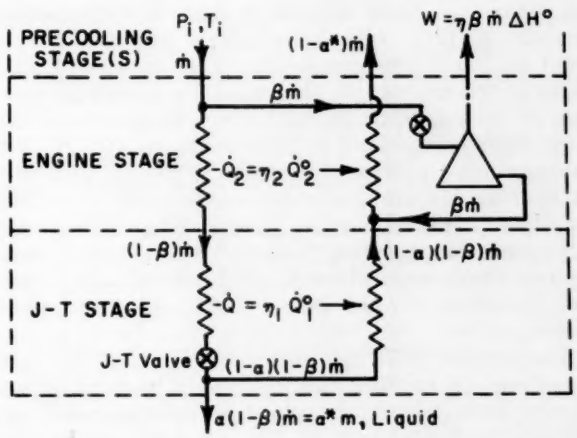

FIGURE 1. *Flow diagram of simple expansion engine and J–T stages.*

[1] This work was supported by the U.S. Atomic Energy Commission.
[2] Figures in brackets indicate the literature references at the end of this paper.

higher—preferably ambient—temperature where it can be used (or dissipated, if it is not large) without being reintroduced to the gas as heat.

Power-output problems are less important for low-speed engines since shafts or connecting rods can be long enough to make heat conduction negligible. Thus, such engines can be directly coupled with a variety of ambient temperature devices, including water-cooled brakes, oil pumps, fans, and motors. High-speed turbines, however, require short, thick shafts to maintain high critical speeds and thus would have higher heat flows if directly connected to ambient temperature output devices. More important, high temperature-gradients would increase the danger of shaft warpage during operation.

Since high-speed (75,000 to 250,000 rpm) turbines appear to be particularly applicable to hydrogen liquefiers in the 5,000 to 50,000 liter/hr range, practical solutions are desirable. Two immediate alternatives may be considered. The first, a direct-coupled high-speed hydrogen compressor operating in a liquid nitrogen bath, might be feasible if a high compressor efficiency could be achieved. The second, and thermodynamically more satisfactory method, a direct-coupled, two-pole, high-speed alternator driving a multipole, low-speed motor at ambient temperature, is especially appealing, since electrical energy is "unaware" of temperature level, and since a simpler arrangement of liquefier components could be made. For such an alternator, the large decrease in conductor resistivity would result in much lower I^2R losses than at ambient temperature; the increased core permeability would permit higher flux densities and, thus, higher voltages; operation of the rotor in a low temperature hydrogen atmosphere (with low viscosity) would make rotor windage losses negligible. High efficiency would be important (since losses would be immediately returned to the hydrogen stream as heat), but the above temperature effects should allow exceptionally high performance.

2. Types of Expansion Engines

Reciprocating expansion engines have been used for years in both liquefiers and low-temperature process plants. Crankshaft-type engines (in contrast to walking-beam) are used in the Amarillo plant of the Bureau of Mines for the quantity separation of helium from natural gas. Engines with very long, thin connecting rods operate to 10° K in the commercially produced Collins' cryostat, and in the 45 liter/hr helium liquefier constructed by Collins for the Massachusetts Institute of Technology Cryogenic Engineering Laboratory. Application of reciprocating expanders in medium capacity hydrogen liquefiers should involve only size and details of design.

The upper limiting liquefier capacity for which reciprocating engines can profitably be used depends on the bulk which the plant designer is willing to insulate and maintain at the required temperature level. Therefore, this limit must depend to some extent on good engineering judgement. For the above reasons, this study was restricted to problems in the application of rotary expanders. However, a brief consideration of such possible upper limits for reciprocating expanders indicated that their use remains practical in liquefiers up to a capacity of at least 10,000 liters/hr.

For other reasons—lack of data—the possible application of the Lysholm "positive-displacement" machine has only been noted. A compressor built by the Svenska Rotor Maskiner AB has been tested as an expander for air at pressure ratios from 3 to 9 and flows from 8 to 28 lb/min. A graph showing resultant test efficiencies (on a temperature, rather than enthalpy basis), furnished by the Stratos Division, Fairchild Engine & Airplane Corp., is included in figure 2 of this report. Maximum efficiency does not appear to be exceptionally high—approximately 73 percent for pressure ratios 6 to 9 and flows from 20 to 28 lb/min at a speed of 40,000 rpm. Since a large part of the losses in such machines can be ascribed to leakage, their application to hydrogen liquefiers is uncertain.

Turbine expanders may be classified by flow direction and type of blading. Three main flow types are: axial flow, radial inward flow (centripetal turbine), and radial outward flow (centrifugal turbine). Radial outward flow turbines have smaller pressure and enthalpy drops and somewhat poorer efficiencies than radial-inflow turbines. Probably, an outward flow turbine would only be advantageous in a plant without a final J–T stage, since cycling of fluid that might condense within a stage would be prevented.

The choice between axial-flow and radial-inflow turbines depends on a number of complicated factors, including required volume flow and pressure ratio and allowable efficiency. Because of the centrifugal field, a radial stage will permit higher pressure and enthalpy drops, and may be as much as 10 percent higher in stage efficiency (78 percent is usually considered a maximum for axial stages: efficiencies of 90 percent are not uncommon for well-designed radial stages). Pressure ratios as high as 17 have recently been obtained in a commercially produced supersonic radial inflow turbine with total peak test efficiency remaining over 72 percent (supersonic flow will ordinarily result in lower efficiency).

Four major losses exist in a turbine stage: nozzle flow loss, rotor flow loss, leakage, and disk friction. In small mass-flow machines operating on large heads, leakage may be a decisive factor in determining the efficiency, especially with hydrogen. The leakage loss in an axial-flow stage may be as high as nine times the leakage loss of a radial stage.

If the required pressure ratio is such that a few radial stages can be used, better performance can be expected. For very high pressure ratios, however, despite the smaller stage drop, an axial-flow turbine would be preferable since there would be no turning losses such as are associated with the repeated change from axial to radial flow in multi-stage radial turbines. Configurations of typical axial-flow and radial-inflow stages are shown in figure 3.

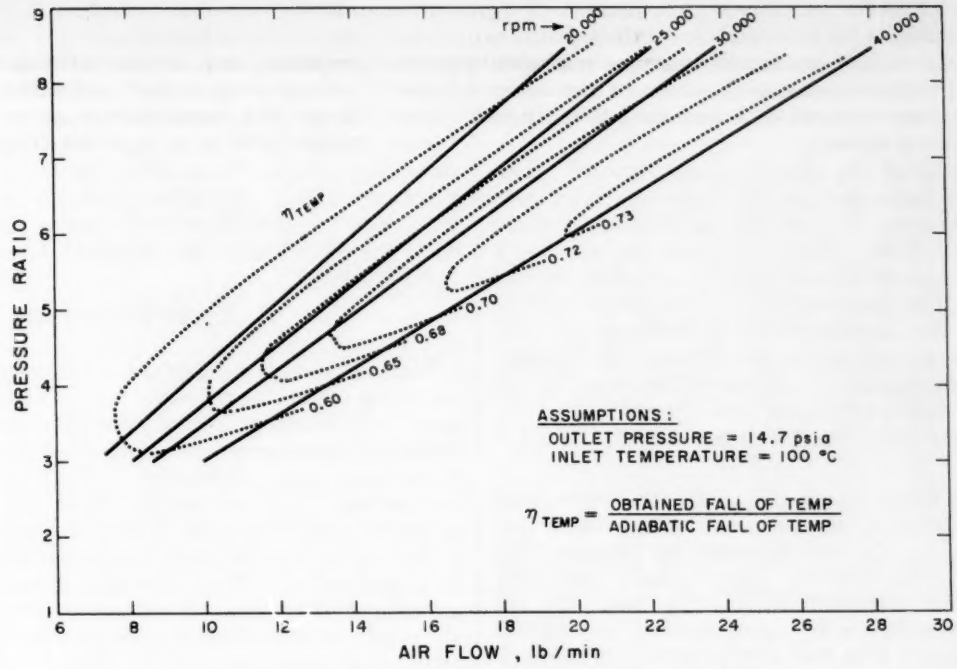

FIGURE 2. *Performance chart for Lysholm expander.*

FIGURE 3. *Typical radial and axial flow stages.*

Dimensional analysis can be used to give some indication of the proper choice of flow-type for a particular application. Such an analysis shows that an important dimensionless parameter in turbine design is the specific speed $n_s = n\sqrt{W/\rho(\Delta H°)^{5/2}}$, where n is the actual speed in rps, W the power output in watts, ρ the gas density in kilograms per cubic meter, and $\Delta H°$ the isentropic enthalpy change in joules per kilogram. Using the relation $W = \eta\beta\dot{m}\Delta H°$, the expression can be transformed to $n_s = n\sqrt{\eta\beta\dot{V}/(\Delta H°)^{3/2}}$, where the actual volume flow $\beta\dot{V}$ through the turbine is usually specified at outlet conditions. Thus, with equal speed and head, larger volume flows imply greater specific speeds.

The above equation for specific speed can be expressed in terms of a number of velocity and diameter ratios. By varying these ratios in a range about their optimum values, the performance of any type of turbine can be determined graphically as a function of specific speed if reasonable values of certain loss factors are assumed. Such a calculation has been made by von der Nuell [4] and leads to the conclusion that, up to a specific speed of about 0.1, the radial-inflow turbine is preferable to the axial-flow turbine. One of his graphs, showing ranges for n_s as a function of the velocity ratio r_v (the ratio of the tip speed u and the isentropic head velocity $c_0 = \sqrt{2\Delta H°}$) is given here in adapted form as figure 4. (Note that in *consistent* units, n_s should be dimensionless; however, von der Nuell's equations are in the English gravitational system using hp, rpm, and head in feet, while his graphs are in a metric gravitational system using metric hp, rpm, and head in kilogram-meters

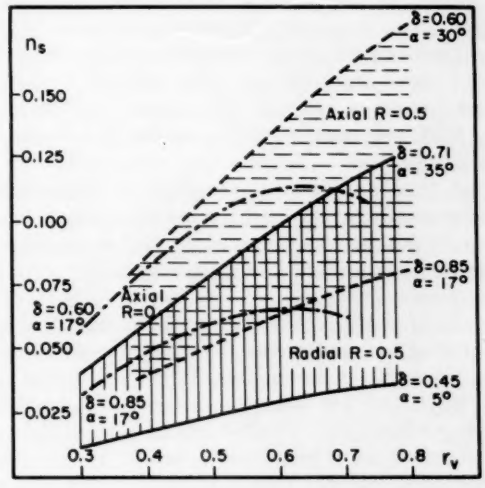

FIGURE 4. *Ranges of application for 50 percent reaction axial-flow turbines – – – –, impulse* (R=0%) *turbines — · — · — · —, and 50 percent reaction radial-inflow turbines ———, in terms of specific speed* n_s *and velocity ratio* $r_v = u/c_o$ *for practical diameter ratios* $\delta = d/D$ *and nozzle angles* α. *(From von der Nuell.)*

per kilogram; thus his equations give values of n_s which are 0.9 times the values shown in his graphs; in this paper, all values are in the absolute mks system and, thus, will be the same as values in any other consistent absolute system, but will be 0.026 times the values in his graphs.)

As an example of the specific speed concept, cycle calculations [5] indicate that, for expander inlet conditions $P_i=30$ atm, $T_i=65°$ K, an optimum mass flow ratio is $\beta=0.46$. With an expander efficiency of only 80 percent an overall yield of $\alpha^*=0.35$ should be obtained. The theoretical head would be $\Delta H°=$ 429,000 j/kg, the isentropic head velocity $c_0=927$ m/sec, and, at actual outlet conditions, the density would be 13 Amagats. In terms of liquefaction capacity, C_L, in liters per hour, the specific speed for these conditions can then be expressed as $n_s=0.5\times 10^{-6}\, n\sqrt{C_L}$.

If $n_s=0.1$ is taken as an approximate upper limit for the practicable application of radial inflow expanders, then the limiting liquefaction capacity for this case is $C_L=4\times10^{10}/n^2$. The highest operating speed for which standard antifriction bearings are commercially available is approximately $n=2{,}000$ rps (120,000 rpm), which would permit a maximum liquefaction rate of 10,000 liters/hr. Similarly, for a more conservative speed of 60,000 rpm, the maximum rate would be 40,000 liters/hr.

A similar calculation can be made using the same conditions, but a minimum specific speed of approximately $n_s=0.025$. Here, it should be emphasized that many other factors must be considered in a detailed design, such as minimum practicable dimensions and the increasing percent tolerances that must be allowed with decreasing dimensions. However, using specific speed merely to obtain an approximate range of applicability, the lower limit for liquefaction capacity can be expressed as $C_{L(\min)}=25\times10^8/n^2$. For a 120,000 rpm turbine, this minimum capacity would be 600 liters/hr; and, for a 60,000 rpm turbine, 2,500 liters/hr. Minimum liquefaction rates are estimated more exactly in section 7, and in addition, the effect of the use of cold gas bearings (permitting speeds up to approximately 250,000 rpm) on the minimum liquefaction rate is evaluated.

In conclusion, the entire range of foreseeable required liquefaction capacity can evidently be covered by two types of expansion engines: reciprocating expanders for small to medium capacity, and radial-flow turbines for medium to large capacity. The radial inflow turbine will have the advantage of high stage enthalpy and pressure drops, and high efficiency. A further advantage is that a given turbine can be adjusted for a large range of flows, without sacrificing efficiency, by the use of adjustable nozzle blades—a frequent practice in small radial-flow aircraft turbine design. Such variable flow characteristics are desirable to cover uncertainties in the original cycle design and fluctuating conditions during operation.

The application of radial turbines requires solutions to several problems: (a) Proper design of the turbine, itself, for the conditions imposed by the cycle; (b) determination of the important fluid properties, and, for the particular case of hydrogen, their effect on output and performance; (c) proper design of a power-output device which, since the radial turbine is a characteristically high-speed machine, might take the form of a high-speed alternator; and (d) proper design of turbine (and generator) bearings which—again, because of the high speeds—might be required to operate at low temperature.

3. Fluid Properties

Values of the density and enthalpy of hydrogen required for turbine design can be obtained from the paper of Woolley, Scott, and Brickwedde [6]. In order to determine the compatibility of the turbine expansion stage with the J–T stage, curves were calculated (and extrapolated at the extremes of pressure) for the yield α as a function of pressure with the inlet temperature to the J–T heat exchanger as a parameter. These curves, determined for heat exchanger efficiencies of 100, 95, and 90 percent using the method described by Brown and Dean [7], are given in figures 5, 6, and 7. For an efficiency of 100 percent, the low temperature limiting curve was obtained by integrating the expression $(\partial h/\partial p)_T = V-T(\partial V/\partial T)_p$ using the liquid PVT data of Friedman [8]. Higher isotherms were obtained from the enthalpy data of [6] up to about 120 atm. The remainder is based on extrapolation and general

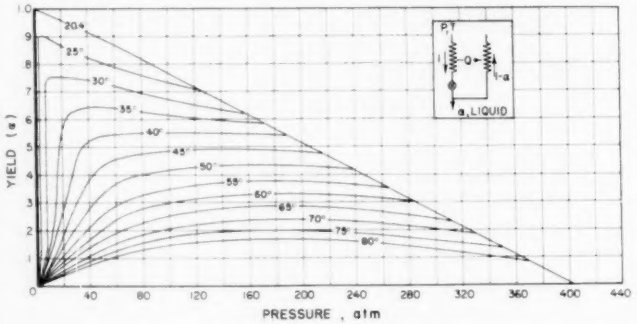

FIGURE 5. *Yield α of the* J–T *stage for a heat exchanger efficiency, $\eta=100$ percent for normal hydrogen.*

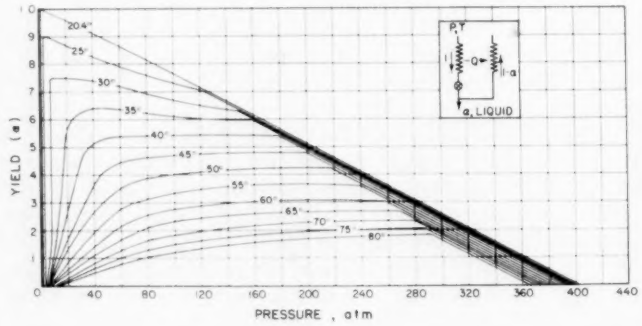

FIGURE 6. *Yield α of the* J–T *stage for a heat exchanger efficiency, $\eta=95$ percent for normal hydrogen.*

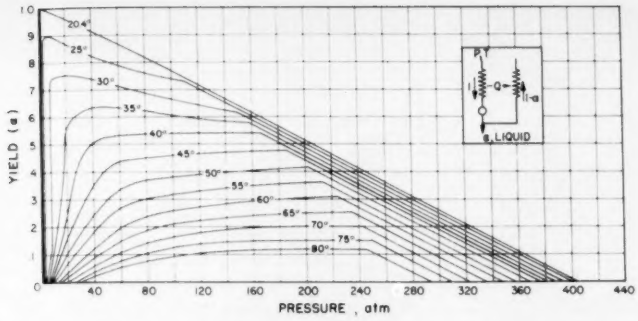

FIGURE 7. *Yield α of the* J–T *stage for a heat exchanger efficiency, $\eta=90$ percent for normal hydrogen.*

thermodynamic tendencies and, thus, should only be considered to show the general behavior of the yield curves. These curves emphasize an important design factor: for small liquefiers using turbine expanders it is desirable to keep the expander inlet pressure low enough that reasonable flow areas can be maintained; the optimum pressure for the J–T stage alone will ordinarily be much higher; thus, some compromise is required, preferably a pressure on, or just above the "knee" of the yield curve. If the temperature is low enough, however, such pressures should require only two, or, at the most three, radial stages in a subsonic turbine, and one or two stages in a supersonic turbine.

In addition to density and enthalpy, the sonic velocity c and kinematic viscosity ν are properties of primary importance in turbine design. The stage work that can be produced under comparable conditions is directly dependent on the sonic velocity. Similarly, the major part of the stage losses—and, thus, the efficiency—is a function of the kinematic viscosity.

Only a small amount of data is available on the sonic velocity of hydrogen. NBS Circular 564 [9] gives values at 0, 1, 10, and 100 atm, but includes only a few points below 80° K. For this reason, a detailed calculation of the thermostatic sonic velocity $c=1/\sqrt{\rho k_s}$ was made from the identity

$$\frac{Mc^2}{RT}=\left(\frac{\partial \rho Z}{\partial \rho}\right)_T+\frac{R}{c_v}\left(\frac{\partial TZ}{\partial T}\right)_\rho^2$$

using the PVT and specific heat data of [6], where R is the gas constant, M the molecular weight, T the absolute temperature, ρ the density, c_v the specific heat at constant volume, and Z the compressibility factor. The results are given by the combination of the results in table 1 of the sonic velocity in the perfect gas state $c^\circ=\sqrt{RT\gamma^\circ(T)/M}$ and the ratio $c(\rho, T)/c^\circ(T)$ given in figure 8 as a function of temperature at densities from 0 to 500 Amagats (units of density reduced by the density at standard conditions of 1 atm and 0° C).

The isentropic critical velocity and critical pressure ratio of a nozzle can be obtained from the curves of figure 8 together with a T–S chart by an approximation process. Maintaining a constant entropy corresponding to the initial conditions P_i, T_i, the final value of the static enthalpy h_f can be estimated. This estimate would result in a final velocity $v_f=\sqrt{2(h_i-h_f)}$ which can be compared with the sonic velocity from figure 8 based on the same assumed P_f and T_f. By adjusting the final state until $v_f=c(P_f, T_f)=v_c$, both the critical velocity and pressure ratio are determined.

TABLE 1. *Sonic velocity $c^\circ(T)=\sqrt{\frac{R}{M}T\gamma^\circ(T)}$ of normal hydrogen in the perfect gas state*

T° K	c° m/sec	T° K	c° m/sec
20	370.8	56	619.4
22	388.8	58	630.1
24	406.1	60	640.6
26	422.7	65	665.7
28	438.7	70	689.4
30	454.1	75	711.8
32	469.0	80	733.0
34	483.4	85	753.1
36	497.4	90	772.3
38	511.0	95	790.6
40	524.3	100	808.1
42	537.2	150	959.2
44	549.8	200	1089
46	562.1	250	1208
48	574.1	300	1318
50	585.8	400	1519
52	597.3	500	1697
54	608.5	600	1858

Similar calculations of the kinematic viscosity ν of hydrogen were made using data for the absolute shear viscosity and density from [6,8,9], and some unpublished data of D. B. Chelton et al., of the National Bureau of Standards, Cryogenic Engineering Laboratory. The results, in figure 9, give the kinematic viscosity ν in square meters per second in the range 14° to 100° K at pressures up to 100 atm.

4. Comparison of Different Fluids

In order to determine the effect of differing fluids on turbine output and performance, some reasonable basis for comparison must be assumed. Since the final goal is liquefaction, it appears reasonable to compare only turbines at similar points in similar cycles in plants having the same liquefaction capacity in kilograms per second. In addition, it is clear that the comparison of a hydrogen expander and a nitrogen expander at the same inlet temperature would not be significant: $T_i=60°$ K would be reasonable for hydrogen, but at this same point nitrogen would be a solid. To obtain a practical basis for comparison, reduced quantities can be defined in a number of ways, one of which is

$$\tau=\frac{\ln T/T_b}{\ln T_c/T_b}=\tau_0 \ln \frac{T}{T_b},\ \pi=\frac{p-p_b}{p_c-p_b},$$

where c and b refer to the critical point and normal boiling point. This set is particularly suitable in that it relates the temperature and pressure to the values at which liquid is to be produced as well as to the critical point values characteristic of the particular gas.

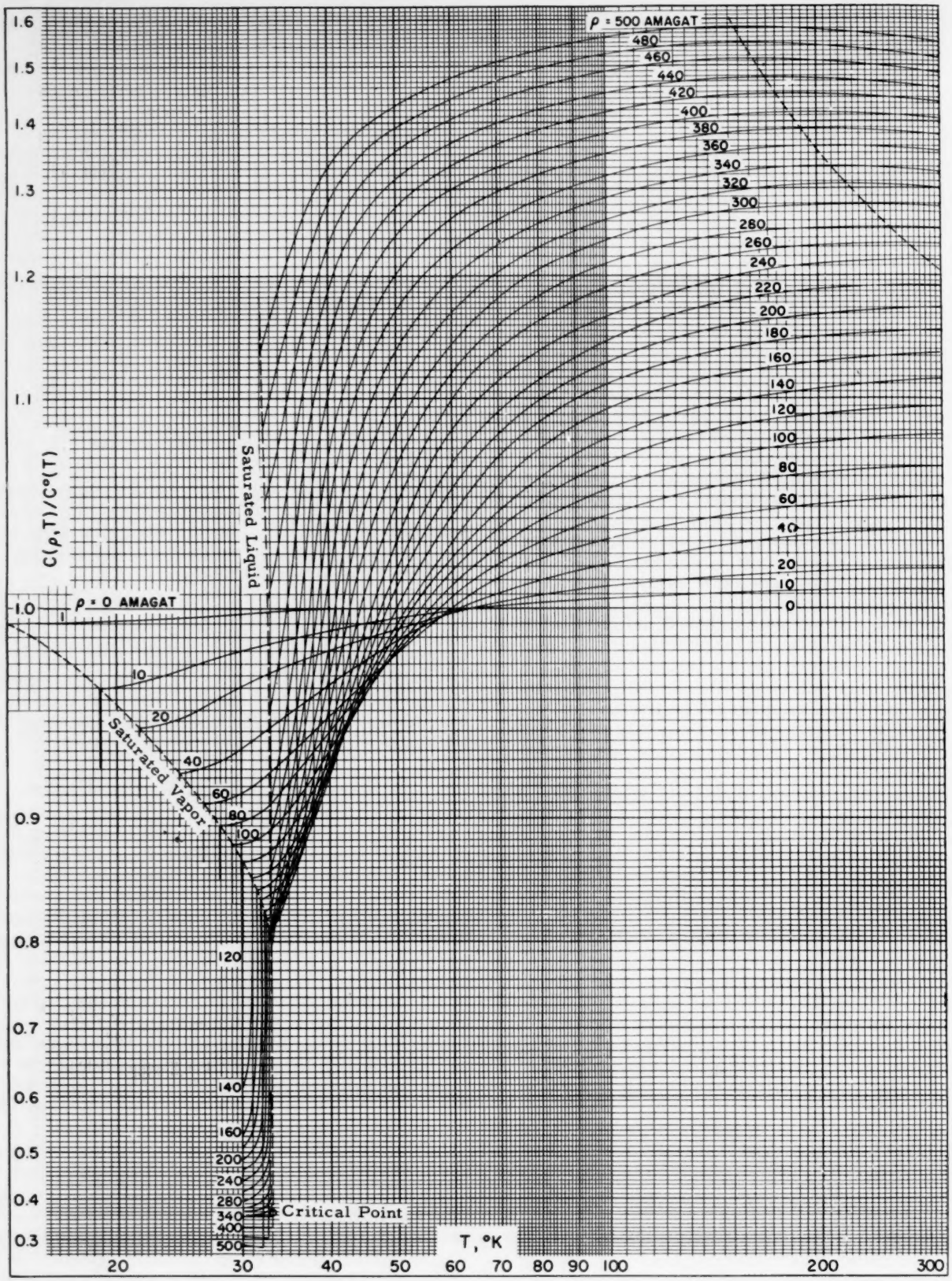

FIGURE 8. *Sonic velocity of normal hydrogen reduced by perfect gas values.*

NOTE: A large size copy of figure 8 is available upon request to Cryogenic Data Center, National Bureau of Standards, Boulder Laboratories Boulder, Colo.

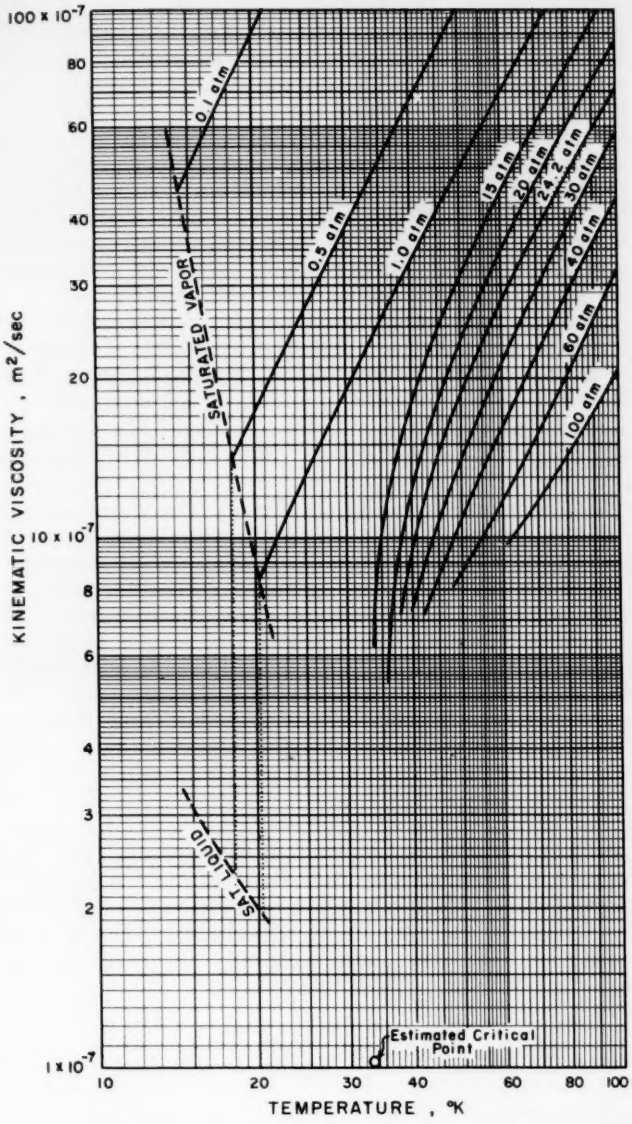

FIGURE 9. *Kinematic viscosity of normal hydrogen.*

The purpose of the expander is to supply refrigeration to a heat exchanger so that the gas to be liquefied can be cooled sufficiently for introduction to the J–T stage. However, temperature drop is not significant by itself, but must be related to a temperature level: e.g., a 1° K drop in a gas initially at 1° K would be impossibly large. Use of the reduced temperature τ provides a meaningful measure of cooling. For small increments, equal values of $\Delta\tau=\tau_0\Delta T/T$ can be considered to signify equivalent cooling for different gases.

Using this measure, enthalpy balance for the first and second streams of a heat exchanger for a particular gas a requires that

$$\dot{m}_1^a\bar{c}_{p1}^a\overline{T}_1^a\Delta\tau_1^a=\dot{m}_2^a\bar{c}_{p2}^a\overline{T}_2^a\Delta\tau_2^a,$$

where mean specific heats and temperature levels over each stream are used as an approximation which is sufficiently justified for the present purpose—determining a practical basis for comparison of turbines using different fluids. To the same degree of approximation, the mean temperature levels of each stream can be considered the same, $\overline{T}_1^a\approx\overline{T}_2^a$. Writing a similar equation for another gas b, and combining the two equations gives

$$\frac{\dot{m}_1^a/\dot{m}_2^a}{\dot{m}_1^b/\dot{m}_2^b}=\frac{\bar{c}_{p1}^a/\bar{c}_{p2}^a}{\bar{c}_{p1}^b/\bar{c}_{p2}^b}\cdot\frac{\Delta\tau_1^a/\Delta\tau_2^b}{\Delta\tau_1^b/\Delta\tau_2^b}.$$

For equivalent cooling, $\Delta\tau_1^a=\Delta\tau_1^b$ and $\Delta\tau_2^a=\Delta\tau_2^b$, and since the specific heat curves of all gases have a common characteristic behavior, at the same reduced pressure and temperature $\bar{c}_{p1}^a/\bar{c}_{p2}^a$ will be approximately equal to $\bar{c}_{p1}^b/\bar{c}_{p2}^b$. Thus, the following equation,

$$\frac{\dot{m}_1^a}{\dot{m}_2^a}=\frac{\dot{m}_1^b}{\dot{m}_2^b},$$

must hold. Stated simply, the fact that one refrigerating gas has a higher specific heat than another does not change the required mass flow ratio, since a gas of correspondingly higher heat capacity must be cooled.

To make the transition from refrigeration mass flow to turbine mass flow, a second assumption—that for the same reduced pressure and temperature the yield α of the J–T stage will be approximately equal for different gases—must be introduced. A comparison of figures 5, 6, and 7 with the similar curves for helium in [7] shows that this assumption is good: for example, the limiting pressure for hydrogen is roughly 400 atm, the limiting pressure for helium is 42 atm; thus, limiting reduced pressures are $\pi=(42-1)/(2.3-1)=31.5$ for helium, and $\pi=(400-1)/(13-1)=33$ for hydrogen. Together with the previous equation for refrigeration mass flow, this assumption requires that $\beta^a\dot{m}^a=\beta^b\dot{m}^b$; that is, for similar liquefiers with the same mass rate of production of different liquids, turbines at the same reduced pressure and temperature levels must have the same mass flow as each other to give equivalent refrigeration. A practical basis for comparison of similar turbines using different gases has thus been obtained.

5. Turbine Output

The theoretical output of a turbine stage can be obtained from the Euler turbine equation $\Delta H=\Delta(\mathbf{u}\cdot\mathbf{v})$, or

$$H_i-H_f=u_1v_1\cos\alpha_1-u_2v_2\cos\alpha_2,$$

where 1 and 2 refer to conditions at the inlet and exit of the rotor, u is the tip speed, and v the absolute gas velocity. The inlet gas velocity $\mathbf{v}$ can be assumed approximately equal to the nozzle exit velocity—that is, having the same magnitude and direction, with the direction, also, approximately equal to the actual nozzle blade angle. To obtain maximum work, the rotor blading is ordinarily designed to make the exit whirl as small as possible.

With such a design, the second velocity term in the above equation can usually be neglected. Thus, the theoretical output is given approximately by

$$|\Delta H| = \mathbf{u}_1 \cdot \mathbf{v}_1.$$

Since the Euler turbine equation in the above form is already in terms of mass flow (the units of ΔH could be watts per kilogram per second), one of the requirements for comparison of turbines with different fluids is already satisfied. Therefore, similar turbines having identical tip speeds and inlet velocities must have the same theoretical output for all fluids.

The assumption of identical nozzle exit velocities, however, cannot be made if similarity in the flow is to be maintained. A value of v_1 which indicated subsonic nozzle flow for hydrogen might require supersonic flow for nitrogen. To avoid this difficulty, the Euler equation can be transformed by defining a nozzle Mach vector $\mathbf{M}_1 = \mathbf{v}_1/c$, where c is the sonic velocity for the actual static temperature and pressure which occur at the throat, and an overall "turbine Mach vector" $\mathbf{M}^* = \mathbf{u}_1/c$, giving

$$|\Delta H| = c^2 \mathbf{M}^* \cdot \mathbf{M}_1$$

If the vectors $\mathbf{M}^*$ and $\mathbf{M}_1$ are maintained constant with different gases the flow conditions and velocity triangles will remain the same. For sonic conditions, where $M_1 = |\mathbf{M}_1| = 1$, since $(\partial G/\partial p)_s = 0$, the mass flow per unit area G will be maximum and c will be equal to the nozzle critical velocity v_c. Since $(\partial c/\partial p)_s \geq 0$ the local sonic velocity c will always be less than the sonic velocity c_i for the initial conditions P_i, T_i. However, c and v_c will always be increasing functions of c_i, so that gases with higher values of c_i will also have higher values of c and v_c. In terms of reduced pressure and temperature the Euler equation can then be expressed as

$$|\Delta H| = c_i^2 \phi^2 (M_1 \pi_i, \tau_i) \mathbf{M}^* \cdot \mathbf{M}_1,$$

where ϕ is a function too complicated to be evaluated other than by approximate methods; however, for the approximation needed for this comparison such evaluation is not necessary.

The last equation shows that more power output can be obtained under similar conditions from a turbine operating on hydrogen than any other gas, since the sonic velocity of hydrogen at the same reduced temperature and pressure is greater than for any other gas. As an example, for the conditions in section 2, $T_i = 65°$ K, $P_i = 30$ atm, the sonic velocity of hydrogen is 680 m/sec. At similar conditions ($\tau_i = 2.38$, $\pi = 2.42$), the inlet pressure and temperature for a nitrogen turbine would be $P_i = 79$ atm, $T_i = 249°$ K, and the initial sonic velocity, $c_i = 336$ m/sec. Thus, the hydrogen turbine would have approximately four times the output of the nitrogen turbine.

6. Turbine Losses

The four main losses in a well-designed turbine operating near its design point are: Nozzle flow losses, rotor flow losses, disk friction, and leakage. For a turbine operating away from its design point, secondary flow losses may become as great or greater than all other losses combined. In addition, a supersonic turbine may have large shock losses which would be very difficult to predetermine analytically. In this discussion, however, only losses at the design point will be considered.

An exact determination of nozzle flow losses would include effects due to the compressibility of the fluid and the change in flow area. Similarly, rotor flow losses should also include effects of turning and the centrifugal and Coriolis fields. Despite the probable importance of these effects, however, it is common practice in turbine analysis to avoid the formidable difficulties presented by them and base estimates of turbine losses on semiempirical equations such as the Prandtl-Karman law for the flow of incompressible fluids in stationary straight pipes of constant cross section. Such estimates have been found to be in approximate agreement with the results of actual tests [10] and also [1, 4]. The drop in total pressure P over a mean flow path length L is given by

$$\Delta P = \lambda \cdot \frac{L}{D} \cdot \frac{1}{2} \rho \bar{v}^2,$$

when D is a mean hydraulic diameter. This equation can be considered, not as a physical law, but merely a definition of the dimensionless resistance coefficient λ. Since such a loss in total pressure represents a conversion of mechanical energy into unusable heat, the total enthalpy loss δH can be determined from $\delta H = \Delta P/\rho$, that is

$$\delta H = \lambda \cdot \frac{L}{D} \cdot \frac{1}{2} v^2 = \lambda \cdot \frac{L}{D} \cdot \frac{1}{2} c_0^2 \cdot M^2 \cdot \left(\frac{c}{c_0}\right)^2$$

Defining $\psi = c_0/c_i$ and using $\phi = c/c_i$ as before, the relative loss can then be written

$$\frac{\delta H}{\Delta H^\circ} = \lambda \cdot \frac{L}{D} \cdot M^2 \left(\frac{\phi}{\psi}\right)^2,$$

where the loss coefficient λ is given by the Prandtl-Karman law [11]

$$\frac{1}{\sqrt{\lambda}} = 2 \log (\mathrm{Re}\sqrt{\lambda}) - 0.80.$$

Graphical solutions of the above equation show that λ is a monotonically decreasing function of the Reynolds number. Since $\mathrm{Re} = \bar{v}D/\nu = MD\,c/\nu$ can be expressed in the form

$$\mathrm{Re} = 2\sqrt{\frac{\dot{m}\bar{M}\bar{c}}{\pi \rho \nu^2}}$$

the assumption of equal mass flow and Mach number

for different gases requires that the loss coefficient decrease as the factor $\sqrt{c/\rho\nu^2}$ increases. Comparing hydrogen with other fluids, the kinematic viscosity ν at similar reduced pressures and temperatures will be approximately constant—at least for diatomic gases, while the sonic velocity c will be greater and the density ρ less. Thus, the flow losses in a comparable hydrogen turbine can be expected to be somewhat less.

Disk friction losses can be treated in a similar way. The moment acting on both sides of a disk of radius R rotating with an angular velocity ω is given by [12]

$$\mathcal{M}=\lambda^* \cdot \frac{1}{2}\rho\omega^2 \cdot R^5 .$$

Using the specific speed at 100 percent efficiency n_s^*, the relative disk friction loss can be expressed as

$$\frac{\delta H}{\Delta H^\circ}=\lambda^* \frac{M^{*5}\left(\frac{\phi}{\psi}\right)^5}{\pi^2\sqrt{2}\, n_s^{*2}}.$$

The value of the rotational loss coefficient λ^* depends on whether the turbine Reynolds number $\mathrm{Re}^*=u_1 D_1/2\nu=cM^*D_1/2\nu$ is in the laminar or turbulent range. For $\mathrm{Re}^*<2000$, λ^* is given by

$$\lambda^*=\frac{\pi D_1}{h}\cdot\frac{1}{\mathrm{Re}^*},$$

where h is the spacing between rotor and casing. For large Re*, the value of λ^* is independent of the spacing, and can be conservatively estimated from the Goldstein law [13] for a free disk

$$\frac{1}{\sqrt{\lambda^*}}=1.97\log\left(\mathrm{Re}^*\sqrt{\lambda^*}\right)+0.03,$$

which is identical, except as to constants, with the Prandtl-Karman law.

Although in either case λ^* is a monotonically decreasing function of Re*, a comparison of Re* for different gases cannot be made directly, since the rotor diameter D_1 cannot be immediately replaced by an expression involving mass flow. However, the larger volume flow in a comparable hydrogen turbine will require a larger rotor diameter to maintain good rotor passage design. Since c/ν will also be greater, the disk friction losses can be expected to be less.

The *volume* flow leakage of hydrogen will be much greater than other gases, since for comparable conditions the absolute shear viscosity will be much smaller: for $\tau=2.38$, $\pi=0$, the viscosity of hydrogen is $\mu=3\times10^{-6}$ dekapoise (=kg/meter-sec) while the viscosity of nitrogen is $\mu=15\times10^{-6}$ dekapoise. However, it is the loss of *mass* from the primary stream rather than volume which must be used to determine the leakage loss. The pressure drop through a leakage orifice can be written

$$\Delta P=\lambda\cdot\frac{L}{D}\cdot\frac{1}{4}\rho v^2$$

where the pressure coefficient λ, assuming laminar flow, is given by $\lambda=64/\mathrm{Re}$. Solving this equation for the leakage mass flow $\dot{m}_L$ in terms of reduced pressure drop gives

$$\dot{m}_L=\frac{A_L^2}{4\pi D_1}\cdot\frac{\Delta\pi}{\pi_0}\cdot\frac{1}{\nu}.$$

where A_L is the leakage area, and $1/\pi_0=P_c-P_b$. Both $1/\pi_0$ and $1/\nu$ will be smaller for hydrogen than other gases (except helium) which will tend to offset the unfavorable increase in A_L^2/D_1 with the larger hydrogen turbine; thus, with careful design of seals and leakage passages it should be possible to maintain equivalent leakage losses.

A general conclusion can be drawn from the above discussions. The formulas used are somewhat oversimplified: an actual turbine designer would, for air, use more complex equations based on test data, with appropriate corrections in empirical constants. However, if the design analysis used for air turbines, together with all the factors based on air tests, are used for a comparable hydrogen turbine, the results should be reasonable and the performance actually better than indicated.

7. Turbine Design

After the above considerations it is possible to sketch a tentative design for a turbine in a specific application. Using as an example the conditions stated in section 2, that is, $T_i=65°\mathrm{K}$, $P_1=30$ atm, $\rho_i=138$ Amagats, $c_i=680$ m/sec, and $h_i=1{,}100{,}000$ j/kg, an expected efficiency of 80 percent would result in the outlet conditions $T_f=23.5°\mathrm{K}$, $P_f=1$ atm, $\rho_f=13$ Amagats, and $h_f=756{,}000$ j/kg. The theoretical required isentropic head is $\Delta H^\circ=429{,}000$ j/kg and the isentropic head velocity is $c_0=\sqrt{2\Delta H^\circ}=927$ m/sec. If the nozzles were designed for $M=1$, the critical nozzle velocity would be $v_c=480$ m/sec and the critical pressure ratio would be $X_c=3.53$. An additional velocity is of some interest: the maximum theoretically possible nozzle velocity, which in this case is $v_m=\sqrt{2h_i}=1483$ m/sec, which can occur only for an infinite Mach number and pressure ratio.

The first question that should be answered is whether the required conditions can be met with a single stage turbine. This can be done using the Euler equation assuming negligible outlet whirl, $\Delta H^\circ=c_0^2/2=u_1 v_1\cos\alpha_1$. As a first possibility, assume a tip speed $u_1=500$ m/sec, which would not be considered unreasonable in the small aircraft turbine industry, and a minimum nozzle angle of 7° (for an axial-flow turbine a larger minimum nozzle angle would have to be assumed, since in that case the nozzle angle is with respect to a plane surface rather than a cylinder). These conditions result in an outlet nozzle velocity $v=875$ m/sec, and a nozzle Mach number of M=2.5 which must be considered to be much too high if the desired efficiency is to be obtained. Thus, using conventional rotor materials and limiting tip speeds, the desired head cannot reasonably be obtained in a single stage.

530231—60——3

The possibility of newly developed materials, however, tempers this negative answer. Recent tests on specially prepared aluminum alloys indicate tip speeds as high as 915 m/sec (=3000 fps) may be obtained in medium sized rotors [14]. Using the same nozzle angle as above and assuming 90° blades for greatest strength (and simplest fabrication), the equation $c_0^2=2u_1v_1 \cos \alpha_1$ becomes $c_0^2=2v_1^2 \cos^2 \alpha_1$ and results in a tip speed of $u_1=655$ m/sec (which should be reasonable with these newer materials) and a nozzle outlet velocity of $v_1=660$ m/sec. At the nozzle outlet, the Mach number would be M=1.3, which would not result in unreasonable losses.

Since it is at least possible to design a single-stage turbine for the above conditions, it is of considerable interest to determine more precisely the minimum capacity liquefier which might use such a turbine. Again neglecting outlet whirl, the Euler equation can be written

$$\Delta H^\circ=\frac{n\beta\dot{m} \cot \alpha_1}{b_1\rho_1}$$

where b_1 is the blade depth at the tip. To make the results most favorable, extreme conditions of $n=2{,}000$ rps (commercially available in an 8-mm ball bearing) and a probably minimum machinable value of $b_1=2$ mm will be chosen. To obtain the required tip speed of $u_1=655$ m/sec, the rotor diameter would be approximately 10 cm. With the calculated nozzle velocity $v_1=660$ m/sec, the density would be 75 Amagats, but the assumption of a 3-percent relative nozzle loss would reduce this to an actual value of 65 Amagats. With these figures, the minimum total volume flow at standard conditions becomes 7.38 m^3/sec (=15,600 scfm), corresponding to a minimum liquefaction capacity of approximately 9,000 liters/1 hr.

Gas bearings have recently been the subject of intensive development. Air bearings for service up to 250,000 rpm have been developed for commercial high speed grinding machines, and it seems clear that such bearings should be adaptable to low temperature service with hydrogen gas. Considering the use of such gas bearings, and choosing $n=4{,}000$ rps, with the other thermal conditions as in the above example, would result, for a 5-cm rotor, in a minimum liquefaction rate of 4,500 liters/hr. Since a number of parameters have been chosen at extreme limits to obtain this result, it would appear more practicable to use a turbine of more than one stage or a reciprocating expander for liquefiers of smaller capacity.

8. Bearing Tests

The combination of high tip speeds required to make use of the enthalpy head of hydrogen, and minimum practicable flow areas for turbines used in small liquefiers, make the necessity of relatively high rotational speeds evident. Such speeds introduce a number of problems in bearing design, especially since, for several reasons, it is desirable to keep the bearings cold. Tanza [15] has found that small stainless steel ball bearings with Micarta retainers will operate satisfactorily at 10,000 rpm without lubrication when surrounded by a cooling and inert (hydrogen) atmosphere.

In order to determine whether similar bearings would operate at higher speeds, a small turbine-driven bearing tester was constructed. This was designed to test 10-mm bearings at 100,000 rpm at low temperatures. The turbine was an impulse type using a rotor that could be easily machined, and mounted on the same shaft as the pair of bearings being tested. The rotor was 1 in. in diameter, made of 24ST–4 aluminum, and pressed on a hard-chromed Inconel shaft. Bearing races and balls were 440C stainless steel, held in a 440A stainless steel cylindrical block containing an adjustable spring to allow various axial loadings. The entire mechanical assembly fitted into a brass case of which the nozzle ring was an integral part. This case was designed to mount on the end of a Collins' ribbon-packed heat exchanger, and at the lower end had a filter to remove water or oxygen particles from a liquid nitrogen bath. The bearings themselves operated in nitrogen gas, but were cooled (and possibly partly lubricated) by liquid nitrogen jets directed between the races. A cross section of the tester is shown in figure 10 and several views of the tester and components in figures 11, 12, and 13.

Tests were completed on only one type, a bearing manufactured by the Barden Corp. using composition retainers. Preliminary runs at room temperature with oil-mist lubrication were highly successful, top speeds of 130,000 rpm being attained, and resulted in only one minor modification: the addition of

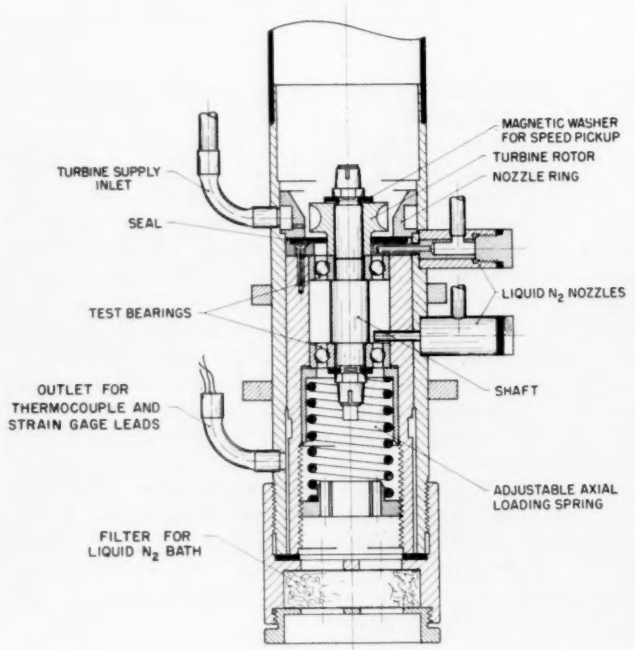

FIGURE 10. *Cross section of high-speed low-temperature bearing tester.*

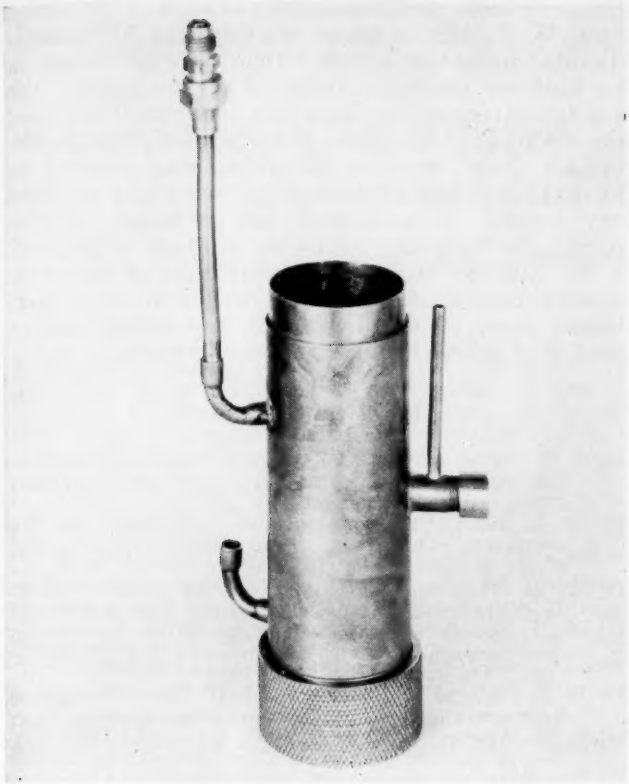

FIGURE 11. *Bearing tester: outer case.*

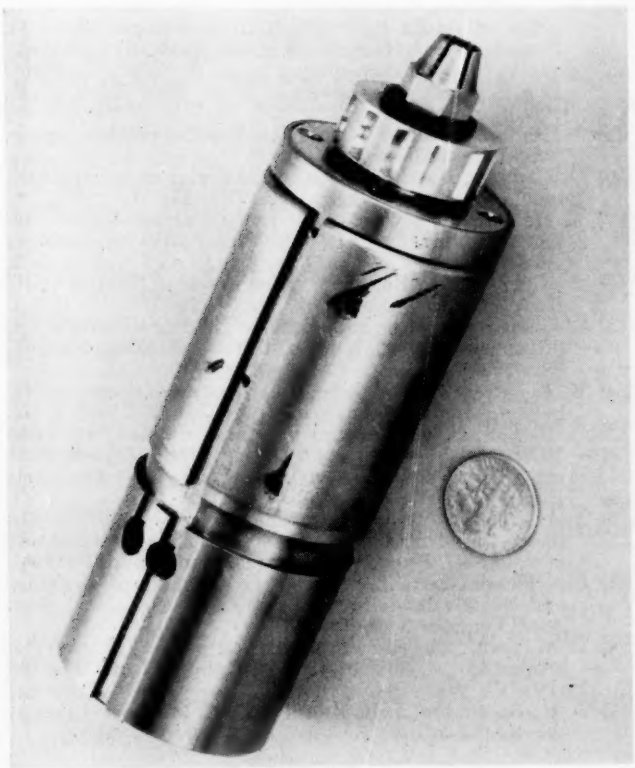

FIGURE 12. *Bearing tester: mechanical assembly.*

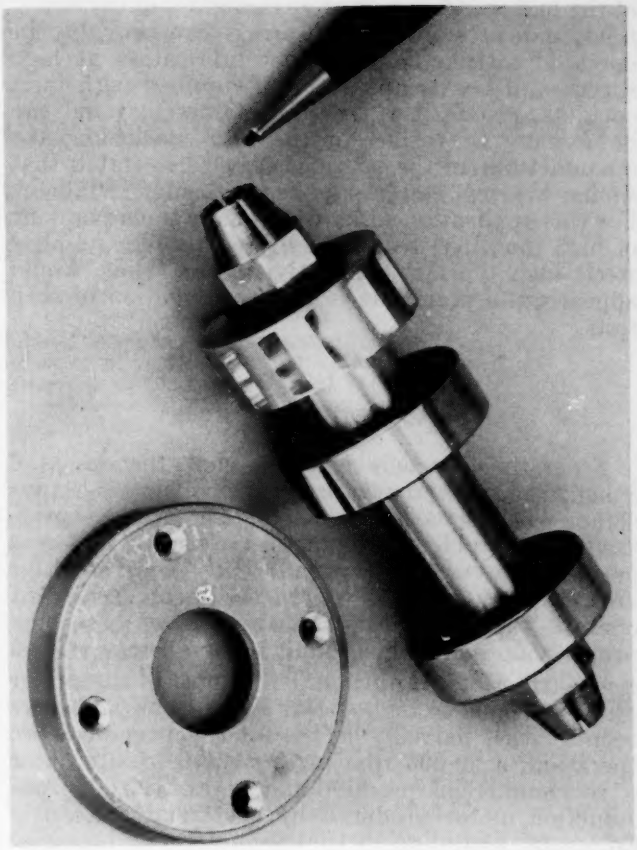

FIGURE 13. *Bearing tester: assembly of rotor, shaft, and bearings.*

stiffening rings to the outer brass case to raise its fundamental four-nodal frequency above 100,000 rpm—exactly the designed operating speed.

At low temperature (liquid nitrogen) the bearing tester itself operated just as satisfactorily, but the bearing retainers (which had appeared very promising from Tanza's similar low speed tests) failed in apparently brittle fracture at the ball holes. It is assumed that the different results are due to the greater impact at high speeds of the balls oscillating about their mean rotating positions. The possibility of a difference in the low temperature brittle behavior of the retainer material should be investigated further, however, by standard notch impact methods. The highest speed attained at low temperature was 60,000 rpm with one retainer cracked completely across at one hole. At this speed centrifugal force was great enough to deflect the broken retainer and stop the turbine until the retainer could return to its normal shape. In most tests retainer damage was considerably greater, large fragments frequently being broken completely away.

Three conclusions can be drawn from the tests: (a) A satisfactory bearing tester for operation at 100,000 rpm and 80° K or lower has been constructed; (b) bearings with composition retainers are probably not suitable for the *combination* of low temperatures and high speeds; and (c) microscopic examination

of the ball tracks, which were straight and extremely faint, indicates that ball bearings can probably be operated satisfactorily without lubrication at high speeds and low temperatures if supplied with inert coolants, provided a suitable retainer material can be found. In regard to the last conclusion, the manufacturer of the bearings tested has stated that similar bearings can be supplied with silver retainers. For this application silver would have the advantage of high ductility, low friction, and (unlike stainless steel) high thermal conductivity, and, thus, would appear quite promising in any continuation of such tests.

9. Generator Design

From the cryogenic point of view, the design of a high speed alternator as a possible power-output component for a turbine expander presents practically no problems; conductor resistivity and core permeability are known sufficiently accurately for any temperature at which the generator might operate that the designer can merely obtain the proper values and thus eliminate temperature level from further consideration. Thus, most of the major problems, such as high speed, are not new and have been at least partially solved for room-temperature operation; a 90,000 rpm permanent field alternator is in commercial production and an 120,000 rpm induction motor produced by the General Electric Co. could, according to the manufacturer, be easily modified for use as an induction generator.

Unlike present applications, however, the use of such generators with turbine expanders at low temperatures would require high generator efficiencies since losses would be returned to the system as heat. With one exception, all such losses can be calculated with existing data and will apparently be much lower than at ambient temperature.

The exception—hysteresis loss in the core—has evidently been of little interest: tests by Fleming and Dewar [16, 17] in 1896 showed no change in hysteresis loss in transformer iron at liquid air temperatures; tests by Terry [18] in 1910 indicated a rapidly increasing loss in electrolytic iron with decreasing temperature, but were not made at constant flux densities and thus are of questionable significance.

Due to the scarcity and conflicting information on hysteresis loss, a modified "Epstein-test" was performed on silicon steel transformer laminations. The detailed results are reported separately by Brown and Brennand [19], but show the following behavior: (a) At any temperature the hysteresis loss increases with induction, following the Steinmetz law $W=aB^n$ quite well; (b) at any induction the hysteresis loss increases with decreasing temperature; (c) the relative increase in the loss is independent of induction: at 20° K, for instance, the loss appears to have increased by 20 percent over the loss at ambient temperature for all inductions between 2 and 10 kilogauss.

Among those contributing to the work of this study were: W. F. Mayer (guest worker from AiResearch Manufacturing Co., summer 1956) to whom credit is due both for the basic design of the turbine for the bearing tester, and guidance in the initial stages of the study; R. J. Corbett (guest worker from Beech Aircraft Corp., summer-fall 1956) who assisted in the detailed design of the bearing tester and was also very helpful in comments and criticism of this report; the following part-time student employees: D. W. Murphy (who carried out most of the sonic velocity calculations), J. R. Brennand (who performed most of the hysteresis loss tests), and a number of others who assisted on occasion.

10. References

[1] S. C. Collins and R. L. Cannaday, Expansion machines for low temperature processes (Oxford University Press, Oxford, England, 1958).
[2] M. L. Land, Expansion turbines and engines for low temperature processing, Proc. 1956 Cryogenic Eng. Conf., Boulder, Colo. (1956).
[3] W. K. Jekat, An impulse type expander turbine, Proc. 1956 Cryogenic Eng. Cong., Boulder, Colo. (1956).
[4] W. T. von der Nuell, Single-stage radial turbines for gaseous substances with high rotative and low specific speed, Trans. ASME **74,** 499 (1952).
[5] D. B. Chelton, J. Macinko, and J. W. Dean, Methods of hydrogen liquefaction (informal communication).
[6] H. W. Woolley, R. B. Scott, F. G. Brickwedde, Compilation of thermal properties of hydrogen in its various isotopic and ortho-para modifications, J. Research NBS **41,** 379 (1958) RP1932.
[7] E. H. Brown and J. W. Dean, Joule-Thomson process in the liquefaction of helium, J. Research NBS **60,** 161 (1958) RP2834.
[8] A. S. Friedman, The thermodynamic and transport properties of liquid hydrogen and its isotopes, Part II, Compressibility factors, viscosity, dialectic constants, and surface tension, quoted in R. B. Scott, Cryogenic Eng. (D. van Nostrand Co., Inc., New York, N.Y., 1959).
[9] J. Hilsenrath, et al., Tables of thermal properties of gases, NBS Circ. 564 (1955).
[10] O. C. Balje, A contribution to the design of radial-turbomachines, CADO Tech. Data Dig. **15,** 21 (1950).
[11] A. H. Shapiro, Dynamics and thermodynamics of compressible fluid flow (Ronald Press, New York, N.Y., 1953 to 1954).
[12] H. Schlichting, Boundary layer theory (McGraw-Hill Book Co., Inc., New York, N.Y., 1955).
[13] S. Goldstein, On the resistance to the rotations of a disc immersed in a fluid, Proc. Cambridge Phil. Soc. **31,** 232 (1935).
[14] N. L. Baker, Industry spotlight: Alcoa develops new impellers, Missiles and rockets, **2,** No. 7, p. 202 (July1957).
[15] G. F. Tanza, Development program for a non-lubricated 10,000 RPM bearing operating over a temperature range from 40° R to 560° R, Proc. 1956 Cryogenic Eng. Conf., Boulder, Colo. (1956).
[16] J. A. Fleming and J. Dewar, On the changes produced in magnetized iron and steel by cooling to the temperature of liquid air, Proc. Roy. Soc. (London) **A60,** 57 (1896).
[17] J. A. Fleming and J. Dewar, On the magnetic permeability and hysteresis of iron at low tempertures, Proc. Roy. Soc. (London) **A60,** 81 (1896).
[18] E. M. Terry, The effect of temperature upon the magnetic properties of electrolytic iron, Phys. Rev. **30,** 133 (1910).
[19] E. H. Brown and J. R. Brennand, Jr., Magnetic losses at low temperatures, J. Appl. Phys. **30,** 112 (1959).

Boulder, Colo. (Paper 64C1–21)

JOURNAL OF RESEARCH of the National Bureau of Standards—C. Engineering and Instrumentation
Vol. 64C, No. 1, January–March 1960

A Statistical Chain-Ratio Method for Estimating Relative Volumes of Mail to Given Destinations

Norman C. Severo [1] and Arthur E. Newman

(August 31, 1959)

A sampling method, called the chain ratio method, is applied in estimating the distribution of mail by destination. Variances and coefficients of variation for the estimators are given. The details and results of three applications of this sampling method to outgoing first-class letter mail are given. These studies were conducted by the National Bureau of Standards in San Francisco, Los Angeles, and Baltimore.

1. Introduction

The National Bureau of Standards has been active in developing equipments and systems for improved letter sorting by automation. To develop design parameters it is necessary to determine the physical characteristics of mail and the proportion of mail going to various *destinations*.[2] Since the volume of mail is much too large for complete piece counts to be feasible, sampling methods of known and adequate accuracy must be used. The present paper is the first step by NBS in the effort to develop such methods as applied to mail distribution. Studies and results concerning letter-size characteristics are reported by Severo, Newman, Young, and Zelen in [1][3] and a general background to the mechanization program is given by I. Rotkin [2].

This paper discusses a sampling procedure designed to estimate the proportion of mail going to each *destination*. The sampling plan used in this study is referred to as the "chain-ratio" method because the nature of the formulas involved in the analyses resembles a chain of ratios. The method has been applied to outgoing first class letter-mail at the San Francisco, Los Angeles, and Baltimore Post Offices.

It was intended, initially, to study five cities: Baltimore, Washington, Philadelphia, Chicago, and Los Angeles. Philadelphia, Baltimore, and Washington were chosen because they would tend to give a pattern of postal operations on the East Coast. Chicago was chosen to show Midwest influence, and Los Angeles was selected to show the West Coast influence. San Francisco was added to the list in an effort to find out whether Los Angeles was atypical, because Los Angeles serves an unusually large area.

The Post Office Department made special studies in Philadelphia, Chicago, and New York, where in each case a complete count was made of the *total volume* of mail to each *destination* for either a 24- or 48-hour period of time. Actually this complete count was obtained by footage measurements of stacks of mail and a conversion factor of 290 letters per foot of mail was used. The NBS also made a modified version of the complete count on November 5, 1956, in Baltimore. In this count, only the *total volume* entering the system between 4 P.M. and 7 P.M. was included.

However, any complete count of large volumes of mail, even for short periods of time such as 3 hours, involves a considerable number of man hours and invariably tends to delay the normal function of sorting mail. Furthermore, any such complete counts are open to criticisms that may be leveled against complete enumeration methods. (The literature contains many examples [3, 4, 5, 6] comparing complete enumeration methods with statistically designed sampling procedures, and shows the desirability, from the economics and reliability point of view, of the sampling techniques.) A complete count of mail, properly done, say, for 24 hours, gives a good indication of what happens during a particular $^1/_{365}$ part of a year. If one wishes to enlarge this fraction then additional complete counts can be made. Thus to represent a particular $^5/_{365}$ part of a year one might take 5 consecutive days—e.g., Monday through Friday or Thursday through Monday depending upon whether or not the weekend is to be included. This is expensive and time consuming. Furthermore tremendous effort is needed on the part of all concerned to keep track of all the mail to each *destination*. Thus errors are bound to occur. Finally, the mail itself will tend to be delayed during such exhaustive counts. A sampling study, on the other hand, enables one to check the flow pattern of mail from time to time during any interval of time and with far less effort and disruption to routine operations than in a complete enumeration and hence may more accurately represent normal operations. Thus, for example, to obtain information about mail for some given week, samples may be taken for short intervals several times each day throughout the week. (Actually in the application discussed here, two samples a day were taken during a 5-day period excluding the weekends.) Or if one wanted to check

[1] Present address: University of Buffalo.
[2] Italicized terms have special meanings in this study and are defined in section 2.1 of this paper or in the *Postal Term Glossary*, U.S. Post Office Department, August 1956, P.O.D. Publication 18.
[3] Figures in brackets indicate the literature references at the end of this paper.

the behavior of mail for any other given time period, say some particular month or during the Christmas rush, then samples could be taken from time to time during that particular time period.

The destination data obtained by application of the chain-ratio method has been used as basic input for: (1) Simulation studies of the effectiveness of an NBS proposed sorting machine; (2) studies of comparative costs for various types of mechanized letter sorting systems, including the one embodied in the machine mentioned in (1); (3) analytic comparisons of suggested configurations for automatic mail sorting equipment [7]; and, (4) improvement of current sorting procedures.

Only some typical results of the San Francisco study are presented here. The reader is referred to [8] for detailed results of the San Francisco, Los Angeles, and Baltimore studies.

Section 2 gives the definitions as used in this paper and the model of the flow of mail that is studied. Section 3 presents in detail the sampling procedures, analysis, and the volume counts used for the particular applications discussed. Section 4 defines precisely the types of mail that were studied at San Francisco, Los Angeles, and Baltimore. Section 5 presents the details of the San Francisco study.

2. Definitions and the Model

2.1. Definitions

A list of definitions of terms, as used in this paper is given here for reference. These definitions are given in order to avoid misinterpretation and ambiguity because of postal language differences between post offices.

1. SEPARATION: a classification characterized by a labeled pigeonhole on a sorting case.
2. DESTINATION: a final *separation* made at a given post office. All *directs* and *residues* are included in this classification.[4]
3. DIRECT: a *destination* to a single given post office.
4. DISTRIBUTION: the function of physically sorting letters into their respective *separation* boxes.
5. PRIMARY: the first stage of *distribution* of outgoing mail.
6. SECONDARY: the second stage of *distribution* of outgoing mail.
7. TERTIARY: the third stage of *distribution* of outgoing mail.
8. BYPASS: mail which receives its first *distribution* in the *secondary* and *tertiary* cases. Also mail which goes directly to the city section.
9. RESIDUE: mail destined for post offices for which no direct *separation* is provided in a case or rack.
10. TOTAL VOLUME: the defined classes of mail studied. (*Total volume* is defined more explicitly as used in this study in section 4.)

The expression "off the *primary*, *secondary*, or *tertiary*" indicates mail which has just undergone that stage of *distribution*.

[4] *Air* mail and foreign mail off the *primary* are also considered *destinations* in this study.

2.2. The Model

The model for the operation of outgoing mail consists of a three stage sorting scheme which can be represented by a flow chart as given in figure 1. The *total volume* in the top box consists of those types of mail indicated in section 4. This volume then divides into two parts, that which goes to the *primary* and that which bypasses the *primary*. The *bypass* mail is sent either to the city section or to the *secondary*. Mail leaving the *primary* may go either to its *destinations* or to the *secondary*. The *secondary* consists of sections which can be numbered 1, 2, 3, . . . and which correspond to *primary separations* needing further *distribution*. We call the i-th section the "i-th *secondary*." From any section in the *secondary*, mail can go either to its *destination* or to one of the *tertiary* sections which can be numbered 1, 2, 3, . . . Therefore sections in the *tertiary*, corresponding to *separations* from the i-th *secondary* can be numbered $i1$, $i2$, $i3$, . . . The ij-th section is called the "ij-th *tertiary*." Mail leaving the *tertiary* goes directly to its *destinations*. A more detailed description of how a letter flows through this system is given in [9].

Since the model for incoming mail is similar to that for outgoing mail, the procedures discussed below may also be applied in studies of incoming mail.

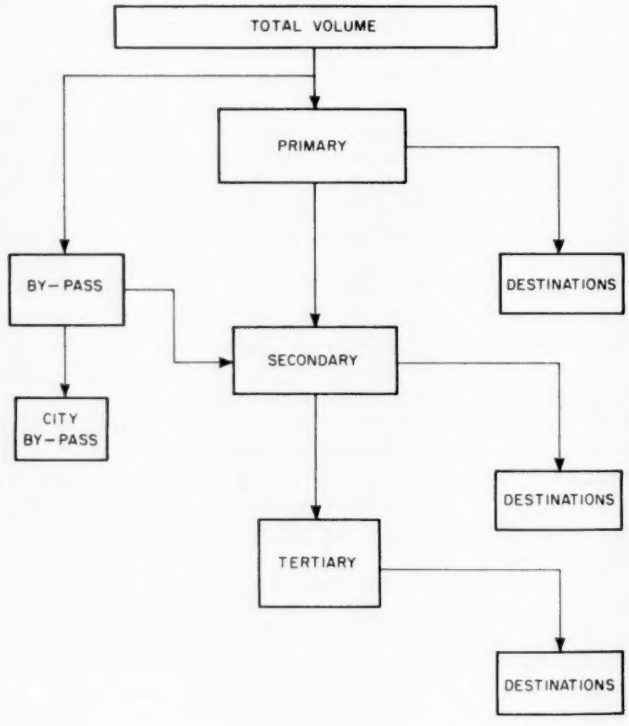

FIGURE 1. *Flow chart model for the distribution of outgoing mail.*

3. Chain-Ratio Estimates

In this section we discuss the estimation formulas and their associated variances and coefficients of variation for estimating the proportion of mail to a given *destination*. We also present a list of notations and specific formulas used in the applications given in section 5 and in [8].

3.1. The General Method

The basic idea involved in the estimation formulas consists of multiplying together a chain of ratios. Two conditions are required for setting up the chain. The first is that each ratio must be one that can be estimated conveniently. This can often be done by using volume count data customarily recorded by the particular post office. If such records are not kept then it must be possible either to arrange that they be kept or to devise appropriate sampling plans that would provide estimates of each ratio. It is essential that such plans be simple to implement and not interrupt the flow of the mail.

The second requirement is that the ratios must be linked together in chain form so that the desired ratio is all that remains after "canceling." This is similar to the usual chain differentiation carried out in the calculus. There if it is desired to obtain $\delta f/\delta x$, where $f=f[z[y[x]]]$, then one writes

$$\frac{\delta f}{\delta z}\times\frac{\delta z}{\delta y}\times\frac{\delta y}{\delta x}$$

and a "cancellation" check gives the desired results; i.e.,

$$\frac{\delta f}{\delta z}\times\frac{\delta z}{\delta y}\times\frac{\delta y}{\delta x}=\frac{\delta f}{\delta x}.$$

Such a "cancellation" is, of course, only a convenient artifice. It must be proved that the multiplication of such a chain of derivatives actually does yield the desired derivative $\delta f/\delta x$.

Here we have a similar situation. Suppose we are interested in estimating the ratio of mail to a *primary destination* to the *total volume*. Let us denote this ratio by the parameter D_P/T. Suppose that (1) the particular post office under study keeps records which enable us to obtain an unbiased estimate of the ratio of *primary* mail to the *total volume*, call this estimate T_P/T, and (2) it is possible to set up a simple sampling plan which yields an unbiased estimate of the ratio of mail to the *primary destination* to the *primary volume*, call this estimate D_P/T_P. Then we write $(D_P/T_P)(T_P/T)$, cancel, as in the calculus, and obtain the desired ratio estimate D_p/T. That such "cancellation" is permitted is seen as a special case of the following:

Let $R_1, R_2, \ldots, R_K$ be a set of K statistically independent random variables such that

$$E(R_i)=\frac{r_{i-1}}{r_i},\quad i=1,2,\ldots,K.$$

Then for any $j\leq K$

$$E(R_1R_2\ldots R_j)=E(R_1)E(R_2)\ldots E(R_j)$$

$$=\frac{r_0}{r_1}\times\frac{r_1}{r_2}\times\ldots\times\frac{r_{j-1}}{r_j}$$

$$=\frac{r_0}{r_j}.$$

Thus $R_1R_2\ldots R_j$ is an unbiased estimate of the ratio r_o/r_j.

It is important to point out that the chain of ratios used for a particular application should be devised with that application in mind. By so doing, optimum use may be made of records already being kept by that post office. No single set of formulas can be used easily in every case because not all post offices maintain the same volume count records.

The variance of $R_1R_2\ldots R_K$, which we symbolize by $\sigma^2_{R_1\ldots R_K}$ may be easily obtained. Denote the mean and variance of R_i by m_i and σ_i^2, respectively. Then, for $K=2$,

$$\sigma^2_{R_1R_2}=E(R_1^2R_2^2)-[E(R_1R_2)]^2$$

$$=(\sigma_1^2+m_1^2)(\sigma_2^2+m_2^2)-m_1^2m_2^2$$

$$=\sigma_1^2\sigma_2^2+\sigma_1^2m_2^2+m_1^2\sigma_2^2.$$

Similarly, for $K=3$ and 4 we obtain

$$\sigma^2_{R_1R_2R_3}=\sigma_1^2\sigma_2^2\sigma_3^2+m_1^2\sigma_2^2\sigma_3^2+\sigma_1^2m_2^2\sigma_3^2$$
$$+\sigma_1^2\sigma_2^2m_3^2+m_1^2m_2^2\sigma_3^2$$
$$+m_1^2\sigma_2^2m_3^2+\sigma_1^2m_2^2m_3^2,$$

and

$$\sigma^2_{R_1R_2R_3R_4}=\sigma_1^2\sigma_2^2\sigma_3^2\sigma_4^2+m_1^2\sigma_2^2\sigma_3^2\sigma_4^2+\sigma_1^2m_2^2\sigma_3^2\sigma_4^2$$
$$+\sigma_1^2\sigma_2^2m_3^2\sigma_4^2+\sigma_1^2\sigma_2^2\sigma_3^2m_4^2+m_1^2m_2^2\sigma_3^2\sigma_4^2$$
$$+m_1^2\sigma_2^2m_3^2\sigma_4^2+m_1^2\sigma_2^2\sigma_3^2m_4^2+\sigma_1^2m_2^2m_3^2\sigma_4^2$$
$$+\sigma_1^2m_2^2\sigma_3^2m_4^2+\sigma_1^2\sigma_2^2m_3^2m_4^2+m_1^2m_2^2m_3^2\sigma_4^2$$
$$+m_1^2m_2^2\sigma_3^2m_4^2+m_1^2\sigma_2^2m_3^2m_4^2+\sigma_1^2m_2^2m_3^2m_4^2.$$

In general

$$\sigma^2_{R_1\ldots R_K}=\sum\prod_{i=1}^{K}t_i-\prod_{i=1}^{K}m_i^2, \tag{1}$$

where the summation is over all possible 2^K combinations obtained by letting each t_i take on either the value m_i^2 or σ_i^2.

Let k_i denote the coefficient of variation of R_i $\left(\text{i.e., } k_i=\frac{\sigma_i}{m_i}\right)$ and let $k_{R_1\ldots R_K}$ denote the coefficient of variation of $R_1R_2\ldots R_K$. Then it follows from

eq (1) that

$$k^2_{R_1 \cdots R_K} = \sum \prod_{i=1}^{K} t_i - 1 \qquad (2)$$

where now the summation is over all possible 2^K combinations obtained by letting each t_i take on either the value k_i^2 or 1. Thus for the case $K=2$,

$$k^2_{R_1 \cdots R_2} = k_1^2 k_2^2 + k_1^2 + k_2^2.$$

For k_1 and k_2 small, we obtain by neglecting terms of higher order

$$k^2_{R_1 R_2} \doteq k_1^2 + k_2^2 \leq 2 \max (k_1^2, k_2^2).$$

Therefore, for k_1 and k_2 sufficiently small

$$k_{R_1 R_2} \leq \sqrt{2} \max (k_1, k_2).$$

In a similar way it is easy to show that

$$k_{R_1 \ldots R_K} \leq \sqrt{K} \max (k_1, k_2, \ldots, k_K) \qquad (3)$$

for the k_i sufficiently small. This says, essentially, what we would intuitively expect; namely that the coefficient of variation of the chain is bounded by a multiple of the coefficient of variation of the "weakest link." This weakest link is that ratio which has the greatest percent variability.

The estimates of the R_i used in the applications in later sections are of the form X/n where X is either a binomial or a multinomial random variable and n is the sample size. Such being the case, the coefficient of variation of any ratio estimate is $k = \sqrt{(1-p)/np}$ where p is the expected value of X/n. Since the sample sizes used here are large, the value k is indeed small. For example if $p=0.05$ and $n=5{,}000$ then the *relative* standard error of X/n is $k=0.0616$ or 6.2 percent and the *absolute* standard error is $0.062 \times 0.05 = 0.0031$. Thus the overall uncertainty is of the order of $3 \times 0.0031 = 0.0093$ so that in repeated drawings of 5,000 samples we would expect almost all of the estimates X/n to be between 0.05 ± 0.0093.

3.2. Notations and Formulas Used in the Applications

In the preceding section we presented the general method for setting up a chain-ratio estimate for the percentage of mail to a given *destination*. In this section we give the specific chain-ratio formulas used in the San Francisco, Los Angeles, and Baltimore studies. We list the notations of the ratios involved, and the related formulas for determining the percentage of mail to a *destination* off the *Primary*, *Secondary*, and *Tertiary* stages.

a. Notations

In the discussion of the general method in section 3.1, ratios appear with and without parentheses. In the list of notations that follows, all ratios appear within parentheses. Throughout this paper we shall always denote parameters by ratios without parentheses, and unbiased estimates of these parameters will always be denoted by ratios within parentheses.

$\left(\frac{D_P}{T_P}\right)$ = Ratio of mail to a *primary destination* to the *primary volume*. Obtained from *primary* samples.

$\left(\frac{S_i'}{T_P}\right)$ = Ratio of mail to an i-th *secondary* to the *total primary volume*. Obtained from *primary* samples.

$\sum\left(\frac{S_i'}{T_P}\right)$ = Sum of ratios of mail to all *secondaries* to *total primary volume*. Obtained from *primary* samples.

$\left(\frac{S_i}{S_i'}\right)$ = Ratio of mail to an i-th *secondary* including *bypass* mail to the i-th *secondary* excluding *bypass* mail. Obtained from volume counts.

$\left(\frac{D_{S_i}}{S_i}\right)$ = Ratio of mail to an i-th *secondary destination* to the i-th *secondary*. Obtained from i-th *secondary* samples.

$\left(\frac{t_{ij}}{S_i}\right)$ = Ratio of mail to a j-th *tertiary* (off i-th *secondary*) to i-th *secondary*. Obtained from i-th *secondary* samples.

$\left(\frac{D_{t_{ij}}}{t_{ij}}\right)$ = Ratio of mail to a j-th *tertiary destination* (off i-th *secondary*) to the j-th *tertiary*. Obtained from the ij-th tertiary samples.

$\left(\frac{D_P}{T}\right)$ = Ratio of mail to a *primary destination* to the *total volume*. Obtained from chain-ratio formula.

$\left(\frac{D_{S_i}}{T}\right)$ = Ratio of mail to an i-th *secondary destination* to the *total volume*. Obtained from chain-ratio formula.

$\left(\frac{D_{t_{ij}}}{T}\right)$ = Ratio of mail to a j-th *tertiary destination* (off i-th *secondary*) to the *total volume*. Obtained from chain-ratio formula.

$\left(\frac{T_P}{T}\right)$ = Ratio of *primary* mail to the *total volume*. Obtained from volume counts.

$\left(\frac{B_S}{T}\right)$ = Ratio of *by-pass* mail entering at the *secondary* to the *total volume*. Obtained from volume counts.

$\left(\frac{T_S}{T}\right)$ = Ratio of total *secondary* mail to *total volume*. Obtained from volume counts.

$\left(\frac{\Sigma D_P}{T}\right)$=Sum of ratios of mail to all *destinations* off the *primary* to the *total volume*. Obtained from volume counts.

$\left(\frac{S_i}{T_S}\right)$=Ratio of mail to an i-th *secondary* to the total *secondary volume*. Obtained from volume counts.

$\left(\frac{D_P}{\Sigma D_P}\right)$=Ratio of mail to a *destination* off the *primary* to the sum of all *destinations* off the *primary*. Obtained from the *primary* samples.

b. Related Formulas

Two essentially different sets of formulas were used. The choice between the two depended upon whether or not the percentage of *secondary* mail that entered the system at each specific *secondary* case was readily available. This often entailed setting up special and difficult procedures for obtaining this ratio. In Baltimore we made special volume counts. In all cases the aim was to estimate the ratio of mail going to a given *destination* to the sum of *primary* and all *bypass* mail.

(1) For Baltimore, where the percentage of *bypass* mail entering the system at the *secondary* was large, the following formulas were used:

a. For a *destination* off the *primary:*

$$\left(\frac{D_P}{T}\right)=\left(\frac{D_P}{\Sigma D_P}\right)\times\left(\frac{\Sigma D_P}{T}\right). \tag{4}$$

b. For a *destination* off the *secondary:*

$$\left(\frac{D_{S_i}}{T}\right)=\left(\frac{D_{S_i}}{S_i}\right)\times\left(\frac{S_i}{T_S}\right)\times\left(\frac{T_S}{T}\right). \tag{5}$$

c. For a *destination* off the *tertiary:*

$$\left(\frac{D_{t_{ij}}}{T}\right)=\left(\frac{D_{t_{ij}}}{t_{ij}}\right)\times\left(\frac{t_{ij}}{S_i}\right)\times\left(\frac{S_i}{T_S}\right)\times\left(\frac{T_S}{T}\right). \tag{6}$$

It is to be noted that formulas (5) and (6) of this section depend upon special volume count data that give (S_i/T_S).

For examples worked out in detail, see the San Francisco study, section 5.

(2) For both San Francisco and Los Angeles, where the percentage of *bypass* mail entering the system at the *secondary* was very small, no special volume counts of mail into the *secondary* were made. Instead, the following formulas were used:

a. For a *destination* off the *primary:*

$$\left(\frac{D_P}{T}\right)=\left(\frac{D_P}{T_P}\right)\times\left(\frac{T_P}{T}\right). \tag{7}$$

b. For a *destination* off the *secondary:*

$$\left(\frac{D_{S_i}}{T}\right)=\left(\frac{D_{S_i}}{S_i}\right)\times\left(\frac{S'_i}{T_P}\right)\times\left(\frac{T_P}{T}\right)\times\frac{\left(\frac{T_P}{T}\right)\Sigma\left(\frac{S'_i}{T_P}\right)+\left(\frac{B_S}{T}\right)}{\left(\frac{T_P}{T}\right)\Sigma\left(\frac{S'_i}{T_P}\right)}. \tag{8}$$

c. For a *destination* off the *tertiary:*

$$\left(\frac{D_{t_{ij}}}{T}\right)=\left(\frac{D_{t_{ij}}}{t_{ij}}\right)\times\left(\frac{t_{ij}}{S_i}\right)\times\left(\frac{S'_i}{T_P}\right)\times\left(\frac{T_P}{T}\right)\times\frac{\left(\frac{T_P}{T}\right)\Sigma\left(\frac{S'_i}{T_P}\right)+\left(\frac{B_S}{T}\right)}{\left(\frac{T_P}{T}\right)\Sigma\left(\frac{S'_i}{T_P}\right)}. \tag{9}$$

The justification for eqs (8) and (9) is the following: Set up the chain

$$\frac{D_{S_i}}{S_i}\times\frac{S_i}{S'_i}\times\frac{S'_i}{T_P}\times\frac{T_P}{T}.$$

Note that S_i/S'_i involves obtaining an estimate of the ratio of mail to an i-th *secondary* including *bypass* mail to the i-th *secondary* excluding *bypass* mail. As mentioned above this was difficult to accomplish in practice. However if $S_i/S'_i=S_j/S'_j$ for all i and j, then

$$\frac{S_i}{S'_i}=\frac{\sum S_i}{\sum S'_i}.$$

The quantity $\sum S_i/\sum S'_i$ can be written as

$$\frac{\frac{T_P}{T}\sum\frac{S'_i}{T_P}+\frac{B_S}{T}}{\frac{T_P}{T}\sum\frac{S'_i}{T_P}}. \tag{10}$$

Using the "propagation of error" formula, we obtain an estimate of (10) as

$$\frac{\left(\frac{T_P}{T}\right)\Sigma\left(\frac{S'_i}{T_P}\right)+\left(\frac{B_S}{T}\right)}{\left(\frac{T_P}{T}\right)\Sigma\left(\frac{S'_i}{T_P}\right)}. \tag{11}$$

Each of the estimates involved in (11) could be easily obtained. Thus we have eq (8). Justification for eq (9) follows similarly.

If the assumption $S_i/S'_i=S_j/S'_j$, for all i and j, is not true then eq (8) and (9) still apply approximately providing the ratio $\sum S_i/\sum S'_i$ is close to one. We confined the use of these formulas to those ap-

plications where the ratio of *bypass* mail to the *secondary* to the total *secondary* mail was small (San Francisco, 0.8 percent; Los Angeles, 2.5 percent).

3.3. Methods of Collecting Data

a. Volume Data

Certain ratios needed to be established in order to relate the pieces of mail counted in each *separation* of the sample to the *total volume* of mail. It was therefore necessary to acquire from volume counts in the post office the following data.

Daily volume information expressed in footage for: *a*. All mail into the *primary*; *b*. all mail bypassing the *primary* and entering the *secondary*; *c*. all *bypass* mail to the city; *d*. all mail into each individual type *secondary* case. (This count may not be necessary, see section 3.2(b).)

Items *a*, *b*, and *c* above are normally maintained daily by the post office. Item *d* usually involves special volume counts. From the data listed above it is possible to determine the ratio of each class and type processed to the *total volume* of mail. Several of these ratios are then utilized in the formulas of section 3.2(b) to estimate the percentage of the *total volume* going to each *destination*. These volume figures were obtained at least 1 day prior to drawing the sample so that decisions regarding the type of analysis to be used could be made early. Very often the analysis did not make use of certain volume ratios, such as those of *d* above, and therefore the particular volume counts could be discontinued. (See section 5.1 for example.)

b. Sample Data

(1) *Primary*. Two feet of mail was selected as it flowed into the *primary* cases from the canceling machines. It was placed on the ledge of the "test" case and distributed by a clerk. Special care was taken to make sure that no mail was added to or subtracted from the sample. After *distribution* had been made, the contents of each separation box were counted by the distributor and recorded by the supervising clerk (e.g., see fig. 3).

Special care was given to the choice of the sample. The randomness of the selection of the 2-ft tray was assured by choosing the first 2 feet flowing into the *primary* from the canceling machines at the predetermined time for drawing the sample. The mail accumulating in the stackers of a cancellation machine is fed from a moving conveyor belt that passes 7 or 8 persons, each of whom faces and places on the belt letters selected from those within his reach. Thus the letters undergo a fairly thorough mixing as they are being stacked so that the letters in any tray of mail sampled at this point would tend to have the property of randomness which is necessary in sampling studies. This method of sampling was selected in order to help eliminate the possibility of personal bias, conscious or unconscious, or personal responsibility for actual allocations.

However, *metered* mail and *patron segregated* mail, which does not undergo this mixing process at the facing table, was sampled differently. Any "bite" or "bunch" of this kind of mail may be addressed to the same *destination* and therefore would not have the required property of randomness. In this case successive letters were selected every few inches apart from each tier of mail until the required 2 feet was obtained. The distance between successive letters was predetermined and constant.

Two samples, each of which consists of about 580 letters, were drawn during the morning peak period and 2 during the evening peak period. Samples were taken for 5 successive days, exclusive of Saturday and Sunday, in order to obtain a fairly representative picture of the mail throughout the sampling period.

(2) *Secondary*. Mail flowing into the *secondary* comes either from the *primary* or from *bypass* mail. *Secondary* cases do not continuously generate enough mail to be sampled at any given moment. Each sample was drawn when enough mail was generated. In each case the sample used in the study was the first 2 feet of mail that accumulated after a case had been selected for sampling. After *distribution* had been made, the contents of each separation box was counted by the distributor and recorded by the supervising clerk. One sample was taken in the morning peak and one in the evening peak periods throughout the week.

(3) *Tertiary*. Mail flowing into the *tertiary* cases usually comes from the *secondary*. Therefore, it was possible to make counts on these cases only when enough mail was generated.

However, in cases where the required 2 ft did not generate, then smaller samples (i.e., whatever was available) were counted. Here again, after *distribution* had been made the contents of each separation box were counted by the distributor and recorded by the supervising clerk. Samples were taken once in the morning and once in the evening at peak periods throughout the week.

In order to satisfy the condition of statistical independence, we avoided, as much as possible, having the same letters represented in samples from more than one stage. Care was taken to record any mail dispatched during the sample period prior to the final count of each *destination* on *primary*, *secondary*, and *tertiary* cases. Thus missing observations were avoided.

4. Type of Mail Studied at San Francisco, Los Angeles, and Baltimore

The *total volume* of mail studied in the San Francisco, Los Angeles, and Baltimore Post Offices may be classified as outgoing first class letter mail of the following types:

1. Cancellation mail (machine and hand).
   a. *Stamped* mail to *primary*
   b. *Air* mail to *primary*
   c. *Specials* to *primary*

d. *Stamped* mail to *secondary* bypassing *primary*
e. *Stamped bypass* mail to city.

2. Noncancellation mail
   a. *Metered* to *primary*
   b. *Metered* to *secondary* bypassing *primary*
   c. *Air* mail to *primary*
   d. *Specials* to *primary*
   e. *Permit* to *primary*
   f. *Permit* to *secondary* bypassing *primary*
   g. *Penalty* to *primary*
   h. *Metered* and *permit bypass* to city.
3. Transit mail [5]
   a. *Transit* to *secondary*
   b. *Transit* to city.

Not included in this study is any type of incoming letter mail nor outgoing first class letter mail of the following types:

1. All mail to *air* mail and *special delivery* sections bypassing *primary*.
2. *Transit* mail receiving no *distribution*.
3. Large special mailings which would tend to bias the sample.

5. San Francisco Study

In this section we present a rather detailed description of the application of the chain-ratio method in the study conducted in San Francisco.

5.1. Volume Count Data

Volume counts made in San Francisco enabled us to determine what percentage of the *total volume* flowed into the *primary*, how much bypassed the *primary* and flowed either into the city section for local *distribution* or into the *secondary*. These counts were made on 6 days, June 21, 24, 25, 26, 27, and 28, 1957, between the hours of 10 a.m. and 10 p.m. Control counts were begun one day prior to drawing samples, so that decisions regarding sample size and optimum sampling periods and areas could be made. Volume control counts showed that mail flowing into the *secondary* that bypassed the *primary* was less than 1 percent. Thus San Francisco was analyzed according to part 2 of section 3.2(b). Therefore, it was established early that a footage count of mail flowing into the *secondary* could be discontinued.

Percentages corresponding to the *total volume* figures are summarized in table 1. The flow chart given in figure 2 contains the basic proportion figures which are then applied in the appropriate formula, as well as certain other summary figures that are a result of the sampling study.

5.2. Sampling Procedure

The sampling procedure adopted for San Francisco is the same as that described in section 3.3(b) with the modification that, wherever possible, the samples were made to consist of equal parts of the following: Stamped long; stamped short; metered long; and metered short letters. This was done because San Francisco makes a separation between long and short letters which is maintained throughout the *primary* and *secondary* cases but not, however, in the *tertiary* cases. Furthermore, metered and nonmetered mail are worked separately throughout the *primary* and *secondary* cases. Moreover the volume of the different classifications were relatively equal. The volume of mail generated in the *tertiary* cases was very small during the morning sampling period. Therefore, no *tertiary* samples were taken during this period.

Figure 3 shows copies of sample field data for the *primary*, a typical *secondary*, and a typical *tertiary* at the San Francisco post office. Each column represents samples taken on each of the 5 consecutive sampling days. Application of the formulas to an example from each stage is shown in section 5.4.

TABLE 1. *Percentages obtained from volume count data supplied by the San Francisco Post Office during the test period*

Date	Primary	City bypass	Secondary bypass
	%	%	%
6-21-57	84.13	15.87	0.00
24	89.44	10.42	0.14
25	89.59	9.97	.46
26	85.66	14.03	.31
27	85.55	14.04	.41
28	86.34	13.40	.26
Average %--------	86.74	13.00	.26

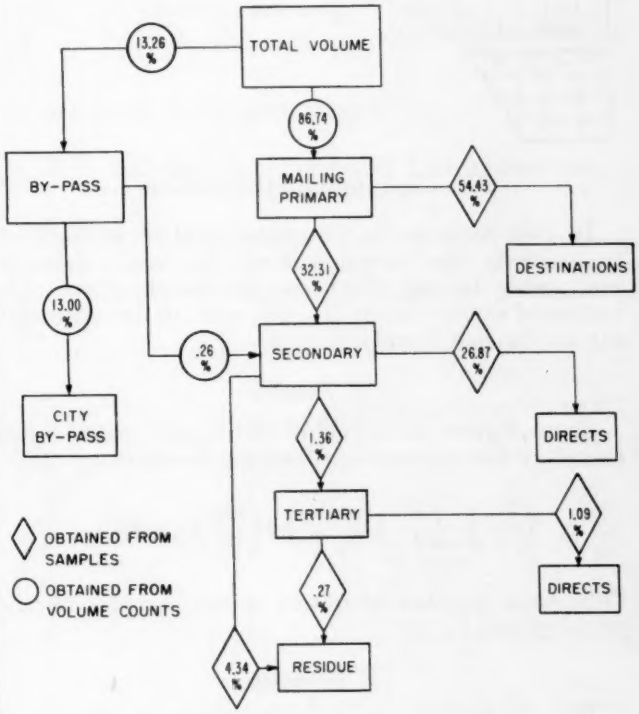

FIGURE 2. *San Francisco flow chart.*

[5] Mail received from another post office for outgoing processing.

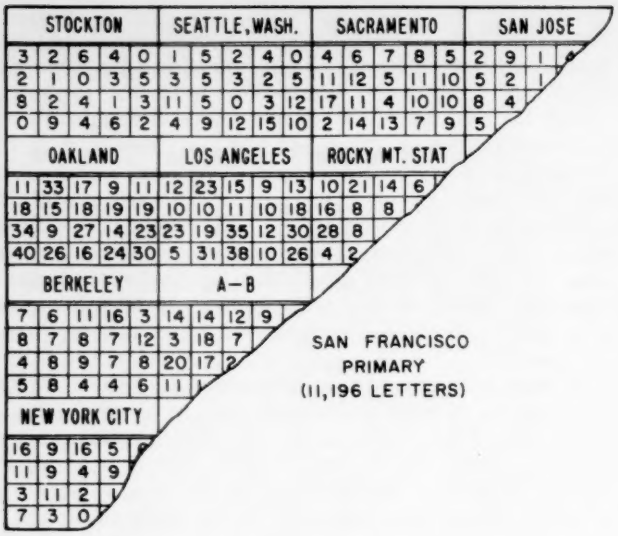

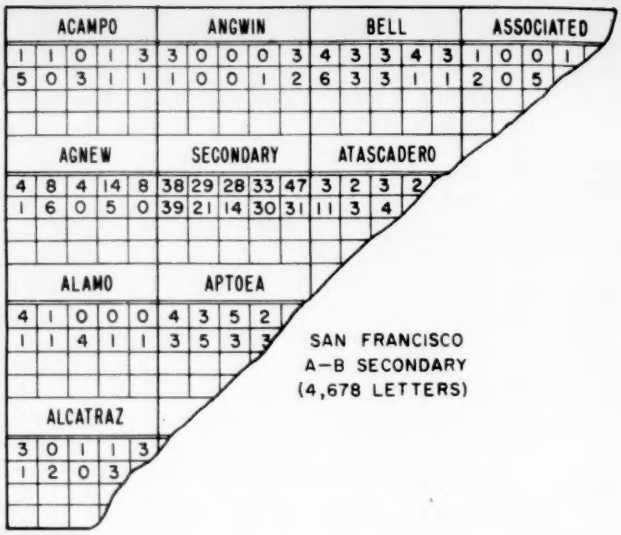

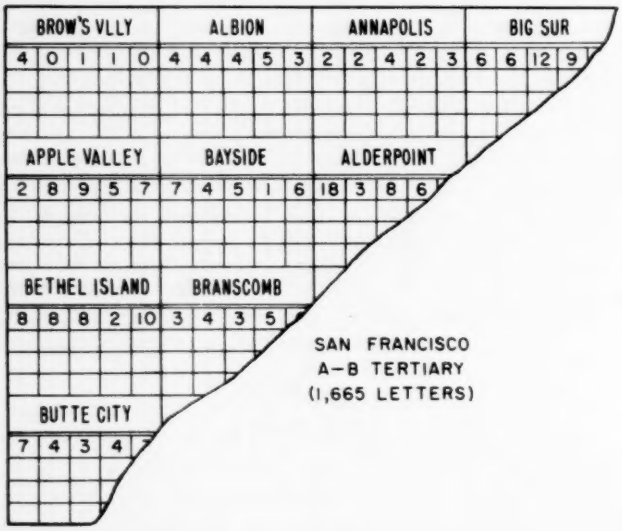

FIGURE 3. *Partial view of sample data for three San Francisco cases (worksheets).*

5.3. Computational Formulas

In this section the computational formulas used to estimate the percentage of the *total volume* of mail going to any given *destination* are given. As indicated above the eq (7), (8), and (9) are appropriate to the San Francisco study.

a. Primary

From figure 2 the value of $(T_p/T)=0.8674$ and therefore the appropriate formula becomes:

$$\left(\frac{D_P}{T}\right)=\left(\frac{D_P}{T_P}\right)\times\left(\frac{T_P}{T}\right)=\left(\frac{D_P}{T_P}\right)\times 0.8674.$$

(The total number of letters in the samples off the *primary* was 11,196.)

b. Secondary

The computational formula for *destinations* off the *secondary* depends upon the ratios obtained at the *primary* as well as the volume counts. Using such ratios gives the formula:

$$\left(\frac{D_{S_i}}{T}\right)=\left(\frac{D_{S_i}}{S_i}\right)\times\left\{\left(\frac{S_i'}{T_P}\right)\times\left(\frac{T_P}{T}\right)\times\frac{\left(\frac{T_P}{T}\right)\Sigma\left(\frac{S_i'}{T_P}\right)+\left(\frac{B_S}{T}\right)}{\left(\frac{T_P}{T}\right)\Sigma\left(\frac{S_i'}{T_P}\right)}\right\}=\left(\frac{D_{S_i}}{S_i}\right)\times c_i,$$

where the c_i are the quantities in brackets which depend upon the particular *secondary*. Values of c_i corresponding to particular *secondaries* are listed in table 2.

These constants actually represent the ratio, as estimated by using volume and *primary* sample counts, of a *secondary* volume of mail to the total *volume*.

TABLE 2. *Number of pieces in sample and constants used in computational formula for destinations off the secondaries for San Francisco*

i	S_i	Number of pieces	c_i
1	Ariz.-N. Mex.-Tex.	5,519	0.01290
2	Ill.-Ind.-Iowa-Mass.-Mich.-Minn.	5,739	.01774
3	Southern States	5,865	.01468
4	Rocky Mountain States	5,252	.02266
5	N.Y.-N.J.-Ohio-Pa.	6,286	.02289
6	Canada-Eastern	5,535	.01797
7	Calif. A–B	4,676	.02180
8	Calif. C–D	4,945	.02367
9	Calif. E–G	4,499	.01351
10	Calif. H–L	4,989	.02383
11	Calif. M–O	4,994	.02702
12	Calif. P–R	5,049	.03024
13	Calif. S	4,759	.02031
14	Calif. San Santa	4,893	.03446
15	Calif. T–Z	4,596	.02203
	Total	77,596	0.32571

C. Tertiary

The computational formula for *destinations* off the *tertiary* depends upon ratios obtained at the *primary* and *secondary*, as well as the volume counts. Using such ratios gives the formula:

$$\left(\frac{D_{t_{ij}}}{T}\right)=\left(\frac{D_{t_{ij}}}{t_{ij}}\right)\times\left\{\left(\frac{t_{ij}}{S_i}\right)\times\left(\frac{S_i'}{T_P}\right)\times\left(\frac{T_P}{T}\right)\times\frac{\left(\frac{T_P}{T}\right)\Sigma\left(\frac{S_i'}{T_P}\right)+\left(\frac{B_S}{T}\right)}{\left(\frac{T_P}{T}\right)\Sigma\left(\frac{S_i'}{T_P}\right)}\right\}=\left(\frac{D_{t_{ij}}}{t_{ij}}\right)\times k_{ij},$$

where the k_{ij} are the quantities in brackets which depend upon the particular *tertiary*. Values of k_{ij} corresponding to particular *tertiaries* are listed in table 3.

These constants actually represent the ratio, as estimated by using volume counts and *primary* and *secondary* sample counts, of a *tertiary* volume of mail to the *total volume*.

TABLE 3. *Number of pieces in sample and constants used in computational formula for destinations off the tertiaries for San Francisco*

i,j	t_{ij}	Number of pieces	k_{ij}
7,1	Calif. A–B	1,665	0.00145
8,1	Calif. C–D	2,507	.00277
9,1	Calif. E–G	1,727	.00081
10,1	Calif. H–L	2,648	.00229
11,1	Calif. M–O	2,086	.00185
12,1	Calif. P–R	2,262	.00135
13+14,1	Calif. S	1,118	.00107
15,1	Calif. T–Z	2,152	.00202
	Total	16,165	.01361

5.4. Examples

Applications of the formulas for each stage are given here.

Primary: (Seattle, Wash.)

D_P=111 pieces—Seattle, Wash.

T_P=11,196 pieces—Total primary

where the numbers are taken from figure 3. Thus,

$$\left(\frac{D_P}{T}\right)=\left(\frac{D_P}{T_P}\right)\times 0.8674=\frac{111}{11,196}\times 0.8674=0.0085996.$$

Secondary: (Bell, Calif.)

D_{S_7}=31 pieces—Bell, Calif.

S_7=4,676 pieces—Total Calif. A–B Secondary

where the numbers are taken from figure 3. Thus,

$$\left(\frac{D_{S_7}}{T}\right)=\left(\frac{D_{S_7}}{S_7}\right)\times c_7=\frac{31}{4,676}\times 0.02180=0.0001445$$

where the constant c_7 is taken from table 2.

Tertiary: (Albion, Calif.)

$D_{t_{7,1}}$=20 pieces—Albion, Calif.

$t_{1,1}$=1,665 pieces—Total Calif. A–B Tertiary

where the numbers are taken from figure 3. Thus,

$$\left(\frac{D_{t_{7,1}}}{T}\right)=\left(\frac{D_{t_{7,1}}}{t_{7,1}}\right)\times k_{7,1}=\frac{20}{1,665}\times 0.00145=0.0000174$$

where $k_{7,1}$ is taken from table 3.

5.5. Tabulation of Estimated Distribution and Observations

Part of the tabulation of the estimated proportions of the *total volume* mail going to each *destination* is given in table 4. Figure 4 graphically portrays the

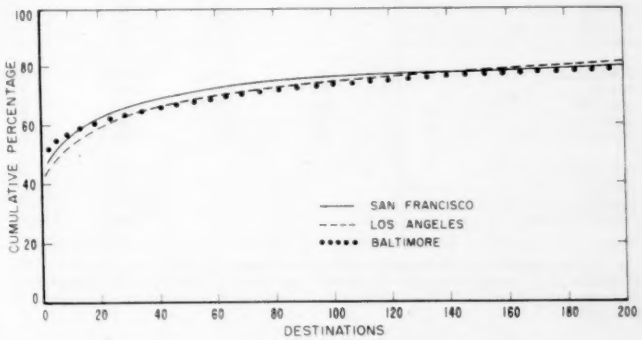

FIGURE 4. *Graph of largest 200 destinations for San Francisco, Los Angeles, and Baltimore post offices.*

TABLE 4.—*Tabulation of estimated percentages of the total volume to each direct destination for San Francisco*

Largest 200 direct destinations	Percent *	Cumulative percent
1. San Francisco Inc. City bypass	38.501	38.501
2. Oakland, Calif	8.158	46.659
3. Los Angeles, Calif	2.789	49.448
4. Sacramento, Calif	1.364	50.812
5. Washington State	1.155	51.967
6. Berkeley, Calif	1.147	53.114
7. New York City, N.Y	1.116	54.230
8. San Jose, Calif	0.961	55.191
9. Seattle, Wash	.860	56.051
10. Oregon State	.775	56.826
11. San Mateo, Calif	.759	57.585
12. Redwood City, Calif	.679	58.264
13. Daly City, Calif	.670	58.934
14. Palo Alto, Calif	.654	59.588
15. Fresno, Calif	.612	60.200
16. Portland, Oreg	.605	60.805
17. South San Francisco	.574	61.379
18. Chicago, Ill	.566	61.945
19. San Rafael, Calif	.521	62.466
20. Stockton, Calif	.504	62.970
21. Burlingame, Calif	.396	63.366
22. Menlo Park, Calif	.394	63.760
23. Santa Rosa, Calif	.352	64.112
24. San Diego, Calif	.349	64.461
25. Vallejo, Calif	.295	64.756
. . .	.	.
. . .	.	.
. . .	.	.
196. Wilmington, Calif	0.030	79.907
197. Lakeport, Calif	.030	79.937
198. Willits, Calif	.029	79.966
199. Porterville, Calif	.029	79.995
200. Placerville, Calif	.029	80.024

Rank	Number in group	Individual percent	Group percent	Cumulative percent
201–204	4	0.029	0.116	80.140
205–207	3	.028	.084	80.224
208–214	7	.027	.189	80.413
215–220	6	.026	.156	80.569
221–225	5	.025	.125	80.694
226–231	6	.024	.144	80.838
232–239	8	.023	.184	81.022
240–249	10	.022	.220	81.242
250–256	7	.021	.147	81.389
257–264	8	.020	.160	81.549
265–281	17	.019	.323	81.872
282–292	11	.018	.198	82.070
293–304	12	.017	.204	82.274
305–321	17	.016	.272	82.546
322–335	14	.015	.210	82.756
336–360	25	.014	.350	83.106
361–380	20	.013	.260	83.366
381–401	21	.012	.252	83.618
402–429	28	.011	.308	83.926
430–467	38	.010	.380	84.306
468–505	38	.009	.342	84.648
506–550	45	.008	.360	85.008
551–604	54	.007	.378	85.386
605–667	63	.006	.378	85.764
668–729	62	.005	.310	86.074
730–798	69	.004	.276	86.350
799–919	121	.003	.363	86.713
920–1087	168	.002	.336	87.049
1088–1271	184	.001	.184	87.233
1272–1296	25	<.001	.006	87.239
Air mail			3.200	90.439
Foreign			0.201	90.640
Residues			4.617	95.257
Miscellaneous			4.743	100.000

* The standard error of the estimated percentages, expressed as percents of the estimates, are between 10 and 15 percent for most of the first 200 *destinations*. For the very small percents the standard error may increase to as high as 35 percent.

largest 200 *destinations* by percentage for the Los Angeles and Baltimore studies as well as for San Francisco. Several observations, based on the tabulation, are given here:

1. The largest 200 *destinations* received 80 percent of the *total volume*.
2. Seventy-six percent of the *total volume* remained in the State of California (not including *air* mail).
3. Thirty-nine percent of the *total volume* remained in San Francisco.
4. Seven *destinations:* San Francisco, Oakland, Los Angeles, Sacramento, Washington State, Berkeley, and New York City were the only *destinations* to receive more than one percent of the *total volume*.
5. Eighty percent of the *total volume* remained on the West Coast (not including *air* mail).

An outstanding feature of the chain-ratio method of sampling is that emphasis may be placed on estimating relatively small percentages. Adaptation of the formulas of section 3.1 shows that the standard errors of the estimated percentages of mail to the various *destinations* considered in table 4 expressed as percents of the estimates, are between 10 and 15 percent for most of the first 200 *destinations*. Thus for Oakland, the estimated *relative* standard error is 10.4 percent so that the *absolute* standard error of the percentage of San Francisco mail having Oakland for its destination is 0.104×8.158 percent$=0.85$ percent so that the overall uncertainty is of the order of 3×0.85 percent$=2.6$ percent and there is very little likelihood that it has been misranked in order of volume.

For the examples in the "tail" of the distribution cited in section 5.4, the relative standard errors are somewhat larger. Thus for Bell, Calif., which ranks about 350, the relative standard error is 21 percent. Likewise for Albion, Calif., which ranks in the 920 to 1087 group, the relative standard error is 34 percent, or 0.0007 percent on an absolute basis, so that its overall uncertainty is of the order of ± 0.002 percent and its "true" ranking position may be as high as 730.

Examination of the complete listings of the San Francisco study given here and of the Los Angeles and Baltimore studies presented in [8] suggests that the proportion of mail to any given *destination* is related to (a) some measure of the "size" of the *destination*, and (b) the distance of the *destination* from the point of origin. Finally, there appears to be rather strong evidence that the distribution of mail plotted against the ranked *destinations* is rather close to a straight line on log-log paper.

Among the many colleagues who assisted in various ways toward the completion of this study, the authors particularly thank Marvin Zelen of NBS for his enthusiastic encouragement and helpful suggestions and Inspector John Falconer of the Post Office Department for assistance in implementing and supervising the collection of the data involved in the sampling procedures.

6. References

[1] N. C. Severo, A. E. Newman, S. Young, and M. Zelen, Some applications of statistical sampling methods to outgoing letter mail characteristics, NBS Tech. Note No. 16 (PB151375).

[2] I. Rotkin, The mechanization of letter mail sorting, Proc. Eastern Joint Computer Conf., Dec. 1957.

[3] W. A. Wallis and H. V. Roberts, Statistics, A new approach (The Free Press, Glencoe, Ill., 1956).

[4] H. A. Freeman, M. Friedman, F. Mosteller, and W. A. Wallis, Sampling Inspection, p. 10 (McGraw-Hill Book Co., New York, N.Y., 1948).

[5] W. E. Deming, Some theory of sampling, p. 40, Chapters 2 and 7 (John Wiley & Sons, Inc., New York, N.Y., 1950).

[6] B. Epstein, R. Bacon, G. Prittham, L. Lewis, F. Grossman, and G. Miller, Jr., No. 561 Memorandum for Record, Eng. Branch, S.A.A. Division, Frankford Arsenal (August 1943).

[7] B. K. Bender and A. J. Goldman, Analytic comparison of suggested configurations for automatic mail sorting equipment, J. Research NBS, **63B**, 83 (1959).

[8] N. C. Severo and A. E. Newman, Distribution of mail by destination at the San Francisco, Los Angeles, and Baltimore Post Offices, NBS Tech. Note 27 (PB151392).

[9] N. C. Severo, A statistician and the post office; A case history in operations research, Transactions of the 1959 Conference of the Administrative Division of ASQC (March 1959).

WASHINGTON, D.C. (Paper 64C1–22)

JOURNAL OF RESEARCH of the National Bureau of Standards—C. Engineering and Instrumentation
Vol. 64C, No. 1, January–March 1960

Standard Free-Air Chamber for the Measurement of Low Energy X-rays (20 to 100 Kilovolts-Constant-Potential)[1]

Victor H. Ritz

(October 2, 1959)

A description of the new National Bureau of Standards "low" energy free-air chamber is given. The standard chamber is designed to measure the exposure dose in roentgens for X-ray beams generated at potentials from 20 to 100 kilovolts-constant-potential (kvcp) with filtrations ranging from 2 millimeters of beryllium to 2 millimeters of beryllium plus 4 millimeters of aluminum. The chamber has been compared with the National Bureau of Standards "medium" energy standard at 60, 75, and 100 kvcp with filtrations of 3, 3, and 4 millimeters of aluminum, respectively. The two standard chambers agreed to within 0.3 percent.

1. Introduction

The roentgen has been recommended [1][2] by the International Commission on Radiological Units and Measurements as the unit of exposure dose. A measurement with a free-air ionization chamber is the most convenient way to accurately determine the exposure dose in the low energy X-ray region. Design criteria for standard free-air chambers have been summarized by Wyckoff and Attix [2] in National Bureau of Standards Handbook 64 for moderately and heavily filtered X-rays generated at potentials from 50 to 500 kilovolts-constant-potential (kvcp).[3] Agreement to about 0.5 percent has been reached in international intercomparisons of the roentgen in this energy region. However, differences of 1 percent or more have been observed [3, 4] in intercomparisons involving lightly filtered low energy X-rays. Design criteria have recently been obtained [5] for 20 to 100 kvcp X-rays with filtrations ranging from 2 mm of beryllium to 2 mm of beryllium plus 4 mm of aluminum. The present paper will discuss the application of these criteria to the design of a "low" energy standard free-air chamber. The reader is referred to Handbook 64 and reference [5] for background information on the correction factors that are applied to free-air chamber measurements.

A schematic of a parallel plate free air chamber, viewed from above, is given in figure 1. The design of a standard chamber involves many compromises. The factors involved include the air attenuation, electric field distortion, electronic equilibrium, electron ionization loss and scattered photon contribution. The largest correction in the "low" energy X-ray region is for the attenuation of the X-ray beam by the air between the chamber diaphragm and the collecting plate. This may be reduced by decreasing the distance between diaphragm and collector. However, the resultant decrease in the distance between the guard strips and collector plate increases the field distortion in the collecting region [5]. In practice the field distortion limits the decrease in the length of the air path. The distance from the inside of the guard strips to the front edge of the collector must be large enough to achieve electronic equilibrium along the X-ray beam.[4] The resultant larger diaphragm to collector distances at the higher voltages and filtrations are partially offset by the decrease in the air attenuation coefficients at higher energies. The collimated beam of X-rays within the chamber interacts with the air to produce high speed electrons and secondary scattered photons. These scattered photons may in turn produce high speed electrons within the collecting volume. A measurement in roentgens requires a determination of the ionization from the high speed electrons produced by the collimated photons alone. The separation of the collecting and high voltage plates and the height of the collecting plate must be sufficiently large to allow the electrons from the collimated beam to expend most (>99 percent) of their energy in the air before striking the plates or guard strips. An excessively large plate separation will result in an unnecessary increase in the scattered photon contribution. The plate separation and height should be made as small as possible, consistent with the consideration of keeping the electron ionization losses smaller than 1 percent [5].

2. Description of the Low Energy Standard

The chamber is designed for 20 to 100 kvcp. X-rays with filtrations ranging from 2 mm of beryllium to 2 mm of beryllium plus 4 mm of aluminum.

[1] A portion of this work was supported by the U.S. Atomic Energy Commission.
[2] Figures in brackets indicate the literature references at the end of this paper.
[3] Kilovolts-constant-potential applied to the X-ray tube.
[4] Handbook 64 [2] recommends that the distance between the diaphragm and the front edge of the collector be adequate for electronic equilibrium. This assumes that none of the electrons generated between the diaphragm and guard strips are intercepted by the guard strips before reaching the collecting region. The distance from the inside of the guard strips to the front of the collector is the critical one in the chamber described here because its closely spaced guard strips intercept most of the electrons generated between the diaphragm and guard strips.

Various views of the chamber are shown in figures 1 to 4 and a list of important dimensions is given in table 1. The plate system is housed in a lead-lined steel box. All connections passing through the box are vacuum tight so that the box can be evacuated and filled with gases other than air if desired. The design of the diaphragm holder is such that the defining plane of the tungsten alloy diaphragm is inside the box. This reduces the air attenuation correction by decreasing the diaphragm to collector distance.

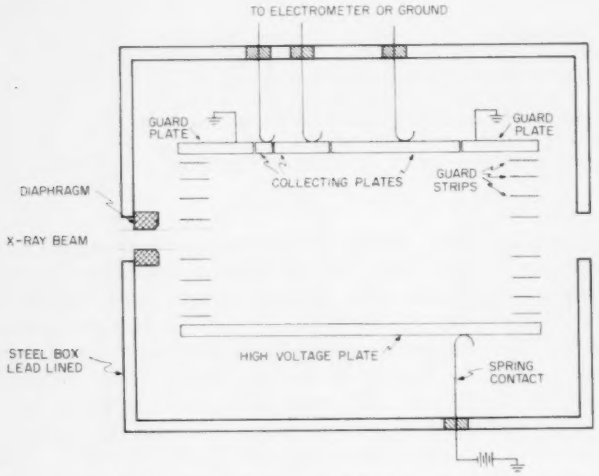

FIGURE 1. *Schematic of a parallel plate free air chamber, viewed from above.*

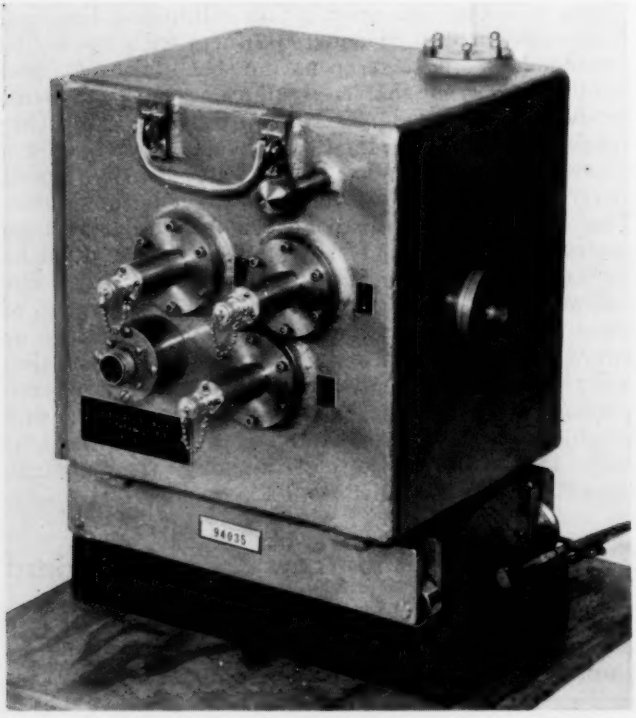

FIGURE 2. *Front, exterior view of the lead lined steel box (27 cm long × 22 cm wide × 27 cm high) housing the plate system.*

Connectors for the collecting plates, guard network monitor, thermocouple and an inlet for gas filling are visible on the side. The diaphragm and thermometer holders are seen on the front and top of the box, respectively.

FIGURE 3. *View of the chamber with the rear cover plate removed, showing the plate system in its normal position.*

The high voltage plate is at the left, the collector with its dust cover is at the right.

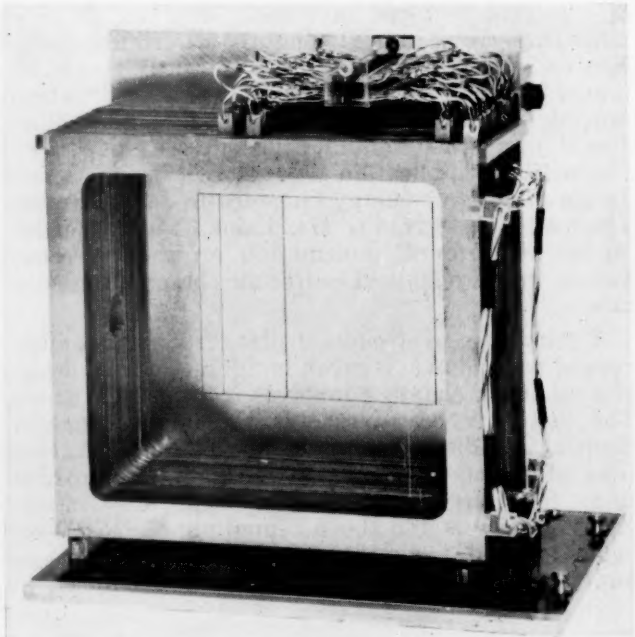

FIGURE 4. *Closeup of the collecting plate assembly and guard strips.*

The high voltage plate has been removed.

TABLE 1. *Important dimensions of "low" energy standard chamber*

Plate separation	9 cm
Collector lengths	1, 3, and 7 cm
Collector height	9 cm
Guard plate width	4 cm
Guard strips:	
Centerline to centerline spacing	0.2 cm [a]
Thickness	0.05 cm
Depth	1.5 cm
Air path from diaphragm to centerline of 1-cm collector	5.7 cm
Air path from diaphragm to centerline of 3-cm collector	7.7 cm
Air path from diaphragm to centerline of 7-cm collector	12.7 cm
Distance from inside of guard strips to closest edge of collector	2.5 cm

[a] Except strips immediately adjacent to the high voltage and collector plates which have a spacing of 0.1 cm.

Three aluminum collecting plates are provided: a 1-cm long collector closest to the diaphragm for use with the lowest energy X-rays; a 3-cm collector further away from the diaphragm for intermediate energy X-rays; and a 7-cm collector at the rear of the chamber for the highest energy X-rays. This arrangement minimizes the air attenuation corrections and provides the distances necessary for electronic equilibrium. Field distortion may be caused by a lack of coplanarity of the collectors with their guards [2]. The collectors and guards in this chamber were machined as a unit until they were coplanar to 0.00025 cm. A similar collecting plate assembly has maintained its planarity since its construction 13 months ago. The details of the collector construction are shown in figure 5. The 1-cm thick collectors are held on a yoke by screws which pass through Kel-F bushings. The collectors are insulated from each other and the guard plate by narrow air gaps ($\approx$0.018 cm wide) and from the yoke by a narrow strip of 0.025-cm-thick polyethylene. The backs of the collectors are shielded from dust by an aluminum cover. Spring-loaded contacts passing through the box and dust cover make contact with the collecting plates. Commercial cable connectors and low noise cable join the spring loaded contacts to the electrometer. Shorting caps on the connectors ground those collectors that are not in use.

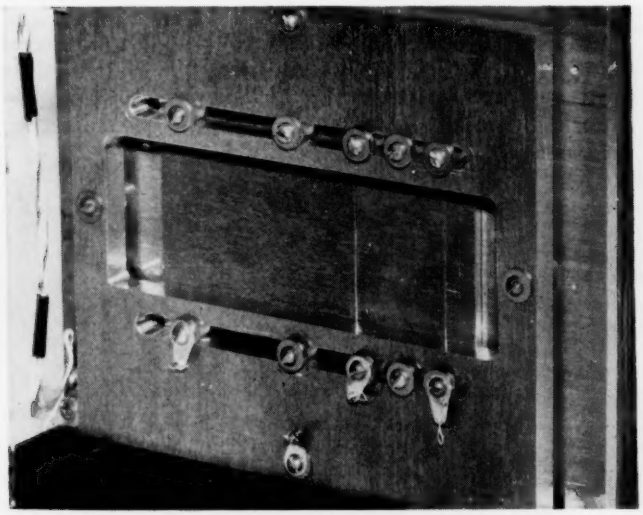

FIGURE 5. *Closeup of the back of the collecting plate assembly with the dust cover removed.*

The guard strips were milled from brass sheets and spaced by slotted Lucite bars which were made as small as possible to avoid field distortion effects from exposed insulators [5]. No change in the ionization current was observed when duplicate Lucite bars were added to the guard strip assembly. The potentials of the guard strips are determined by a network of megohm resistors which grades the potential linearly from the high voltage to the collector plate. The current through the network can be monitored by measuring the potential drop across a 50-K resistor in series with resistor chain. This permits easy detection of a shorted guard strip or an open resistor. Field distortion can also be caused by the presence of the grounded box or by the guard strips themselves [5]. The chamber was designed so that distortion from the guard strips was less than 0.1 percent. Distortion caused by the box was determined experimentally by measuring an exposure dose rate with the box alternately at the potential of the high voltage plate and at ground [2]. No change was observed for the 3-cm and 7-cm collectors. The box caused a 0.09-percent distortion at the 1-cm collector. This is not surprising since this plate probably "sees" the box through the entrance hole (2 cm in diam) cut in the guard strips for the X-ray beam.

The ionization measured by the various collectors is compared in table 2. The readings have been normalized so that the reading of the 7 cm collector is unity at each voltage and filtration. The data have been corrected for air attenuation, distortion of the electric field by the box and differences in the collector lengths. An inspection of the data taken for X-rays between 20 kvcp, inherent filtration, and 60 kvcp, inherent +0.5 mm Al filtration, reveals differences of $\pm$0.2 percent in the ionization measured by the collectors. This reflects uncertainties in the collecting volume caused by field distortion and difficulties in measuring the ionization currents and lengths of the collectors. These uncertainties are of the same order as those observed in a previous experiment [5]. The drop in the ionization measured by the 1 cm collector at 60 kvcp inherent +1 mm Al filtration was attributed to a lack of electronic equilibrium caused by an inadequate distance between

TABLE 2. *Ionization measured by the various collectors* [a]

Collector	Tube potential and filtration [b]					
	20 kvcp none	60 kvcp none	60 kvcp 0.5 mm Al	60 kvcp 1.0 mm Al	75 kvcp 3.0 mm Al	100 kvcp 4.0 mm Al
1 cm	0.999	0.998	0.998	[c] 0.994	[c] 0.994	[c] 0.990
3 cm	1.003	1.003	1.003	1.002	[c] 1.000	[c] .998
7 cm	1.000	1.000	1.000	1.000	1.000	1.000

[a] In addition to the inherent filtration of 2 mm of beryllium.
[b] The readings have been normalized so that the reading of the 7-cm collector is unity at each kilovoltage and filtration. The data have been corrected for air attenuation, distortion of the electric field by the box and differences in the collector lengths.
[c] See the text for a discussion of the influence of electronic equilibrium on the entries marked.

the inside of the guard strips and the front edge of the collector. The distance necessary for equilibrium at a particular energy may be taken to be approximately half the plate separation required at that energy [2]. Figures 7 to 10 of reference [5] may be used to determine the plate separation at which the electron ionization losses will be 0.05 percent. A good working criterion is to take half of this plate separation as the required equilibrium distance. Combinations in table 2 marked with "c" do not satisfy this criterion. It is seen that the relative readings of the various collectors is independent of the energy of the X-ray beam within the experimental error if electronic equilibrium has been achieved.

Some typical correction factors for the chamber are listed in table 3. The plate separation had to be adequate for 100-kvcp X-rays filtered by 4 mm of aluminum. This resulted in a chamber that was somewhat oversized for lower energy X-rays. For example, a free-air chamber designed for X-rays generated at or below 50-kvcp, 0.5-mm aluminum filtration, might have a 3-cm plate separation. The electron and scattered photon corrections would be about 0.7 percent and 0.15 percent, respectively, for such a chamber. The same chamber would have electron and photon corrections of <0.01 percent and 0.2 percent, respectively for 20 kvcp inherent filtration X-rays. Thus such a standard would have much smaller correction factors at "low" energies than the one described in this paper. Some accuracy at "low" energies was sacrificed in the present chamber to enable it to overlap the X-ray energy range covered by the NBS "medium" energy free air standard. A description of a comparison between the two chambers is given in the next section.

TABLE 3. *Typical corrections for the "low" energy standard chamber, in percent*

	Tube potential and filtration [a]					
	20 kvcp none	100 kvcp none	50 kvcp 0.5 mm Al	60 kvcp 3 mm Al	75 kvcp 3 mm Al	100 kvcp 4 mm Al
Collector used	1 cm	3 cm	1 cm	7 cm	7 cm	7 cm
Air attenuation	4.5	4.5	0.9	0.6	0.5	0.4
Photon contribution	0.70	0.70	0.54	0.41	0.38	0.30
Electron loss	<0.01	0.02	<0.01	0.02	0.11	0.71

[a] In addition to the inherent filtration of 2 mm of beryllium.

3. Intercomparison of NBS "Low" and "Medium" Energy Free-Air Chambers [4]

Details of the NBS "medium" energy standard instrument have been published elsewhere [6, 7]. The chamber, designed for X-rays generated at potentials up to 250 kvcp, has a 20-cm plate separation and a 30.8-cm air path between the diaphragm and the center of the collector. The "low" and "medium" energy chambers were mounted on carriages that rolled on a track perpendicular to the roentgen beam. Each standard chamber could be brought into the beam in turn. A 1.3-cm diam diaphragm on the tube housing, 17.5 cm away from the target, was used to collimate the beam. The ratio of the two standards was unchanged when the 1.3-cm diaphragm was replaced by one 2.5 cm in diam. The defining planes of the chamber diaphragms (1-cm diam) were 153 cm from the X-ray tube target. The chambers were alined optically and radiographically [2]. The focal spot lay within the "tunnel" formed by the extension of the sides of the chamber diaphragm. Aitken [8] indicates that there will be no alinement error in such a case. Separate charge measuring systems and chamber diaphragms were used in the intercomparison. A field gradient of 250 v/cm was used on both chambers. The inherent filtration of the X-ray tube used for the intercomparison was determined by a comparison of the measured half-value-layers, in mm of aluminium, with those obtained previously with a beryllium window tube [5]. Aluminum was added to the inherent filtration of 1.7 mm of Al to produce the different filtrations used in the intercomparison. The tube potentials, equivalent filtrations and half-value-layers used in the intercomparison are listed in table 4.

Measurements of the exposure dose rate in roentgens per minute were made alternately with each chamber. Corrections for air attenuation, electron losses and the scattered photon contributions were taken from Handbook 64. The ratios of the dose rates measured by the "low" energy standard chamber to those measured by the "medium" energy standard chamber are listed in table 4. The multiple entries at a given energy reflect day to day fluctuations in the ratio of the two chambers. The collecting

[4] April 1 to 9, 1959.

TABLE 4. *Results of the intercomparison*

Tube potential	Equivalent filtration	Half-value layer	"Low" energy chamber / "Medium" energy chamber		"Low" energy chamber / "Medium" energy chamber [a]
100 kvcp	2 mm Be+ 4 mm Al	3.9 mm Al	$.999_7$		
			$.997_7$	$.998_8$	$.997_1$
			$.998_1$	average	
75 kvcp	2 mm Be+ 3 mm Al	2.5 mm Al	$.998_5$	$.998_3$	
			$.998_1$	average	$.996_8$
60 kvcp	2 mm Be+ 3 mm Al	2.1 mm Al	1.000_8		
			$.999_8$	1.000_3	$.998_8$
				average	

[a] Corrected for collector plate warp.

plate of the "medium" energy standard chamber has warped and is no longer coplanar with its guards. It is estimated [2] that this causes it to read 0.15 percent too low. Application of this correction to the average ratios of the two chambers yields the results listed in the last column of table 4. Agreement between the two standard instruments is excellent, well within the ± 0.5 percent expected for such an intercomparison [2].

WASHINGTON, D.C. (Paper 64C1–23)

4. References

[1] NBS Handb. 62, Report of the international commission on radiological units and measurements (Superintendent of Documents, Government Printing Office, Washington, D.C., 1956).
[2] NBS Handb. 64, Design of free-air ionization chambers (Superintendent of Documents, Government Printing Office, Washington, D.C., 1957).
[3] R. Thoraeus *et al.*, Strahlentherapie **98,** 2 (1955).
[4] E. Bunde *et al.*, Acta Radiol. **44,** 163 (1955).
[5] V. H. Ritz, Design of free-air ionization chambers for the low energy X-ray region (20 to 100 kvcp) Radiology **73,** 911 (1959).
[6] H. O. Wyckoff, G. H. Aston and E. E. Smith, Brit. J. Radiol. **27,** 325 (1954).
[7] G. H. Aston and F. H. Attix, Acta Radiol. **46,** 747 (1956).
[8] J. H. Aitken, Phys. Med. Biol. **3,** 27 (1958).

JOURNAL OF RESEARCH of the National Bureau of Standards—C. Engineering and Instrumentation
Vol. 64C, No. 1, January–March 1960

Transmittance of Materials in the Far Infrared

Earle K. Plyler and L. R. Blaine

(October 27, 1959)

The transmittance of several crystalline materials with thicknesses of about 5 mm has been measured from 17 to 55 μ. The crystals are sodium chloride, potassium chloride, potassium bromide, thallium bromide-iodide, cesium bromide, and cesium iodide. Also the transmittance of a polyethylene film containing carbon black has been measured to 100 μ and an example of its use as a transmission filter for the far infrared is given.

Different optical crystals are used for prisms and windows in the infrared region. Another use of these materials is for chopper blades for measurements in the far infrared region. When they are used as choppers, only that radiation is modulated to which the specific crystal is opaque. This provides a powerful tool for eliminating the amplification of short wavelength stray radiation. For example, a chopper of CsBr would transmit all the radiation, except for reflection losses, from the visible to about 35 μ; any stray radiation or higher orders from the grating would not be observed, thus improving the purity of the spectrum at longer wavelengths.

In figure 1 is shown the transmittance of several materials from 17 to 55 μ. The materials are sodium chloride, potassium chloride, potassium bromide, thallium bromide-iodide (KRS–5), cesium bromide, and cesium iodide. All of these crystals are transparent in the near infrared and become opaque by or before 55 μ except CsI. It becomes opaque at about 75 μ for 5-mm thickness.[1] All of these crystals were obtained from the Harshaw Chemical Company, and the absence of absorption bands in the near infrared indicates a high purity. The wavelength range of transmission of the different crystals agree well with the results obtained in this laboratory and with results obtained in other laboratories on other samples of these materials which were characterized by indices of refraction measurements.

A filter which absorbs the short wavelength radiation, but which is transparent at long wavelengths, is useful in removing stray radiation. A good material for this purpose is polyethylene containing carbon black. A filter of this type may sometimes be used in place of the crystal chopper.

In figure 2 is shown the transmittance of polyethylene and polyethylene containing carbon black. The transmittance varies with the thickness of the film and the amount of carbon black included. A film with thickness of 0.05 mm transmits about 40 percent of the radiant energy at 15 μ, while a 0.2-mm film is only slightly transparent at 15 μ. Thicker

[1] Earle K. Plyler and Nicolo Acquista, J. Opt. Soc. Am. **48**, 668 (1958).

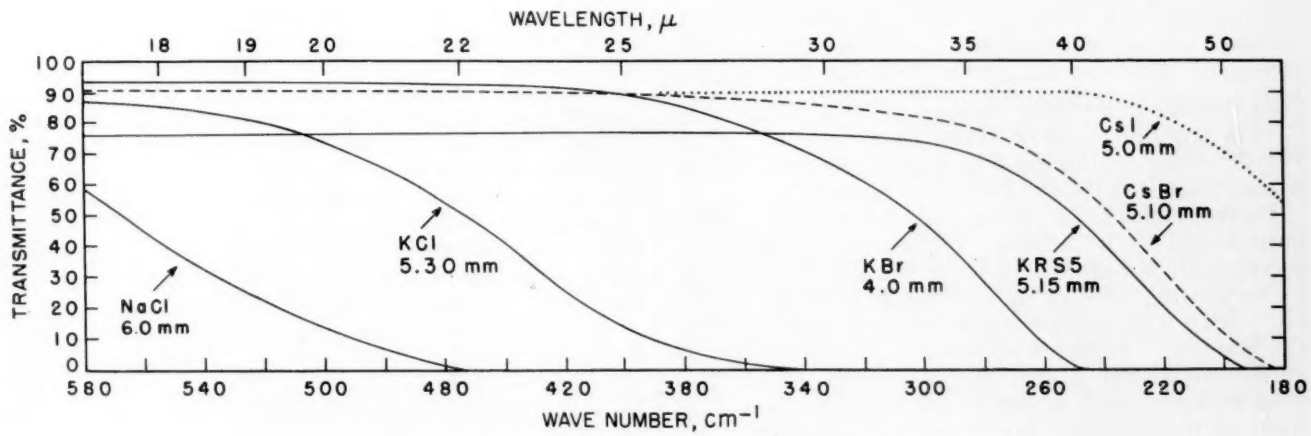

FIGURE 1. *The transmittance of several crystals in the infrared from 17 to 55 μ.*

No correction has been made for reflection losses.

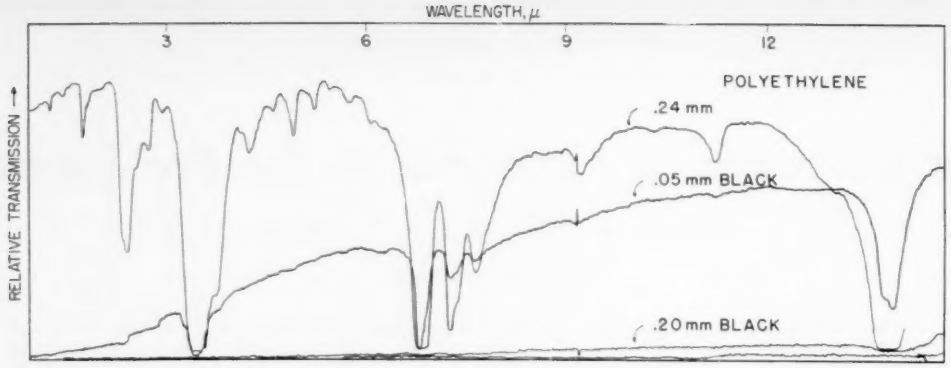

FIGURE 2. *The transmittances of clear polyethylene and polyethylene containing carbon black from 2 to 15 μ.*

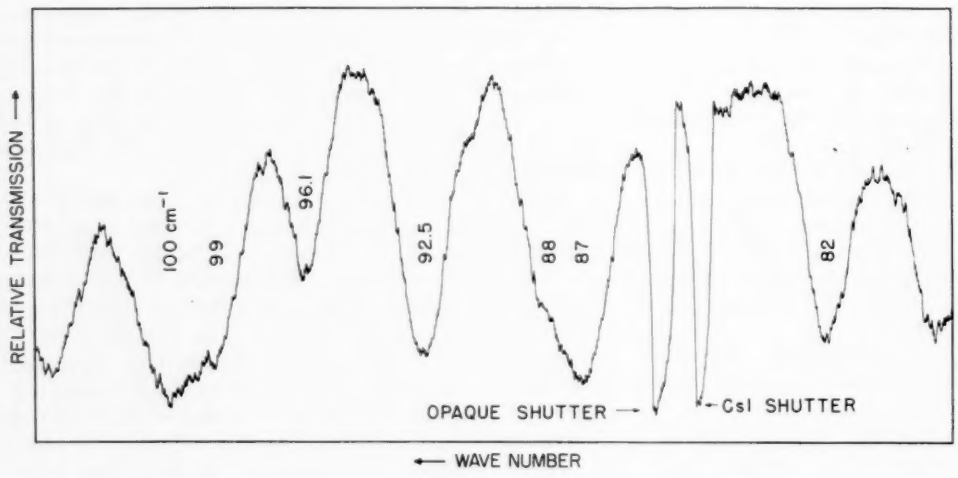

FIGURE 3. *The absorption spectrum of water vapor from 80 to 100 cm⁻¹.*

The amount of stray radiation is shown by a comparison of the two deflections for the interposed shutters.

films remain practically opaque to 30 μ, while they have a transmittance of about 80 percent at 100 μ. Polyethylene containing 2 to 4 percent carbon black is manufactured by the Bakelite Corporation.

Polyethylene films containing carbon black have been found to be efficient for removing the short wavelength radiation and their use has been tested by measuring spectra in the region from 80 to 110 cm^{-1} with a far infrared spectrometer developed at the Bureau.[2] Figure 3 shows a section of the water vapor rotational absorption spectrum which has been recorded with a film of polyethylene placed in front of the entrance slit of the spectrometer. Between the recording of the rotational lines at 82 and 87 cm^{-1}, an opaque shutter was placed in the beam of radiation and the zero deflection was obtained. Then the opaque shutter was removed and a window of CsI was placed in the beam which produces a second zero deflection. The readings of the zero points of the two shutters agreed closely, and the stray radiation in this part of the infrared spectrum has been determined to be less than 2 percent. Without the use of the polyethylene film the stray radiation was about 25 percent. This shows that the polyethylene black is an efficient transmission filter for eliminating all radiation except in the far infrared.

[2] Earle K. Plyler and L. R. Blaine, J. Research NBS **60,** 55 (1958) RP2821.

WASHINGTON, D.C. (Paper 64C1–24)

JOURNAL OF RESEARCH of the National Bureau of Standards—C. Engineering and Instrumentation
Vol. 64C, No. 1, January–March 1960

Equipment and Method for Photoelectric Determination of Image Contrast Suitable for Using Square Wave Targets

Fred W. Rosberry

(September 1, 1959)

Conventional measurements of the resolving power of lenses employ measuring photographs of test charts containing an array of accurately spaced parallel lines. This method has limited precision because of the variability of photographic emulsions and is time-consuming in operation. This paper extends previous work by others in obviating these differences by using a direct photoelectric scanning of a line-pattern image formed by the lens under test. Square wave high contrast resolving power targets with two different line pattern arrangements were used as test objects. The image was moved across a stationary slit and photomultiplier tube. The output was recorded as relative transmission.

1. Introduction

The evaluation of the performance or efficiency of a lens involves, to some degree, the comparison of the output with the input. The respective outputs and inputs are essentially areas of information with input represented by the object or target and the output by the resultant image. A visual comparison of the two represents a typical subjective type of test. An effort was made in the construction of this equipment to minimize the subjective type of test and emphasize the objective. An objective approach includes making some sort of measurements in the object area in order that a numerical comparison might be made with similar measurements in the image. There are several quantities which can be measured in these areas to determine the preservation of information content. It is known that there is a relation between information content and resolving power, the latter of which relates to the smallest distinguishable separation of separate objects and is probably affected by the contrast of the adjacent objects to be distinguished.

Many types of line pattern charts have been developed for testing resolving power. These charts consist of line patterns of varying spacings which proceed in some form of an orderly progression. For example, the ratio of line widths existing between adjacent patterns may be $\sqrt{2}$, $\sqrt[3]{2}$, $\sqrt[4]{2}$, or $\sqrt[6]{2}$. In one chart developed at NBS the values of resolving power, indicated by successive line patterns, vary continuously in a linear manner [1].[1] Each of these charts has some desirable features. Charts having large steps between successive patterns can cover a longer range of values of resolving power with a relatively small target area as compared to charts of a linear nature or those having small steps between successive patterns. Coarse charts permit a higher degree of repeatability, but a lower degree of precision with respect to the actual limit of resolution [2].

[1] Figures in brackets indicate the literature references at the end of this paper.

The actual determination of the focal location of this resolution limit can be avoided and yet similar results produced by a method which is based on the measurement of contrast in each of the line-space patterns in the image as it approaches the limit. Earlier work along these lines consisted of recording the image on a photographic plate and then scanning or measuring the line-space density with a microdensitometer which recorded the measurements in the form of a curve on graph paper, from which density values could be read [3]. This procedure soon led to the discovery that different types of photographic plates gave different results. The slower, fine-grain emulsions gave higher limits of resolution than did the faster coarse-grain emulsions. Different development procedures applied to the same type of plate would also produce a variation in results. It naturally followed that a procedure to eliminate this photographic variable was necessary. A different type of receiver was needed to supplement the photographic emulsion.

The photoelectric tube had already proven itself a suitable and reliable receiver. The linearity of response for increasing quantities of light is superior in the phototube to that of a photographic emulsion. The work of Schade [4] demonstrated one method in which the photographic process could be eliminated completely: Scanning the image with a narrow slit followed by a phototube measuring the flux which entered the slit. Another modification incorporated in this method is the use of a target which has its line-space transmission varying along a curve which is essentially sine wave. Targets used previously were square wave in transmission with the dividing edge between line and space a sharp line. The Schade apparatus, on the other hand, uses a rapidly moving target causing a rapid sinusoidal fluctuation in intensity at the receiving slit. The phototube and accessory equipment received and converted this signal, producing on a meter or recorder, a measurement of the amplitude of the

a-c component. As the test signal emitted from the target is a sine wave and reaches the receiving slit in the same waveform, the effect of the lens under investigation in the system was only to reduce the amplitude of the fluctuations. A comparison of the amplitudes leaving the target with those leaving the lens was handled in a mathematical manner to produce a term called "sine wave response." This equipment is now at the National Bureau of Standards and has been used in a number of investigations. One objection to the system has been the short length of line which it uses. The length of the lines is approximately 2 mm in the target plane as they are located on the sound track of 35-mm film. Rather than try to make a sine wave target with greater line length, an effort has been made to utilize the square wave target and scan it at a slower speed in order to register each individual line and space. Square wave targets are readily available with line lengths of 8 in. and, by using a long target line and relatively short scanning slit, the end effects of the line image are screened out by the scanning slit.

In brief, a method has been developed here involving the use of a microphotometer to study the aerial image of long line target transparencies. This method and a few representative results are described in this paper.

2. Description of Apparatus

The direct scanning of the image with a phototube was accomplished by arranging the microphotometer as shown in figure 1. A schematic layout is shown in figure 2. The source was a ribbon-filament lamp operated at 6 v and 18 amp by a suitable transformer, with a control for varying lamp intensity. Nine inches in front of the lamp were located the filter holder and condenser system. The target was

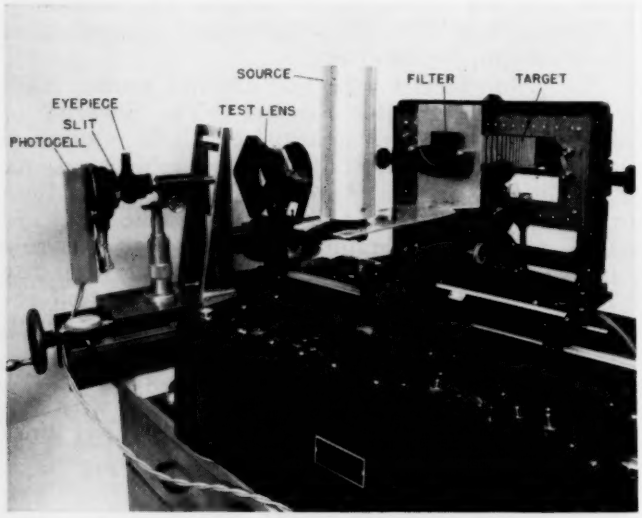

FIGURE 1. *Microdensitometer modified to accommodate lamp house and filter holder.*

The 3-line target is in place on the instrument cross slide. Test lens and receiving unit can be seen at left.

FIGURE 2. *Schematic layout of arrangement of equipment.*

The arrow indicates the component in the system which was moved during a test.

mounted on the traveling carriage of the microphotometer and driven by a motor which was synchronized with the paper drive of the recorder. The plane in which the target moved was perpendicular to the optic axis of the test system. The target was so designed that, to cover the required line-space frequency range in the image plane, it was necessary that the target be reduced in size by a factor of 25, or that it be placed a distance of 26 focal lengths from the lens under investigation. The test lens having a focal length of 6 in. thus required a target-to-lens separation of 13 ft. Available space in this laboratory did not allow such a spread of equipment, so the system was folded almost back upon itself by the use of a high quality front-surfaced mirror. The next component along the optical axis was the lens under test, which in this investigation was a typical distortion-free wide angle mapping lens including anti-vignetting filter. A microscope was focused on the focal plane of this lens which reimaged the target at 10 × magnification on a slit. Immediately behind the slit, in a light-tight enclosure was a phototube, the output of which was amplified and used as the input to a recorder which traced the transmission of the target image lines and spaces on a chart.

2.1. Description of Targets

The two targets used in this work were of the square wave type made at this laboratory. Each is on a 2- by 10-in. photographic plate used as a transparency. The geometry of the scanning system requires that only a small portion of the target be illuminated at one time. The only requirement was that the image of the illuminating aperture be larger than the receiving slit and this was relatively easy to accomplish. Another advantage of this system was that the distribution of light flux need not be exactly uniform over the illuminating aperture, as there was no movement of the illuminating aperture with respect to the slit. The targets were both high contrast, with the lines having a density of approximately 3.0 and the clear spaces a density of 0.05. The target was mounted on the scanning carriage of the microphotometer and moved through the light beam. The target speeds were constant for a given pattern but for coarse patterns the scanning speed was higher than for fine patterns. An effort was made to maintain a constant lines-per-minute scanning rate for the entire target by changing target speed with a gear transmission.

One of the two targets used was a 2-in.-wide strip of the multi-line, as shown in figure 3a. The range of this target is from 0.2 to 2.0 lines/mm which gave a range, in the image plane of the lens under test, of from 5 to 50 lines/mm at 25 times reduction. The second target was a 2-in.-wide strip of the 75-line target (fig. 3b) which is in the form of 25 groups of 3 equally spaced lines. The line and space widths were the same in a given group; however, the spatial frequency values varied from one group to the next by a ratio equal to $\sqrt[6]{2}$. The range of resolving power of this target was from 0.2 to 3.2 lines/mm and gave a corresponding range in the image plane of 5 to 79.6 lines/mm.

2.2. Mirror Assembly

The front-surface mirror used for folding the optical axis to satisfy space limitations does not show in the schematic diagram or the photographs. It was actually an end mirror borrowed from a 4-in. aperture interferometer. The front surface was of very high quality and flatness, aluminized to enhance the reflecting properties. This mirror was in turn supported on a rigid mount, with provision for minute rotational adjustments about horizontal and vertical axes. Adjustments of this unit were necessary only in the initial alinement of the equipment. The distance from the target to the mirror was roughly the same as the distance of mirror to lens under test, making both legs of the folded system approximately equal. A poor quality mirror at this point in the system would have had a disastrous effect on the results.

2.3. Lens Assembly

The lens to be investigated was mounted in a nodal slide as shown in figure 4 and this in turn was mounted on a saddle which slides parallel to the optic axis of the system. When the lens was correctly mounted in the slide, it could be moved about its vertical axis of rotation without displacing the image an appreciable amount to right or left of the receiving slit. This adjustment was not important for data taken only in axial positions as reported in this discussion, but a few trials were made at extra-axial positions. It was found that the equipment functioned equally well in off-axis positions, but results of these extra-axial positions are not reported here.

2.4. Receiving Unit

The receiving unit, shown in figure 1, was composed of the microscope, slit, and phototube with associated equipment such as amplifier and recorder. The microscope was of standard design, with the incorporation of an eyepiece at right angles to the line of sight and focused on the slit by means of a mirror, providing an opportunity to examine the image as it was focused on the slit. This feature was also necessary for making adjustments to render the line pattern in the image and the slit parallel. Adjustments could be made by rotating the slit with respect to the image. The microscope objective used in this work was a 10-power, 16-mm apochromat. The slit size was 35-μ wide by 10-mm long, which was somewhat shorter than the image of the

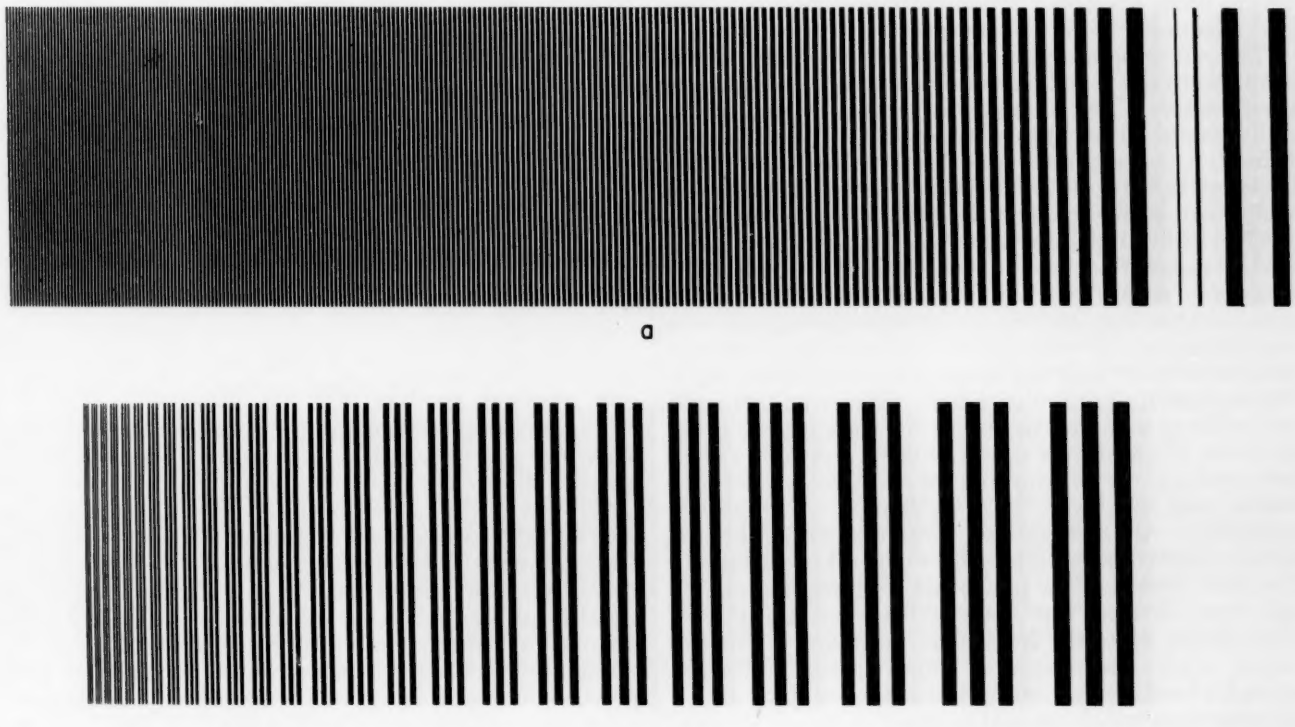

FIGURE 3. *Multiline (a) and 3-line (b) targets used in this investigation.*

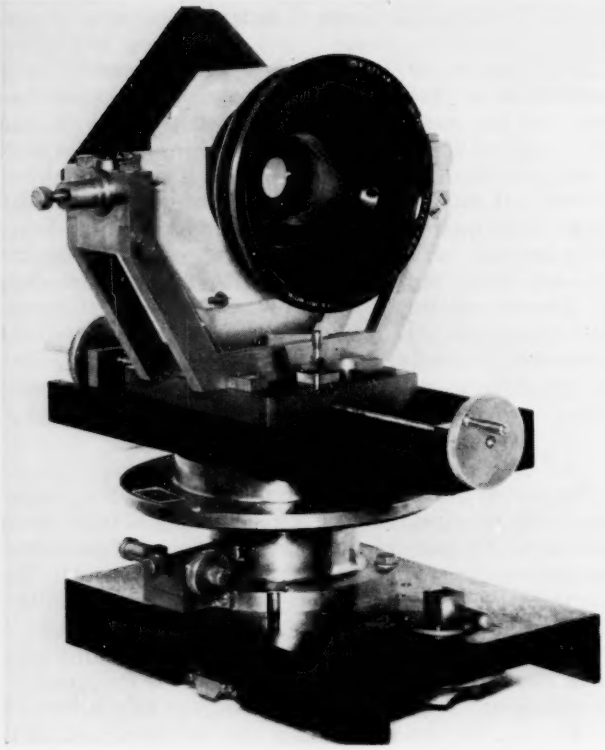

FIGURE 4. *Lens mounted in nodal slide.*

target lines, thereby virtually eliminating any of the end effects in the line patterns.

The slit support, phototube enclosure, and microscope were the standard receiving unit on the microphotometer. The phototube enclosure was originally made to accommodate a 921 type of phototube, but this did not have the necessary sensitivity for successfully recording the small flux densities which sometimes passed the somewhat narrow slit. A 1P21 photomultiplier tube was found to give much better results but would not fit into the standard housing. A new rear cover plate was made for the standard housing and the photomultiplier probe unit was attached to this cover. This separated the photomultiplier and slit about 2 in. which was more than a good design should allow. This was corrected by building a tunnel to collect all the flux emerging from the slit and pipe it to the tube. A high reflective coating on the interior of the tunnel reduced losses from scattering to a minimum. The photomultiplier unit had its own amplifier with four different ranges of sensitivity and a control for adjusting the dark current of the phototube. A small adapting unit was all that was necessary to run the microphotometer recorder from this amplifier. The recorder strip chart was a 100-division, uniformly spaced chart, which made the response plotted on a percent transmission scale.

The receiving unit, consisting of microscope, slit, and phototube, was mounted on one saddle similar to the one holding the nodal slide. Movement of one saddle with respect to the other was used as the means of locating a good focal plane of the lens. The nodal slide saddle was locked in position after the initial setup, and all focusing was done with the receiver unit. A dial indicator was fixed to the ways with its indicating probe in contact with the saddle for measuring the small displacements in focal position.

2.5. Alinement

Proper alinement of some of the components in this system was very important, while small misalinements in others did not appreciably affect the reliability of the data. The nodal slide and receiving unit were mounted on a short length of ways. It was important that the axis of these ways were parallel with the optical axis established by the light source and mirror. The target was mounted on the plate carriage of the microphotometer, thus establishing the direction of travel of the plate carriage perpendicular to the optical axis. Perpendicularity was checked by substituting a mirror for the target and adjusting the direction of the ways until reflected light from the source fell back upon itself.

The lens was mounted in the nodal slide with the aid of an axis finder to assure that the optical axis of the lens was parallel with the line of travel of the saddle on the ways. The lens was also located with its nodal point over the center of rotation of the nodal slide, thus assuring that the image would not move laterally from the receiving slit when the lens was rotated to simulate off-axis positions.

The microscope and slit combination were next alined along the axis established by the lens in the nodal slide. Alinement of these two components was important, as they were mounted on two different saddles, and focusing of the test lens was accomplished by varying the distance separating them. Misalinement here resulted in a lateral shift of the image when the lens-to-receiver distance was changed. The components on the ways were now in alinement with each other and it was relatively easy to make this optical axis coincident with the one for the whole system by moving the ways and saddles as a unit.

2.6. Calibration

The linearity of the amplifier, phototube, and the recorder was checked as a unit by substituting an adjustable slit for the fixed slit in front of the phototube unit. The space between slit and phototube was suitably masked to exclude all extraneous light, thus allowing only the slit to pass the light registering on the phototube. The recorder was then zeroed for dark current conditions. The slit was opened by small but uniform increments to its maximum opening. The amplifier and recorder thus produced a trace which was read and plotted against slit area to indicate the response of the system. The curve produced by these data verified the expected linearity of the system.

3. Description of a Typical Run

A typical run consisted of determining the response of 5 known spatial frequencies at 11 different focal positions on axis of a common type photographic objective. The response in the image was expressed in terms of contrast between lines and spaces. The target, figure 3a, provided a choice of 200 different spatial frequencies but to shorten the scanning and data handling time only 5 preselected frequencies were accurately measured, skipping over all intervening patterns. During a run the target was the only component in the system which moved. It could be moved slowly during measurement of each of the 5 frequencies and then moved rapidly through those between. The 5 spatial frequencies selected for measurement were 10, 20.5, 30.5, 40, and 63.5 lines/mm, but any or all others could have been used. A visual determination was made of the position of best focus and the first scan of the 5 frequencies was made at a focal position 1 mm back from this position. Starting at this long focal position a scan of the 5 frequencies was made at steps of 0.2 mm, to the other extreme of 1.0 mm inside of focus. This procedure produced a scan at 11 different focal positions. Measurement of the changes in focal position was accomplished with the dial indicator attached to the ways and bearing against the receiving unit saddle.

The traces produced by the recorder at each focal position were treated the same in that the maximum and minimum light transmission of each line and space of the predetermined frequency patterns was recorded. The contrast of each frequency was determined from the transmission data by using the formula

$$C=\frac{T_s-T_1}{T_s},$$

where T_s is the transmission of a space and T_1 of the adjoining line. These contrast data are plotted against spatial frequency in figure 5, which includes the 10 most informative of the 11 focal positions. There is a curve for each focal position, showing the manner in which the contrast decays toward zero. The larger numbers along the ordinate axis indicate the focal position and the smaller positive and negative numbers indicate the contrast scale. The abscissae represent the frequency in lines per millimeter. It will be noted that portions of the curves drop below the zero contrast value and have negative values. The negative values indicate the areas in which spurious resolution [5] is present and are only on the extreme short focus positions for this particular lens.

This equipment was found to lend itself very well to producing evidence showing what is taking place in these areas of spurious resolution. Two microphotometer traces of two aerial images are shown in figure 6. The trace which has the larger amplitudes represents a focal position close to best focus,

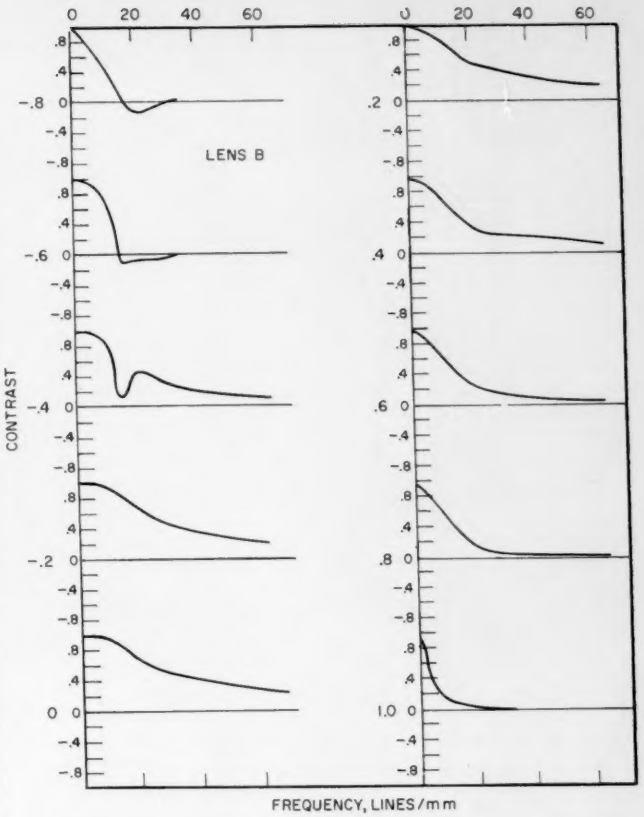

FIGURE 5. *A set of curves showing the contrast at various spatial frequencies of the direct scanned image as recorded at 10 different focal positions.*

Large numbers on the ordinate represent focal positions in millimeters.

and forms a good representation of the actual target in use as each line and space is registered in its relative position. The inner or low-amplitude trade represents a focal position 1.2-mm closer to the lens than the other trace. The two traces have been put in proper register with the maximum of the first line for the two traces in coincidence. It can be seen by following the inner trace that, for parts of the range of spatial frequency, the lines and spaces are registered out of phase and a line is indicated where a space should be. This indicates that, in this first zero point or node, one-half line has been lost, and the indicated resolution in this area to the next node is 180° out of phase. This is spurious resolution. At node two, another one-half cycle is lost. The area extending between nodes two and three shows the lines and spaces back in proper register but 360° out of phase, as one whole cycle has been lost.

The curves in figure 5 show the contrast as negative when the line-space register is out and positive when it is in. All of the contrast curve to the right of the first zero point represents spurious resolution.

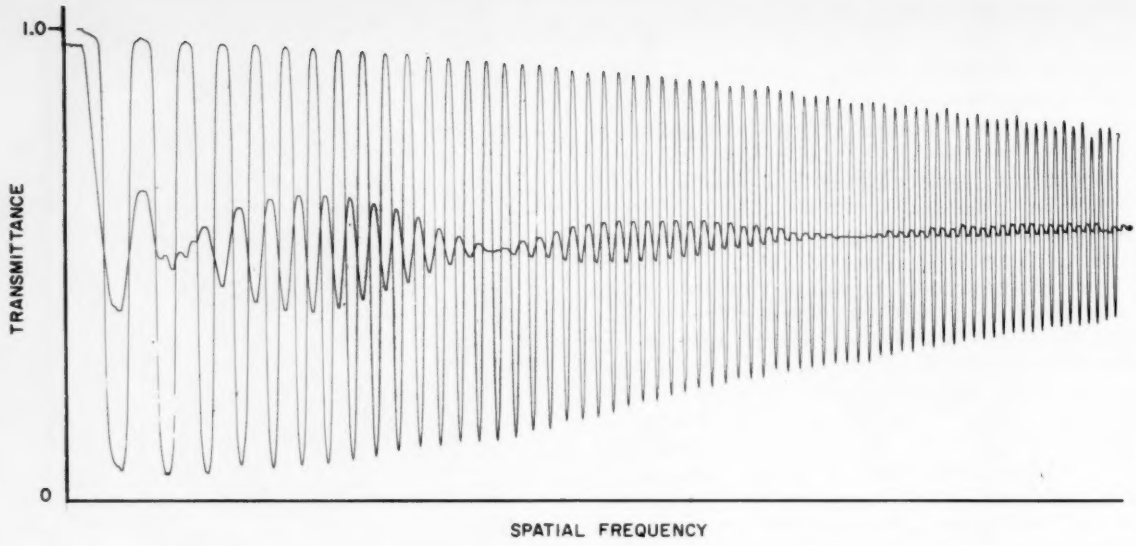

FIGURE 6. *Two microdensitometer traces made by direct scanning of the image.*
The trace with greatest magnitude was made at a position near best focus. Inside trace was made at a focal position 1.2-mm nearer lens. Note changes in phase.

4. Other Uses of Equipment

It is possible to insert color filters in the light path between the light source and target. The effective area of the receiving slit when projected back to the target is small enough to allow the use of standard 2-in. square filters. With the use of a suitable filter, investigative work can be carried out in a narrow spectral region. The use of several different narrow band filters permits the whole range of white light to be broken into as many narrow bands, which greatly reduces the effects of chromatic aberration within each band.

If repeated measurements of the same frequency pattern are made at different focal positions using the three-line target, it can be assumed that a best-focus position could be established by locating the position of maximum contrast rendition. This procedure was followed, using a filter and recording traces at 14 established focal positions. It was noted that at the various focal positions the contrast started at a low value, increased to a maximum, and then diminished. The filter was then changed to one which transmitted light in an adjacent spectral region. Another set of traces was taken using the same focal settings and noting the resultant contrast. This procedure was repeated using 6 different spectral regions to cover the range of visible wavelengths. When the 6 traces were arranged on a common focal position scale the results appeared as shown in figure 7. The numbers along the ordinate represent the Wratten filter number used to produce that trace, otherwise the ordinate scale is in transmittance. The spectral range passed by these filter numbers were: Blue with 45; green with 16 and 60; yellow with 90; orange with 25; and red with 29. Further investigation with different f/values and at off-axis positions could have easily been performed but exploration of the versatility of the equipment was the prime interest at the time.

Another image phenomenon which shows itself rather clearly can be seen by referring to figure 8. This illustration consists of two runs through focus in which the same spatial frequency pattern was scanned for each run. The upper run was the result of repetitive scans of a relatively coarse pattern of 5 lines/mm in the image while the lower run represents the response to the 64 lines/mm pattern. The unrestricted spectral range of a tungsten-lamp source was used for these traces. Close examination of the focal location of the two areas of maximum contrast shows a separation of about 0.2 mm. The values of contrast at each focal position could have been determined for these traces and curves of contrast versus focal position drawn to illustrate the same effect. The added work is not necessary here as the raw data alone indicate the results in a satisfactory manner.

The next experiment showing the possibilities of this apparatus involved making two apertures to be used as stops in the lens under investigation. These were constructed by depositing opaque material in the shape of a circle on thin cover glasses. The diameter of the full aperture of the lens at f/6.3 was measured and an annular ring was deposited which reduced the clear aperture of one-half the original area, or an f/value of 8.9. Another cover glass was used to make a negative of this aperture, which consisted of a circular opaque center with a transparent annular ring to transmit the light. The two apertures contain the same amount of clear area and are therefore the same f/value.

A full aperture (f/6.3) trace was made by again making repetitive scans of a constant spatial frequency 3-line pattern at 10 different focal settings

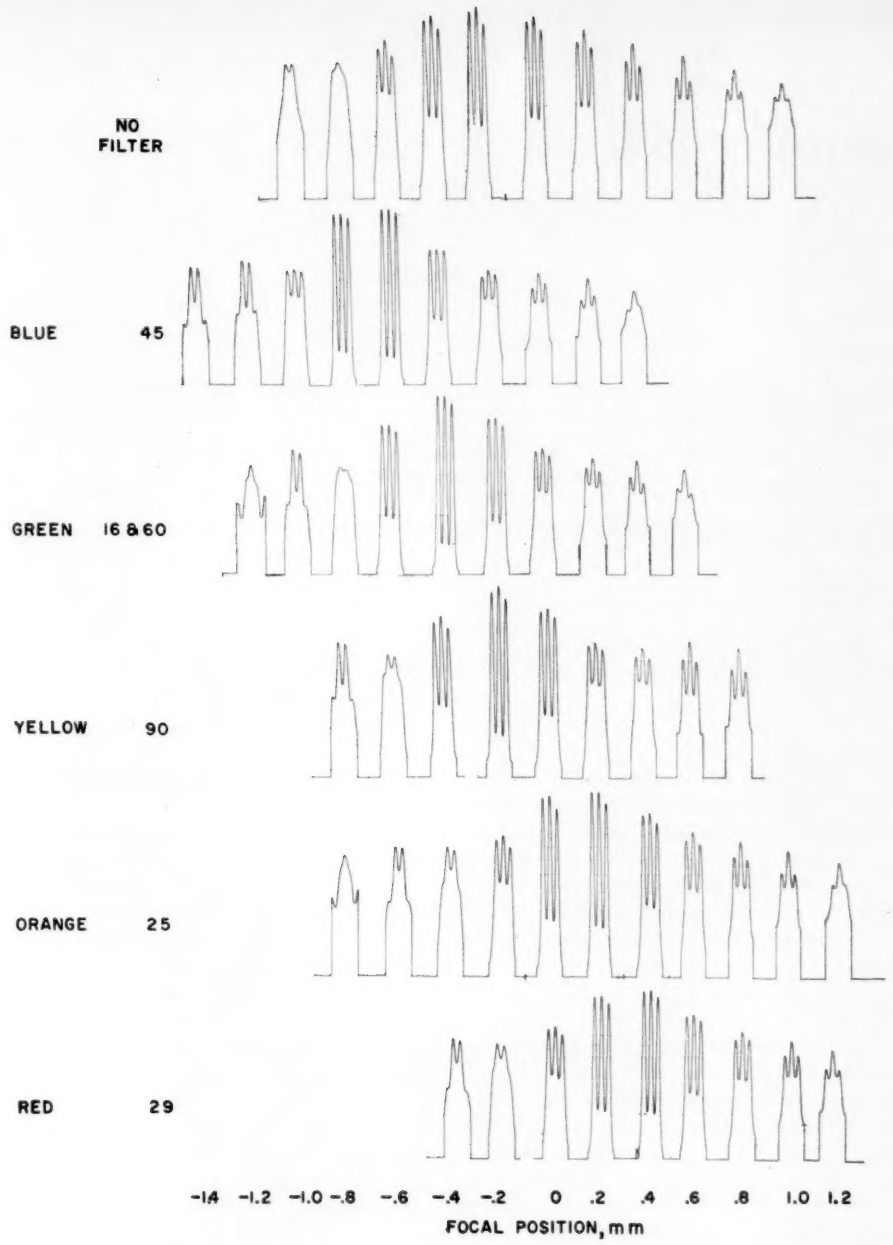

FIGURE 7. *Traces showing the response of a single 3-line pattern made at various focal positions.*
Each horizontal row was made in a different spectral region indicated by the filter number at the left. Note the shift in position of best focus.

while using a tungsten source as an illuminant. The full aperture trace was made with a clear cover glass in the same position the partially opaqued aperture stops were to occupy in the succeeding two runs. This was done to render constant the effect of the 0.1-mm glass thickness which was added to the lens system. Traces were then made with the two f/8.9 apertures, and the three traces arranged according to a common focal-position scale for comparison as seen in figure 9. A test along these lines might be used in a study of longitudinal spherical aberration in a lens system.

There are undoubtedly other areas of image evaluation which could be investigated with this equipment. One such area of study is that of star images, which was accomplished by substituting a camera for the photocell. One of the initial aims in building this apparatus was to reduce the time required for a lens test over the photographic method and this has attained that goal.

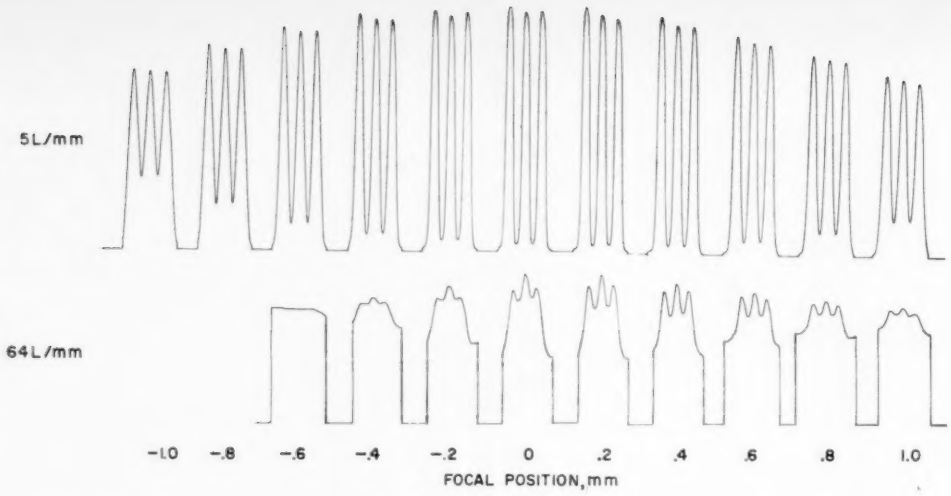

FIGURE 8. *Traces showing the response of two frequency patterns as indicated at left.*

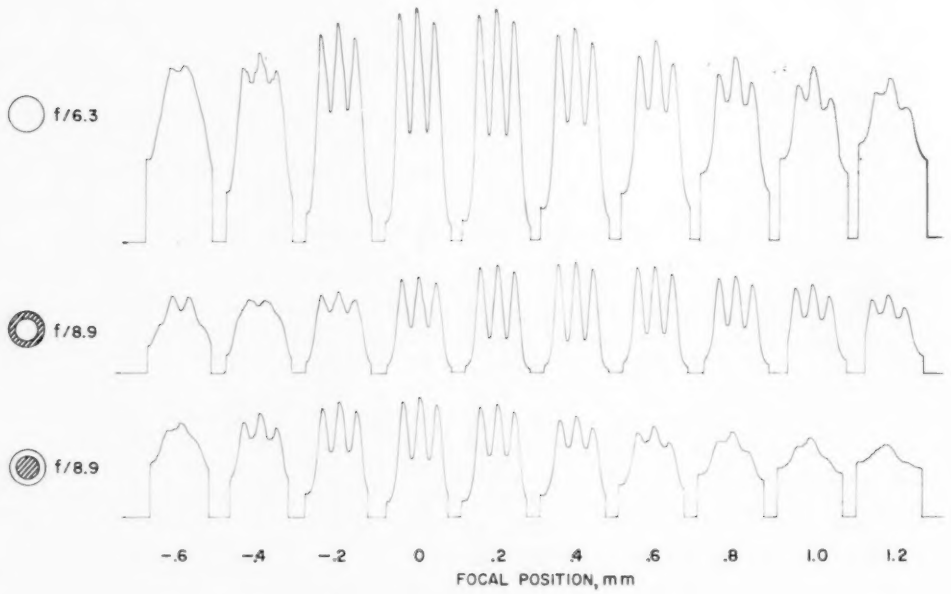

FIGURE 9. *Traces showing the response of repeated measurement of a single 3-line pattern at 10 different focal positions.*

Each horizontal row was made with a different aperture stop, the first stop was the normal, in the second the aperture was stopped down to f/8.9, and in the third the stop opening was shaped in the form of an annular ring with the same f/value as the second.

5. References

[1] F. E. Washer and F. W. Rosberry, New resolving power test chart, J. Opt. Soc. Am. **41** 9 (1951).

[2] F. E. Washer and I. C. Gardner, Method for determining the resolving power of photographic lenses, NBS Circ. 533 (1953).

[3] F. W. Rosberry, Effect of object frequency on focal position of four photographic objectives, J. Research NBS **57** 17 (1956) RP2688.

[4] O. H. Schade, A new system of measuring and specifying image definition, NBS Circ. 526 (1954).

[5] R. N. Hotchkiss, F. E. Washer, and F. W. Rosberry, Spurious resolution of photographic lenses, J. Opt. Soc. Am. **41** 9 (1951).

WASHINGTON, D.C. (Paper 64C1–25)

JOURNAL OF RESEARCH of the National Bureau of Standards—C. Engineering and Instrumentation
Vol. 64C, No. 1, January–March 1960

Formation of Silver Sulfide in the Photographic Image During Fixation

Chester I. Pope

(October 23, 1959)

A photographic silver image is made permanent (fixed) after development by bathing it in a solution containing thiosulfate which forms a soluble thiosulfate complex with the residual silver halide. Some of the silver in the image is sulfided by the thiosulfate during fixation. The purpose of this study was to determine the amount of sulfiding of the silver in the image during fixation of film and paper. The amount of the silver reacting depends on the type of the light-sensitive layer. Also, during bleaching, the residual thiosulfate in the film or paper reacts with silver in a potassium dichromate-sulfuric acid bleach bath to form silver sulfide. For one paper, it was shown that the amount of silver sulfide which was formed in the bleach bath increased with the increase of the concentration of the residual thiosulfate in the paper. A procedure was developed for the reduction of silver sulfide in an emulsion layer to silver so that the silver sulfide may be determined in terms of the optical density of the silver deposit. The use of hypo eliminators was investigated and a test procedure was found for testing the effectiveness of hypo eliminators. A small amount of potassium iodide added to the fixing bath was found effective in preventing most of the sulfiding of the silver image during fixation.

1. Introduction

A photographic silver image is made permanent (fixed) after development by bathing it in a solution containing thiosulfate which forms a soluble thiosulfate complex with the residual silver halide. Some of the silver in the image is sulfided by the thiosulfate during fixation. The permanence of the silver image in processed film and paper is related to the degree of sulfiding of the silver in the image which takes place during fixation and the amount of silver thiosulfate complex and thiosulfate which remain after the washing process. The purpose of this study was to determine the amount of sulfiding of the silver in the image during fixation of film and paper. A brown stain or "ghost" image remains when the silver in an image is removed by most bleaching solutions [1, 5, 6, 7, 8, 9, 11].[1] This stain has been identified as silver sulfide [1, 2, 3].

The silver sulfide residue which remains when a silver image is bleached may have three sources. The first is the reaction of the silver in the image with the thiosulfate during fixation. The amount of this sulfiding of the silver depends on the type of the sensitized emulsion. This silver sulfide is present before and after the silver has been bleached. The second source of silver sulfide is the residual silver thiosulfate complex and thiosulfate which have not been removed in the washing process and have not yet reacted with the silver in the image to form silver sulfide but do react in the bleach bath. This reaction was used to study the effect of different residual thiosulfate concentrations on the amount of silver sulfide formed in the bleach bath for one paper. A third source of silver sulfide may be traced to the residual silver thiosulfate complex and thiosulfate which have not been removed in the washing process but have reacted during storage to form silver sulfide. This silver sulfide is present before and after the silver has been bleached. The silver thiosulfate complex eventually decomposes to form silver sulfide. The residual thiosulfate, because of its labile sulfur, reacts with the silver in the image to form silver sulfide, especially at high relative humidities. The effect of excessive sulfiding of the silver image first appears in the areas of low silver density, the highlights, causing the image tone to become brownish. Eventually silver sulfide, itself, may bleach, particularly at high relative humidities and in the presence of excess salts which have not been removed during the washing process [4].

Levenson and Sharpe [11] made an intensive study of the role of thiosulfate in the formation of silver sulfide stains in a bromide emulsion during the bleaching process. They found that the stain was produced after the silver image had been in contact with thiosulfate either in the developer or after fixing in a sodium thiosulfate fixing bath. They exposed their samples to a step wedge and plotted the silver density and the stain density against relative values of the logarithm of exposure to show the amount of stain produced by the corresponding silver densities for a bromide fine-grain emulsion. They concluded that a certain amount of thiosulfate was strongly absorbed on the silver of the image as thiosulfate or as a thiosulfate complex and that it reacted with silver ions in the bleach to form silver sulfide. This subject is discussed further in section 6.

[1] Figures in brackets indicate the literature references at the end of this paper.

530231—60——5

2. Processing Procedures

Samples of the photographic film and paper were cut to 1⅜ in. by 10 in. and exposed to a step wedge. Not more than eight samples were processed or treated at one time. About 2 liters of fresh solution were used in each processing operation employing nominal 8- by 10-in. enameled trays. The samples were continuously agitated by hand during processing and washed in running tap water. The processing solutions are listed in the appendix, section 8. The temperature of the processing solutions were at room temperature (22° to 28° C).

2.1. Developing and Fixing the Silver Image

The samples were developed 3 min, treated 1 min in the short stop bath, and fixed 10 min in two baths (5 min in each bath). Next the samples were rinsed 1 min in tap water, treated 10 min in the hydrogen peroxide eliminator No. 1, bathed 2 min in a 1-percent solution of sodium sulfite, washed 30 min, and hung to dry at room temperature. Two fixing baths were used to facilitate the removal of the silver thiosulfate complex. Tests showed that the amount of silver sulfide formed in the silver image during fixation reached a maximum in about 3 min in the acid-hardening fixing bath.

2.2. Bleaching the Silver Image

The samples were treated 5 min in the dichromate bleach bath, washed 30 min in tap water at 25° ± 2° C, treated 5 min in the clearing bath, treated 3 min in the thiosulfate eliminator No. 3, and washed 30 min in tap water. The operation was performed in daylight but not in direct sunlight. The bleach removed the silver, leaving the silver sulfide which formed during fixation. Additional silver sulfide was formed when the silver thiosulfate complex or residual thiosulfate was present. The potassium dichromate-sulfuric acid bleach oxidized the silver in the image in 1 to 2 min. The bleach did not dissolve the silver-sulfide residue when the bleaching time was extended to 15 min. The clearing bath, which was used to remove the residual dichromate, was the one employed by Levenson and Sharpe [11] and proved to be quite satisfactory for both films and papers. It was found necessary to fix the samples after clearing to remove the last traces of silver salts which, when present, increased the density of the silver sulfide residue slightly.

2.3. Reduction of the Silver Sulfide to Silver

The samples were treated 2 to 3 min in the permanganate bleach bath, rinsed 10 sec in running tap water, treated 5 min in the clearing bath, washed 30 min in running tap water, blotted to remove surface water, and dried in the dark. The samples were then exposed for 10 min to a 100-w tungsten lamp at a distance of 12 in., developed 5 min in running tap water, and hung to dry. With the exception of the drying of the samples before exposure the operations were performed in daylight but not in direct sunlight.

The permanganate bleach converted the silver sulfide to silver chloride. The potassium bromide in the clearing bath prevented the loss of silver in the gelatin layer because silver chloride is more soluble than silver bromide. There was a partial solution of the silver chloride when sodium chloride was used in the clearing bath. Unfortunately, the gelatin layer was quite soft after treatment in the clearing bath and the high alkalinity of most developers caused the gelatin to break loose from the support. The amidol developer was found to be satisfactory for papers and most films. However, films with a normally soft gelatin layer should be washed 5 min after treatment in the clearing bath, treated 5 min in a 2-percent solution of formaldehyde, and washed 10 min before drying.

The reduction of silver sulfide in the gelatin layer to silver appeared to be quantitative. When this reduced silver was sulfided the original silver sulfide densities were again obtained. The silver was sulfided in an atmosphere of hydrogen sulfide. The sample of film or paper was soaked in water for 5 min and, after removing the surface water with a blotter, it was suspended for 1 hr in a ½-gallon bottle above a solution containing 50 g of sodium sulfide ($Na_2S{\cdot}9H_2O$), 35 g of citric acid ($H_3C_6H_5O_7{\cdot}H_2O$), and 500 ml of water. After this treatment the sample was washed for 30 min in running tap water.

3. Removal of the Thiosulfate During the Washing Process

The thiosulfate must be removed from processed films and papers when investigating the reaction of thiosulfate with the silver of the image during fixation. Solutions which remove the thiosulfate from the gelatin layer and paper base are generally known as "hypo eliminators." Crabtree et al. [13] showed that hydrogen peroxide in an ammoniacal solution eliminates thiosulfate from photographic materials. The hydrogen peroxide oxidizes the thiosulfate to sulfate. This hypo eliminator was used in the experimental work reported in this paper and is listed as formula No. 1 in the appendix, section 8.1. It is the same hypo eliminator used in an American Standards Association photographic standard [16].

Salt solutions have proved effective in removing the thiosulfate from films and papers [12, 13, 14, 15]. Such solutions are convenient because they can be prepared and stored before use and no temperature control is necessary. In the course of this study two salt solutions were developed which proved to be quite efficient in removing the thiosulfate. One solution contained sodium sulfate and ammonium hydroxide and the other sodium sulfate and sodium sulfite. The sodium sulfate helps to prevent undue swelling of the gelatin caused by the alkalinity of the salt solutions. The formulas for these solutions are listed as No. 2 and 3 in the appendix, section 8.1. The two salt solutions have been used in experimental studies only and have not been evaluated for use in large-scale production. The sodium

thiosulfate content of single-weight samples of photocopy, contact, and enlarging papers was reduced to 0.005 mg or less per square inch when treated in these solutions. When the hydrogen peroxide hypo eliminator No. 1 was used no sodium thiosulfate could be found in films or papers. The residual thiosulfate in photographic papers was determined by the method of Crabtree et al. [17] and in photographic films by the method of Crabtree and Ross [22].

4. Results and Discussion

4.1. Silver Sulfide Formed in Photographic Papers During Fixation

The paper sample was exposed to a step wedge, processed and treated in the hydrogen peroxide hypo eliminator No. 1 after fixation. The silver image was removed by the potassium dichromate-sulfuric acid bleach leaving the silver sulfide image or residue which in turn was reduced to silver. During the above procedure reflection density [2] measurements were made of the original silver image, the silver sulfide image remaining after the bleach, and the silver image obtained by reducing the silver sulfide to silver. No filter was used in measuring the densities of the silver sulfide. The density of the paper base was subtracted from the density readings. The densities for the three images obtained from a single sample were plotted against relative values of the logarithm of exposure and the three characteristic curves are shown in figures 1, 2, and 3, respectively, for a photocopy paper, a contact paper, and an enlarging paper. The papers were all single weight. The lowest curve in figures 1, 2, and 3 shows the density of the silver sulfide formed in the image during fixation. The middle curve shows the density of the silver which is obtained by reducing the silver sulfide to silver. The percentage of the original image silver sulfided during fixation may be determined from the density reading in the middle curve and the corresponding density reading in the highest curve which is that for the original silver image. In the region of high-silver densities or full exposure the amount of sulfiding of the silver image is about 25 percent for the photocopy paper, about 17 percent for the contact paper, and about 28 percent for the enlarging paper. At lower silver densities the amount of sulfiding of the silver image is about 20 percent for a density of 0.6 for the photocopy paper, about 9 percent for a silver density of 1.0 for the contact paper, and about 14 percent for a silver density of 1.0 for the enlarging paper. The percentage of the silver sulfided increases as the silver density in the image increases up to the high densities. The amount of silver sulfide formed reaches a maximum in the high densities and levels off as shown by the curve for silver sulfide in figures 1, 2, and 3.

[2] The reflection density was measured by the American Standards Association method [10].

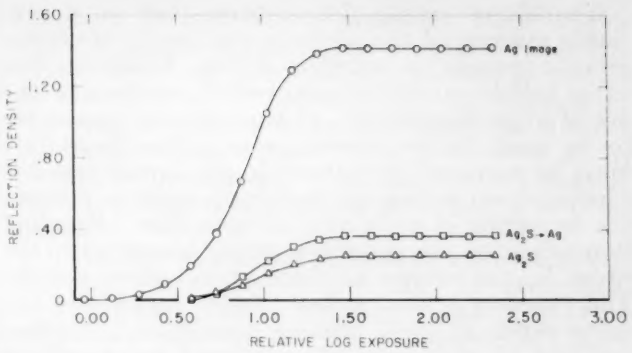

FIGURE 1. *Reflection density versus relative logarithm of exposure for the silver image, the silver sulfide residue, and the silver obtained by the reduction of the silver sulfide, for one sample of a single-weight photocopy paper.*

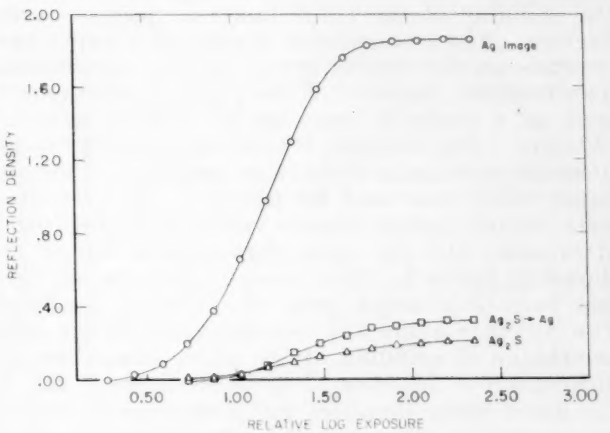

FIGURE 2. *Reflection density versus relative logarithm of exposure for the silver image, the silver sulfide residue, and the silver obtained by the reduction of the silver sulfide, for one sample of a single-weight contact paper.*

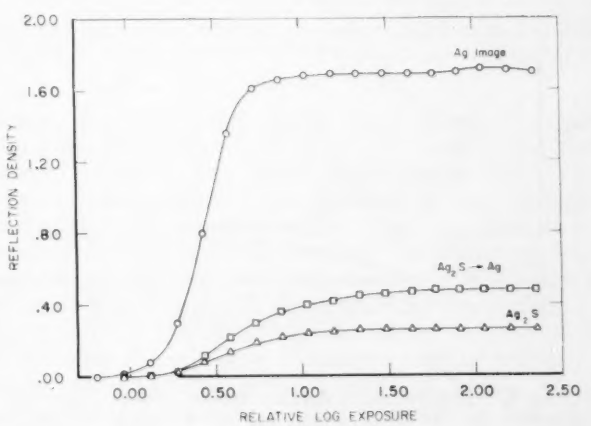

FIGURE 3. *Reflection density versus relative logarithm of exposure for the silver image, the silver sulfide residue, and the silver obtained by the reduction of the silver sulfide, for one sample of a single-weight enlarging paper.*

The above results demonstrate that an appreciable amount of the silver in the image of photographic papers is sulfided during fixation. The silver sulfide cannot be removed by washing or the use of hypo eliminators. If photographic papers are to be used for permanent records the thiosulfate must be removed or reduced to the lowest possible concentration during the washing process to prevent the formation of additional silver sulfide. Residual thiosulfate in the processed paper reacts with the silver in the image to form more silver sulfide. This reaction is slow at low relative humidities but quite rapid at high relative humidities. Further sulfiding of the silver image would be especially objectionable in areas of low silver densities corresponding to the highlights of pictures. The amount of the sulfiding of the silver in films and papers depends on the type of emulsion.

Transmission density measurements were also made of the silver and silver sulfide in this study on the sulfiding of the silver image in papers during fixation. The transmission density of a paper base depends on the optical system of the transmission densitometer; however, if the same densitometer is used in a series of tests useful relative data are obtained. For example, transmission density measurements were made of the same sample of photocopy paper which was used for figure 1. The densities were plotted against relative values of the logarithm of exposure and the three characteristic curves are shown in figure 4. The density of the paper base has been subtracted from the density readings. The curves in figure 4 show approximately the same percentage of sulfiding of the silver image for the highest silver densities as those in figure 1 but in the lower silver densities the transmission density measurements show a higher percentage of silver sulfided than the reflection density measurements. This was found to be true also for contact and enlarging papers.

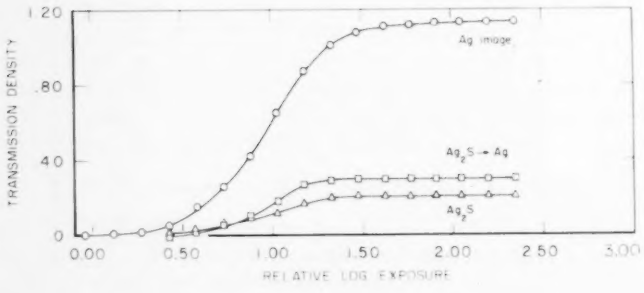

FIGURE 4. *Transmission density versus relative logarithm of exposure for the silver image, the silver sulfide residue, and the silver obtained by the reduction of the silver sulfide, for the same sample of single-weight photocopy paper shown in figure 1.*

4.2. Silver Sulfide Formed in Photographic Films During Fixation

The amount of sulfiding of the silver image during fixation was determined for two microfilms, a photomechanical film, and an X-ray film by the same procedure as that described for photographic papers except that the densities were measured by transmitted light. No filter was used in measuring the densities of the silver sulfide. The transmission densities were plotted against relative values of the logarithm of exposure. From the characteristic curves obtained for each film the density of the silver sulfide and silver obtained when the silver sulfide was reduced to silver were determined for various densities of the original silver image. The results are tabulated in table 1. The characteristic curves for microfilm A are shown in figure 5. The results in table 1 show that the amount of sulfiding of the silver image in the high densities is about 7 percent for microfilm A and 5 percent for microfilm B. These values compare well with the 5 percent found by Levenson and Sharpe [11] for a bromide fine-grain emulsion. This amount of sulfiding of the silver image during fixation should have a negligible effect on the permanency of the image in microfilm. However, the residual thiosulfate must be removed in the washing process to prevent further sulfiding of the silver image.

As in the case of photographic papers, the amount of sulfiding of the silver image in films depends on the type of emulsion. The values for the photo-

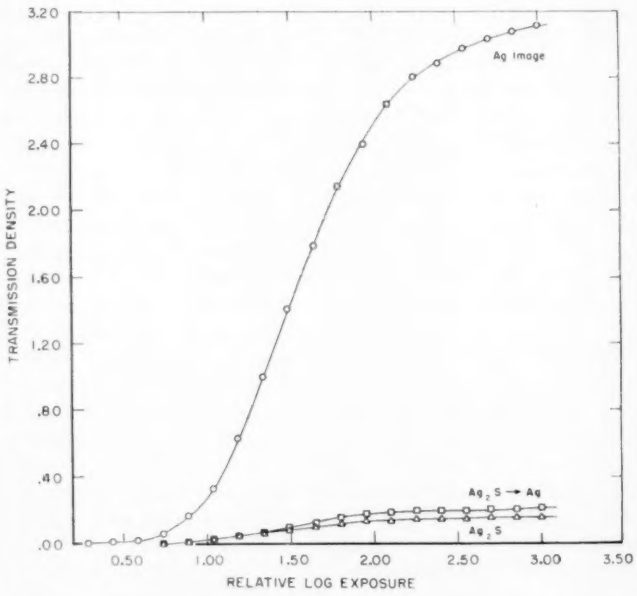

FIGURE 5. *Transmission density versus relative logarithm of exposure for the silver image, the silver sulfide residue, and the silver obtained by the reduction of the silver sulfide, for one sample of microfilm A.*

mechanical and X-ray films are given in table 1 to show the difference in types of emulsions in films. A silver sulfide density of 0.02 was obtained for a silver density of 1.8 for one ciné fine-grain film not shown in the table.

TABLE 1. *Densities of the silver image in films and the corresponding densities of the silver sulfide residue and the silver obtained by the reduction of the silver sulfide*

Density of the silver image	Density of silver sulfide after bleach	Density of the silver obtained by the reduction of the silver sulfide
Microfilm A		
0.50	0.05	0.05
1.00	.07	.07
1.50	.08	.10
2.00	.11	.14
2.50	.13	.18
3.00	.15	.20
Microfilm B		
0.50	0.02	0.03
1.00	.03	.05
1.50	.04	.06
2.00	.06	.08
2.50	.08	.11
3.00	.10	.14
Photomechanical film		
0.50	0.03	0.08
1.00	.06	.12
1.50	.09	.18
2.00	.12	.22
2.50	.14	.26
3.00	.17	.28
3.50	.19	.30
4.00	.20	.31
X-ray film (2 light-sensitive emulsions)		
0.50	0.04	0.05
1.00	.06	.08
1.50	.08	.12
2.00	.10	.14
2.50	.12	.17
3.00	.13	.19
4.00	.16	.23

4.3. A Test for Hypo Eliminators

The potassium dichromate-sulfuric acid bleach which was used in this investigation removes the silver from the photographic image, leaving the silver sulfide formed during fixation by the reaction of thiosulfate with the silver image. Also, any residual thiosulfate reacts with silver ions in the bleach bath to form additional silver sulfide. It seemed feasible to use the latter reaction to determine the effect of different thiosulfate concentrations on the silver image by measuring the increase in the silver sulfide density above that found when the residual thiosulfate is completely eliminated by the hydrogen peroxide hypo eliminator No. 1. A concentration of 0.005 mg of sodium thiosulfate ($Na_2S_2O_3$) per square inch in photographic papers gave a measurable increase in the silver sulfide density above that normally formed during fixation. This type of test for residual thiosulfate in papers and films shows the direct effect of the residual thiosulfate on the silver in the image and should simulate the reaction of residual thiosulfate with the silver in the image during storage. The Crabtree et al. [17] method for determining thiosulfate in paper measures the thiosulfate concentration in a clear area of the paper.

If residual thiosulfate is present when papers are bleached, some silver sulfide may be precipitated in the paper base. Reflection density measures only the density of silver and silver sulfide in the gelatin layer. For this reason, transmission density is recommended instead of reflection density for measuring the silver sulfide in papers as a test procedure for evaluating hypo eliminators.

The effect of different residual thiosulfate concentrations in paper on the increase of the density of the silver sulfide is shown in figure 6. Samples of a

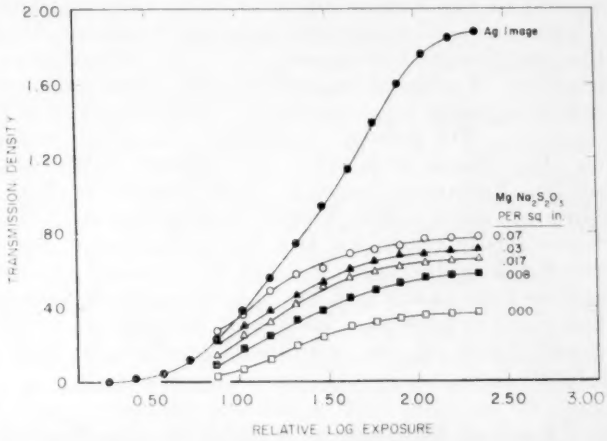

FIGURE 6. *The effect of the residual sodium thiosulfate concentration on the amount of silver sulfide formed in the bleach bath is shown for a single-weight contact paper.*

Characteristic curves are given for the original silver image and for the silver obtained by the reduction of the silver sulfide formed with varying concentrations of residual sodium thiosulfate. The concentration of the residual sodium thiosulfate is shown at the end of the curves.

single weight contact paper were given the same exposure to a step wedge and processed in the same manner and at the same time except that, after fixation, one sample was treated in the hydrogen peroxide hypo eliminator No. 1 and one sample was washed in tap water for each of the following washing times: 120, 60, 30, and 10 min. The samples were bleached and the silver sulfide was reduced to silver. The transmission densities of the silver image and the silver of the silver sulfide reduced to silver were plotted against relative values of the logarithm of exposure. The density of the paper base was subtracted from the density readings. The lowest curve shows the silver of the image sulfided during fixation, where all of the residual thiosulfate had been removed by the hydrogen peroxide hypo eliminator No. 1. The curve for the original silver

image was obtained from the sample which had been treated in the hydrogen peroxide hypo eliminator No. 1. The other curves fall in order of their residual thiosulfate concentrations which are given in milligrams of sodium thiosulfate ($Na_2S_2O_3$) per square inch at the end of the curves. The curves show that the silver sulfide increases appreciably as the residual thiosulfate increases. For a silver image density of about 1.9 the sample containing 0.008 mg of sodium thiosulfate per square inch shows a 57 percent increase in the sulfiding of the silver above that taking place during fixation and the sample containing 0.07 mg of sodium thiosulfate per square inch shows 111 percent increase.

The above results show that the efficiency of a hypo eliminator may be evaluated by testing it against the hydrogen peroxide hypo eliminator No. 1 used as a standard. This test may be made by giving samples of film or paper from the same roll or box the same exposure to a step wedge and processing them at the same time in the same solutions except that, after fixation, one set of samples is treated in the hypo eliminator to be tested and the other in the hydrogen peroxide hypo eliminator No. 1. The samples are then bleached and the transmission densities of the silver sulfide are measured and plotted against relative values of the logarithm of exposure. For greater sensitivity the silver sulfide may be reduced to silver. The characteristic curve for the hydrogen peroxide hypo eliminator No. 1 shows the silver sulfide formed during fixation. The characteristic curve for the hypo eliminator being tested will be the same if all of the residual thiosulfate has been eliminated but will be higher if residual thiosulfate is present. Its height will depend on the concentration of the residual thiosulfate as shown in figure 6.

5. Effect of Potassium Iodide on the Formation of Silver Sulfide During Fixation

The addition of potassium iodide to the fixing bath has been found to prevent the formation of the brown silver sulfide stain which interferes in reversal and reduction operations [7, 18, 19]. Murray [18] added three-fourths of an ounce of potassium iodide to one gallon of the fixing bath. Crabtree et al. [7] found that 0.1 to 1.0 percent of potassium iodide in the fixing bath eliminated the brown stain in positive film.

The effect of potassium iodide in the acid fixing bath on the sulfiding of the silver image was investigated. One gram of potassium iodide was added to each liter of the fixing bath. The samples were given a full exposure, developed, fixed, treated in the hydrogen peroxide hypo eliminator No. 1, and bleached. The density of the silver sulfide ranged from 0.02 to 0.04 for contact and enlarging papers which normally yielded a silver sulfide density of 0.2 to 0.25. The density of the silver sulfide was about 0.005 for two microfilms which normally yielded a silver sulfide density of 0.10 to 0.15. The densities were measured by transmission without a filter. These results show that a small amount of the iodide ion in the fixing bath is quite effective in preventing most of the normal sulfiding of the silver. When processed samples of film or paper, which had been fixed in the acid fixing bath containing potassium iodide, were again treated in the acid fixing bath containing no iodide ion, the amount of sulfiding of the silver was almost as great as that normally obtained.

The effect of the iodide ion in preventing the formation of silver sulfide in the silver image would suggest that silver ions were present in the fixing bath. Silver iodide instead of silver sulfide would be formed because it is less soluble than silver sulfide. It is not known what effect any residual silver iodide or potassium iodide might have on the stability of the silver image. Small concentrations of the iodide ion in the fixing bath retards the rate of fixation [20] and decreases its fixing capacity.

6. Silver Sulfide Formed During Fixation in a Thiosulfate Fixing Bath

Reindorp [1] postulated that the silver sulfide was formed during fixation by the decomposition of a silver thiosulfate complex. Levenson and Sharpe [11] concluded that the thiosulfate was absorbed as a simple ion or a complex ion on the silver in the image during fixing and that the silver sulfide was formed in the bleach bath by the reaction of silver ions with the absorbed thiosulfate. If the thiosulfate is absorbed as a simple ion or as a complex ion on the surface of the silver grains it might be possible to eliminate it and prevent the formation of silver sulfide. But, if the silver sulfide is formed during fixation it could not be removed and would be an integral part of the image. This problem was investigated and the experimental results gave strong evidence that the silver sulfide is formed during fixation.

6.1. Experimental Results

a. Removal of the Silver Sulfide From the Silver Image

An investigation was made to determine if the silver sulfide, which formed during fixation, could be removed from the silver image before it was bleached. A solution containing 30 g of silver nitrate and 180 g of anhydrous sodium sulfite per liter was found capable of removing all of the silver sulfide from a sulfided silver strip. A similar solution was used by Hickman and Weyerts [21] in their studies on optical intensification of silver sulfide images.

A brown coating of silver sulfide was formed on silver strips, ¾-in. by 5-in. and 0.01-in. in thickness, by exposing them to an atmosphere of hydrogen sulfide gas for 1 to 4 hr. The strips were first cleaned in glacial acetic acid, washed, and then suspended in an atmosphere of hydrogen sulfide. The silver nitrate-sodium sulfite solution removed the silver sulfide layer from the silver in 2 to 6 hr at room temperature and in diffuse daylight. The time required for the removal of the silver sulfide layer depended on its thickness and the intensity of the

light. This test shows that the silver nitrate-sodium sulfite solution dissolves silver sulfide.

Processed samples of 2 microfilms, a contact paper, and an enlarging paper were treated for 2 hr in the silver nitrate-sodium sulfite solution in diffuse daylight at 25° C, washed for 30 min in tap water, and bleached. The densities were measured by transmission without a filter. These samples had been treated in the hydrogen peroxide hypo eliminator No. 1 during processing. For areas of high silver density of almost full exposure the silver sulfide density in microfilm A was reduced from 0.10 to 0.00; microfilm B, 0.15 to 0.005; a contact paper, 0.20 to 0.07; and an enlarging paper, 0.26 to 0.09. The first value in each case was the normal silver-sulfide density obtained when the silver image was bleached.

The silver sulfide image or residue, left in the gelatin layer of papers after the removal of the silver by the bleach bath, was only slightly dissolved by the silver nitrate-sodium sulfite solution under the above experimental conditions but, when exposed to direct sunlight during treatment for 4 hr at 28° C, most of the silver sulfide was removed. Densities of 0.2 to 0.3 of silver sulfide residue in papers were reduced to a density of 0.04. It was necessary to rebleach the samples to remove the silver deposited by the silver nitrate-sodium sulfite solution in the gelatin layer and paper base.

The above results indicate that silver sulfide was formed on the silver image during fixation.

b. Staining Effect of the Fixing Bath on a Silver Surface

Glass plates, 3-in. by 4-in., were coated with silver by the Rochelle salts process. The silver coated plates were partially immersed in an acid or neutral fixing bath for 1 min and washed. A brown stain was clearly visible on the surface of the silver in that area treated in the fixing bath. The brown stain was more pronounced when wet but still visible when dry.

Silver strips, ¾-in. by 5-in. and 0.01-in. in thickness, were treated in a solution containing 60 ml of distilled water and 40 ml of concentrated nitric acid, and washed. This operation produced a fine white, mat surface on the silver strip. The silver strips, wet or dry, were partially immersed in an acid or neutral fixing bath for 10 sec and washed. In each case a brown stain was clearly visible on that portion of the strip treated in the fixing bath. The brown stain was assumed to be silver sulfide. These tests show that the thiosulfate in the fixing bath reacts rapidly to stain mirror and fine mat silver surfaces and it would be expected that the silver in a photographic image would react in a like manner with thiosulfate in the fixing bath to form silver sulfide during fixation.

c. Conversion of Absorbed Thiosulfate to Silver Sulfide

It should be possible to increase the density of the silver in the image by converting any thiosulfate absorbed on the silver to silver sulfide. Contact and enlarging papers were subjected to the Crabtree et al. [17] hypo test used for determining residual thiosulfate in papers. The solution used in this test contains silver nitrate and sulfuric acid and reacts quantitatively with thiosulfate to form silver sulfide. Several tests were made on paper samples with high silver densities (full exposure) but no increase in the density of the silver image could be detected. This indicated that no thiosulfate was present in an absorbed state on the surface of the silver in the image. These same paper samples yielded a silver sulfide residue with a density of 0.20 to 0.25 when the silver was removed by the bleach bath. These results indicated that the silver sulfide obtained after bleaching was formed during fixation and not in the bleach bath by the reaction of silver ions with absorbed thiosulfate.

6.2. Formation of the Silver Sulfide

It is well known that thiosulfate in a fixing bath attacks the silver in a photographic image and the rate of attack depends on several factors such as the composition of the bath, acidity of the bath, temperature, and agitation [23]. The silver ion reacts with the thiosulfate anion to form silver sulfide. Experimental evidence indicates that the silver in the image is oxidized in the fixing bath in the presence of oxygen [3, 23] and this reaction would be a source of silver ions. Reindorp [1] suggested that silver ions may be formed in the fixing bath by a secondary dissociation of the anions of a silver thiosulfate complex. More information is necessary to establish the exact mechanism of the formation of silver sulfide in the silver image during fixation.

It is to be noted that no silver sulfide residue is obtained when the silver image is bleached if fixation takes place in a 2-percent solution of potassium cyanide but, if a silver image which has been fixed in potassium cyanide is exposed to an atmosphere of hydrogen sulfide gas for a few minutes, a silver sulfide residue is obtained when the silver is removed in the bleach bath.

7. Summary and Conclusions

Silver sulfide forms in the silver image of photographic materials during fixation. The percentage of the silver sulfide in the image is small in microfilms but is quite large in photographic papers as shown in section 4. The thiosulfate which is not removed by the washing process causes further sulfiding of the image. The extent of the sulfiding depends chiefly on the concentration of the residual thiosulfate and the storage conditions. If the photographic image is to be used for permanent or archival records, the thiosulfate must be removed as completely as possible during the washing process. If the thiosulfate is not sufficiently removed by the wash water, it may be necessary to use a hypo eliminator.

Hypo eliminators may be evaluated for their efficiency by comparing them with the hydrogen peroxide hypo eliminator No. 1. A solution of sodium sulfate together with either sodium sulfite or ammonium hydroxide will reduce the hypo (sodium thiosulfate, $Na_2S_2O_3$) content of single-weight papers to 0.005 mg or less per square inch.

The effect of different residual thiosulfate concentrations on the sulfiding of the silver image can be determined by measuring the density of the silver sulfide formed when the image is bleached. The thiosulfate reacts with the silver ion in the bleach bath to yield silver sulfide and the density of the silver sulfide increases as the residual thiosulfate concentration increases. This method would be more rapid than the oven aging tests used by Crabtree and Ross [22] and in an American Standards Association specification [16] to determine the effect of residual thiosulfate on the silver image.

Silver sulfide, which remains in the gelatin layer after the silver is bleached, may be reduced to silver by the procedure outlined in section 2.3. The percentage of silver sulfide is calculated from the densities of the reduced silver and the silver in the original image.

The addition of potassium iodide to the fixing bath will prevent most of the sulfiding of the silver image which takes place during fixation. The iodide ion increases the fixing time and decreases the fixing potential of the bath.

Experimental evidence is presented to show that silver sulfide is formed in the silver image during fixation. However, more information is necessary to establish the exact mechanism of its formation.

8. Appendix

8.1. Formulas for Developing and Fixing the Silver Image in Films and Papers

Developer

Monomethyl p-aminophenol sulfate	3.1 g.
Sodium sulfite, anhydrous	45.0 g.
Hydroquinone	12.0 g.
Sodium carbonate, anhydrous	67.5 g.
Potassium bromide	1.9 g.
Water to make	1 liter.

Dilute 1 to 1 before use.

Stop Bath

Acetic acid, glacial	12 ml.
Water to make	1 liter.

Fixing Bath

Sodium thiosulfate, $Na_2S_2O_3 \cdot 5H_2O$	240.0 g.
Sodium sulfite, anhydrous	15.0 g.
Acetic acid (28%)	48 ml.
Boric acid	7.5 g.
Potassium aluminum sulfate, $KAl(SO_4)_2 \cdot 12H_2O$	15.0 g.
Water to make	1 liter.

Hypo eliminators

No. 1

Water	300 ml.
Hydrogen peroxide (30%)	50 ml.
Ammonium hydroxide (28%)	10 ml.
Potassium bromide	1.0 g.
Water to make	1 liter.

After fixation the sample of film or paper is rinsed 1 min in running tap water, treated for 10 min in the above solution, bathed for 2 min in a 1 percent solution of sodium sulfite to remove the excess hydrogen peroxide, and washed 30 min in running tap water.

No. 2

Sodium sulfate, anhydrous	140 g.
Ammonium hydroxide (28%)	2 ml.
Water to make	1 liter.

No. 3

Sodium sulfate, anhydrous	71 g.
Sodium sulfite, anhydrous	63 g.
Water to make	1 liter.

When hypo eliminators No. 2 and 3 are used, the sample of film or paper, after fixation, is rinsed 1 min in running tap water, treated for 10 min in the hypo eliminator, and washed 30 min in running tap water.

8.2. Formulas for the Bleaching Process in Which the Silver of the Photographic Image Is Removed and the Silver Sulfide Is Left as a Residue in the Emulsion Layer

Bleach Bath

Potassium dichromate	5.0 g.
Sulfuric acid (95%)	5.0 ml.
Water to make	1 liter.

Clearing Bath

Sodium sulfite, anhydrous	50.0 g.
Sodium hydroxide	1.0 g.
Water to make	1 liter.

Fixing Bath

Sodium thiosulfate, $Na_2S_2O_3 \cdot 5H_2O$	240 g.
Sodium sulfite, anhydrous	15 g.
Water to make	1 liter.

Hypo eliminator

Use hypo eliminator No. 3 which is listed in section 8.1.

8.3. Formulas for Reducing the Silver Sulfide Residue in the Gelatin Layer to Silver

Bleach Bath

Potassium permanganate	5.0 g.
Sodium chloride	10.0 g.
Acetic acid, glacial	50 ml.
Water to make	1 liter.

Clearing Bath

Sodium bisulfite	50.0 g.
Potassium bromide	12.0 g.
Water to make	1 liter.

Developer

Amidol, 2,4-Diaminophenol Dihydrochloride	5.0 g.
Sodium sulfite, anhydrous	30.0 g.
Water to make	1 liter.

Stop Bath

Citric acid, $H_3C_6H_5O_7 \cdot H_2O$	35 g.
Water to make	1 liter.

8.4. Quality of the Chemicals Used for the Formulas Listed in This Appendix

All of the solutions were made up with distilled water. The following chemicals were of reagent quality meeting ACS specifications: sodium sulfite, sodium sulfate, acetic acid, boric acid, potassium bromide, sodium carbonate, citric acid, sodium chloride, potassium permanganate, sodium hydroxide potassium dichromate, ammonium hydroxide, and sulfuric acid. The monomethyl p-aminophenol sulfate, hydroquinone, sodium thiosulfate, and potassium aluminum sulfate conformed to American Standard Specifications for Photographic Grade Chemicals. The Amidol was Eastman Kodak Cat. No. P–614. The sodium bisulfite was Mallinckrodt analytical reagent grade.

9. References

[1] J. H. Reindorp, A contribution to the chemistry of residual images, Brit. J. Phot. **82,** 244 (1935).

[2] L. P. Clerc, Photography theory and practice, p. 298 (Pitman Publishing Corp., New York, N.Y., 1954).

[3] C. E. K. Mees, The theory of the photographic process, p. 715 (The Macmillan Co., New York, N.Y., 1954).

[4] K. C. D. Hickman and D. A. Spencer, The washing of negatives and prints, Brit. J. Phot. **69,** 387 (1922).

[5] Dr. Lüppo-Cramer, Zur konstitution der negativsubstanz Photographische Korrespondenz **49,** 121 (1912).

[6] A. and L. Lumiere and A. Seyewetz, The composition of the developed image, Brit. J. Phot. **59,** 61 (1921).

[7] J. I. Crabtree and L. E. Muehler, Reducing and intensifying solutions for motion picture film, J. Soc. Motion Picture Engrs. **17,** 1025 (1931).

[8] J. I. Crabtree, G. T. Eaton, and L. E. Muehler, The removal of hypo and silver salts from photographic materials as affected by the composition of the processing solutions, J. Soc. Motion Picture Engrs. **41,** 47 (1943).

[9] C. Lighton, Notes on the bleaching and local reduction of bromide prints, Brit. J. Phot. **73,** 643 (1926).

[10] American Standard Sensitometry and Grading of Photographic Papers, PH2.2–1953 (American Standards Association, Inc., 70 East 45th St., New York 17, N.Y.)

[11] G. I. P. Levenson and C. J. Sharpe, The role of thiosulphate in the formation of sulphide stains during bleaching, J. Phot. Sci. **4,** No. 4, 89 (1956).

[12] H. L. Scott and W. F. Hyatt, U.S. Patent 2,688,546 (1954).

[13] J. I. Crabtree, G. T. Eaton, and L. E. Muehler, The elimination of hypo from photographic images, Am. Phot. **35,** No. 4, 272 (1941).

[14] J. I. Crabtree, and R. W. Henn, Increasing the washing rate of motion picture films with salt solutions, J. Soc. Motion Picture & Television Engrs. **65,** 378 (1956).

[15] R. W. Henn, N. H. King, and J. I. Crabtree, The effect of salt baths on hypo and silver elimination, Phot. Eng. **7,** No. 3 and 4, 153 (1956).

[16] American Standard Method for Indicating the Stability of the Images of Processed Black-and-White Films, Plates, and Papers, PH4.12–1954, p. 8 (American Standards Association, Inc., 70 East 45th St. New York 17, N.Y.).

[17] J. I. Crabtree, G. T. Eaton, and L. E. Muehler, The quantitative determination of hypo in photographic prints with silver nitrate, J. Franklin Inst. **235,** No. 4, 351 (1943).

[18] A. Murray, New control methods in chemical retouching, Brit. J. Phot. **77,** 121 (1930).

[19] A. Murray, Chemical retouching, The National Lithographer **36,** No. 11, 29 (1929).

[20] L. P. Clerc, Photography theory and practice, p. 303 (Pitman Publishing Corp., New York, N.Y., 1954).

[21] K. Hickman and W. Weyerts, Optical intensification, Brit. J. Phot. **80,** 482 (1933).

[22] J. I. Crabtree and J. F. Ross, A method of testing for the presence of thiosulfate in motion picture film, J. Soc. Motion Picture Engrs. **14,** 419–426 (1930).

[23] H. D. Russell and J. I. Crabtree, The reducing action of fixing baths on the silver image, J. Soc. Motion Picture Engrs. **18,** 371 (1932).

WASHINGTON, D.C. (Paper 64C1–26)

530231—60——6

JOURNAL OF RESEARCH of the National Bureau of Standards—C. Engineering and Instrumentation
Vol. 64C, No. 1, January–March 1960

Capacitor Calibration by Step-Up Methods

Thomas L. Zapf

(October 8, 1959)

Step-calibration methods are used in many physical laboratories for the extension of measurements to quantities far removed from the magnitude of greatest accuracy at which absolute determinations are made. The excellent precision of repetitive substitution procedures is exploited by step-up or step-down methods to extend measurements to higher or lower magnitudes without serious degradation of accuracy. The application of step-up techniques to the calibration of variable air capacitors is described in this paper as a practical example of the method.

1. Introduction

One of the important statutory functions of the National Bureau of Standards is the calibration of physical standards of measurement used in science and industry. The chain of measurements connecting this calibration service to the national prototype standards of length, mass, and time is complex, and for electrical measurements involves meticulous experiments to assign numerical values to calibration standards and corrections to standard instruments. These devices, designed for excellent stability and definitude, serve as comparison standards basic to the calibration services rendered by the Bureau. Equally important to accurate scientific work is the proper use of these standards to overcome their inherent limitations. Frequently an appropriate choice of method and the employment of suitable techniques are as important as the judicious selection of equipment. The close association between methods, techniques, and equipment is particularly evident when, in the course of calibration activities, it is necessary to obtain accurate measurements at magnitudes far removed from that at which absolute determinations are made. The extension of range of electrical measurements is sometimes accomplished by the establishment of accurately known ratios. For example, ratios very nearly equal to the squares of integers may be obtained through the successive measurement in series and parallel of resistors having nearly equal values [1].[1] Resistance ratios of approximately 10:1 may be realized by the successive measurement of 11 resistors in arbitrary units and the use of these as the 10:1 ratio arms of a bridge. A unique 10:1 ratio apparatus used with a special resistance bridge is described by Wenner [2].

The building-up to ratios larger than 10:1 is particularly well exemplified by the procedure followed in calibrating the standard volt box at the Bureau [3] in which a group of sections of nominally equal resistance is intercompared. These sections, connected in series, form the first section of a group of larger denomination. The buildup to large ratios is rapid and exact. The standard volt box was designed specially for self-calibration by this method.

The calibration of resistance decade boxes and the resistance decades of bridges by the step-substitution or step-up method illustrates yet another technique of obtaining accurate measurements over wide ranges [4]. A similar process is used by the Bureau for the calibration of the capacitance bridges that are used daily to measure standards of capacitance.

In order to obviate the concern over connection errors and avoid the detailed consideration of connectors, it is customary and convenient to use as standards of low grounded capacitance such devices as variable air capacitors and capacitance decade boxes which may be calibrated accurately for capacitance difference from some arbitrary setting. The calibration of such variable capacitors may be accomplished quite effectively by the step-up method employing fixed standards or standards of capacitance difference.

An excellent description of a step-up method applied to the calibration of decade capacitors for both capacitance and dissipation factor has been described by Ford and Astbury of the British National Physical Laboratory [5].

2. Equipment

Very little special equipment is needed to calibrate a variable capacitor by step-up methods. If the variable air capacitor, X, having a range from 100 to 1,100 pf, is to be calibrated at every 100-pf division mark, it is necessary to have a fixed air capacitor, S, of approximately 100 pf that can be connected in parallel with the variable capacitor under test in a precisely repeatable manner. This can be achieved if the mating connectors introduce no significant uncertainties to the capacitance added to the circuit and if the connectors are designed to couple quickly and easily to either the variable capacitor or the

[1] Figures in brackets indicate the literature references at the end of this paper.

bridge that will be used, or if a capacitor can be connected or disconnected by a precise switching arrangement. The 100-pf capacitor should be adjusted close to the nominal value, but it need not be calibrated. It must, however, be free from significant drift over the period of a quarter-hour or so during which the test is being run.

A calibrated 1,000-pf air capacitance standard, S', is needed to relate the results of the step-up test to the national reference standard of capacitance.

The bridge used for this step calibration need not have great accuracy but must be stable, for it is used with a sensitive detector for substitution measurements. A small variable capacitor, V, is required, having a least count (smallest readable increment) one-tenth that of X or smaller. It is advantageous to choose the smallest possible precision variable capacitor, V, consistent with other limitations so that the corrections to V are negligibly small relative to the corrections to X. The total range of V must be at least a little larger than the range of errors in the capacitor to be calibrated. The readable accuracy of this capacitor, if expressed in percent of total range, need not be very great.

The equipment described is assembled as shown in figure 1. It is most important that the cables used to connect components be shielded and rigid, or if flexible cables are used, it should be ascertained that variations in cable capacitance are negligible. The cables must be fixed in position and must not be disturbed during the entire calibration. This precaution is intended to emphasize the importance of particular care to one of those sources of systematic error that could impair good calibration accuracy. The operator must have a good technical appreciation of the apparatus and quantities measured, gained through study and experience.

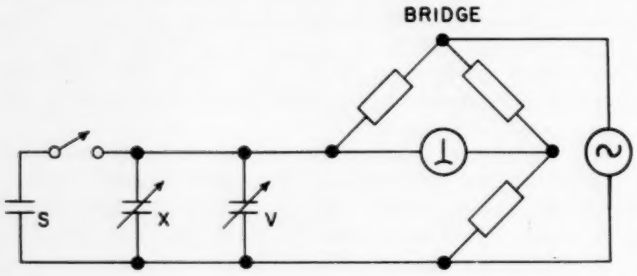

FIGURE 1. *The variable capacitor under text,* X, *is calibrated by a step-up method employing a fixed capacitor,* S, *and a small variable capacitor,* V.

3. Procedure and Computations

The true value of each of the capacitors involved in the calibration may be defined as the nominal value plus a correction; thus, the true capacitance of the uncalibrated 100-pf capacitor is $S=S_n+s$, where $S_n=100$ (exactly) and s is the small correction. Similarly the calibrated 1,000-pf standard has the value $S'=S'_n+s'$, and the variable air capacitor to be calibrated may be represented by $X=X_n+x$, where x is the correction to the reading (or setting) X_n. The calibration will consist of the determination of the relatively small correction, x, to each 100-pf division mark, X_n, and since only capacitance differences are of interest, the observer is free to choose any one of the division marks as a reference point. It is frequently convenient to choose as a reference the first marked point on the dial. In this case the 100-pf mark is considered as a reference and a correction of 0.00 is arbitrarily assigned to it. For this example it will be assumed that the small variable capacitor, V, has corrections that are negligibly small.

The capacitor under test is first carefully set to the 100-pf mark ($X_{n1}=100$ pf) avoiding backlash errors by approaching the mark in the direction of increasing dial readings. The small variable capacitor, V, is set to any convenient mark near the center of its range. The 100-pf capacitor, S, is connected in parallel with X and V. Now the bridge must be balanced using the controls on the bridge itself. If a balance cannot otherwise be obtained, V may be used to attain balance. When the bridge is balanced the reading V_A is recorded. The fixed capacitor, S, is then removed and X set to the 200-pf mark ($X_{n2}=200$ pf), again approaching the mark in the same direction. Without changing any other component the circuit is rebalanced by changing V alone, and the reading V_B recorded as before. In the first balance the external bridge arm consisted of $S+X_1+V_A$, and for the second balance, with the bridge unchanged, the external arm consisted of X_2+V_B. These can be equated to yield

$$S+X_1+V_A=X_2+V_B \tag{1}$$

The cable and connector capacitance, as well as residuals within the bridge, contribute equally to both balances and are therefore deliberately disregarded.

It is convenient to work with small numbers, and eq (1) can be expressed as

$$S_n+s+X_{n1}+x_1+V_A=X_{n2}+x_2+V_B \tag{2}$$

and since

$$S_n=X_{n2}-X_{n1} \text{ and } x_1=0 \tag{3}$$

$$x_2=(V_A-V_B)_2+s \tag{4}$$

where the subscript is appended to the difference (V_A-V_B) to distinguish this set of data from other sets and to appropriately correlate the difference with the setting of X in the second balance of each set.

The quantity x_2 is the desired correction to X_n when $X_n=200$ pf. The difference $(V_A-V_B)_2$ is easily computed from the recorded data.

Without changing X, S is reconnected and the bridge rebalanced using the bridge controls and V, if necessary, to attain exact balance. The reading, V_A, is then recorded. Capacitor S is then removed and X set to the 300-pf mark ($X_n=300$). The bridge is rebalanced using V alone and the reading,

V_B, recorded. When the first balance is equated to the second balance

$$S+X_2+V_A=X_3+V_B \tag{5}$$

or

$$S_n+s+X_{n2}+x_2+V_A=X_{n3}+x_3+V_B \tag{6}$$

and since

$$S_n=X_{n3}-X_{n2} \tag{7}$$

$$x_3=x_2+(V_A-V_B)_3+s. \tag{8}$$

Substituting eq (4) in eq (8)

$$x_3=(V_A-V_B)_2+(V_A-V_B)_3+2s. \tag{9}$$

Continuing this process step-by-step, in general for the mth step

$$x_m=\sum_2^m (V_A-V_B)+(m-1)s \tag{10}$$

and finally

$$x_{11}=\sum_2^{11} (V_A-V_B)+10s \tag{11}$$

A tabulation of the differences and the cumulative sum of the differences is shown in table 1, which shows the data and computations for a typical calibration. It remains to determine the value of s so that the corrections x_2 through x_{11} can be evaluated.

The 1,000-pf standard capacitor, S', accurately calibrated for insertion capacitance, is now connected in parallel with X and V. With X set at 100 pf, the bridge is balanced with the bridge controls and V, if necessary, and the reading, V_A, recorded. S' is removed, X is set to the 1,100-pf mark, the bridge rebalanced using V alone, and the reading, V_B, recorded. Then

$$S'+X_1+V_A=X_{11}+V_B \tag{12}$$

or

$$S'_n+s'+X_{n1}+V_A=X_{n11}+x_{11}+V_B \tag{13}$$

and since

$$S'_n=X_{n11}-X_{n1} \tag{14}$$

$$x_{11}=(V_A-V_B)_T+s' \tag{15}$$

where the subscript T denotes the V difference obtained when the capacitor, S', is used.

In this way x_{11} is determined accurately in terms of a small difference reading of the variable capacitor, V, and the known correction, s', to the standard capacitor, S'. The correction, s, to the fixed capacitor, S, can now be computed from eq (11)

$$10s=x_{11}-\sum_2^{11} (V_A-V_B) \tag{16}$$

or

$$10s=s'+(V_A-V_B)_T-\sum_2^{11} (V_A-V_B) \tag{17}$$

The quantity $10s$ is then added algebraically to the sum of the V differences corresponding to the test of the 1,100-pf mark, the result being the correction to this reading. Similarly $9s$ is added to the sum of the V differences corresponding to the 1,000-pf mark, and so on, until only s is added to the V differences corresponding to the 200-pf mark. These small corrections are listed in table 1 under the heading ns.

The observations can be made rapidly and the computations are simple, since only small differences appear. A second complete calibration, preferably by another observer, enables one to appraise the precision of the measurements including the stability and resetability of the capacitor under test, and serves to reveal measurement and arithmetic errors that might otherwise remain undetected.

In the procedure described above the fixed increment of calibration was 100 pf. It is well to point out that other increments can be accommodated as well. A 50-pf capacitor, if used as a fixed step, would permit calibration at 50-pf intervals. Although the procedure has been described using a fixed capacitor as a step, a continuously variable capacitor or decade capacitor would also be satisfactory if it were used in such a manner as to provide a repeatable difference of capacitance. Care would be necessary to avoid setting errors caused, for example, by backlash in the control mechanism, or by careless setting to the index.

A variable capacitor calibrated for capacitance difference by this method can be used as a standard for extending the method to capacitance calibrations of still lower magnitudes.

TABLE 1. *Observations and calculations*

All values in picofarads

S	X	V	V_A-V_B	$\Sigma(V_A-V_B)$	ns	x
100	100	5.00				
			0.31	0.31	−0.14	0.17
0	200	4.69				
100	200	4.84				
			−.02	.29	−.29	.00
0	300	4.86				
100	300	4.99				
			.06	.35	−.43	−.08
0	400	4.93				
100	400	4.92				
			.41	.76	−.58	.18
0	500	4.51				
100	500	4.65				
			.01	.77	−.72	.05
0	600	4.64				
100	600	4.81				
			.05	.82	−.86	−.04
0	700	4.76				
100	700	4.87				
			.27	1.09	−1.01	.08
0	800	4.60				
100	800	4.73				
			.31	1.40	−1.15	.25
0	900	4.42				
100	900	4.57				
			.04	1.44	−1.30	.14
0	1000	4.53				
100	1000	4.67				
			.55	1.99	−1.44	.55
0	1100	4.12				
1000	100	5.04				
			0.92			
0	1100	4.12				

$s'=-0.37$ pf $10s=-1.44$ pf

4. Dual Calibration

Reviewing the calibration described above, it is noticed that for each set of two balances, one balance is obtained with the bridge controls and V, if necessary. The fact that the change in the bridge reading is always an amount approximately equal to S (or S') leads to the consideration of calibrating two variable capacitors having the same range with practically no extra work.

If X and U, the variable capacitors to be calibrated, are connected as shown in figure 2, the procedure is similar to that described above except that the bridge need not be changed after the initial setting. The settings of X and U are listed in table 2. Care must be taken to apply the proper sign to the differences and to cumulatively add the differences for the calibration of U beginning at the bottom of the table rather than the top.

Lower range capacitors can be calibrated similarly, but extreme attention must be paid to good mechanical rigidity in all parts of the circuit.

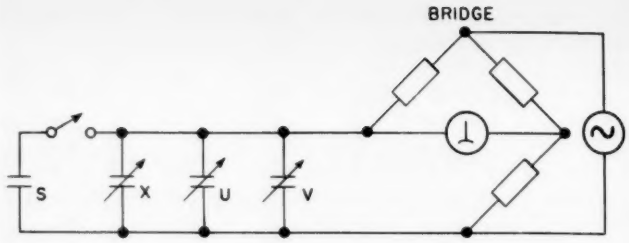

FIGURE 2. *Two variable capacitors, X and U, may be calibrated simultaneously by a step-up method.*

5. Discussion

If attention is confined to the calibration of two-terminal variable air capacitors having a capacitance range from several picofarads to about 1,000 pf, the procedure outlined in this paper demonstrates the ability of step-calibration methods to provide accurate calibrations of capacitors at levels at which good accuracy is otherwise difficult to obtain.

TABLE 2. *Observations and calculations (dual calibration)*

All values in picofarads

S	X	U	V	V_A-V_B	$\Sigma(V_A-V_B)$	ns	x [a]	V_B-V_A	$\Sigma(V_B-V_A)$	ns	u [a]
0	100	1100	5.00								
								0.34	2.05	−1.38	0.67
100	100	1000	5.34	0.31	0.31	−0.14	0.17				
0	200	1000	5.03					.04	1.71	−1.24	.47
100	200	900	5.07	−.03	.28	−.28	.00				
0	300	900	5.10					.07	1.67	−1.10	.57
100	300	800	5.17	.06	.34	−.41	−.07				
0	400	800	5.11					.24	1.60	−0.97	.63
100	400	700	5.35	.37	.71	−.55	.16				
0	500	700	4.98					.36	1.36	−.83	.53
100	500	600	5.34	.02	.73	−.69	.04				
0	600	600	5.32					.31	1.00	−.69	.31
100	600	500	5.63	.05	.78	−.83	−.05				
0	700	500	5.58					.26	0.69	−.55	.14
100	700	400	5.84	.26	1.04	−.97	.07				
0	800	400	5.58					.29	.43	−.41	.02
100	800	300	5.87	.31	1.35	−1.10	.25				
0	900	300	5.56					.01	.14	−.28	−.14
100	900	200	5.57	.03	1.38	−1.24	.14				
0	1000	200	5.54					.13	.13	−.14	−.01
100	1000	100	5.67	.54	1.92	−1.38	.54				
0	1100	100	5.13								
1000	100	1100	5.37	.91							
0	1100	1100	4.46								
1000	1100	100	5.50					1.04			
$s'=-0.37$ pf				$10s=-1.38$ pf				$10s=-1.38$ pf			

[a] The columns x and u are the corrections to the dial readings of the variable capacitors X and U. The good precision of the method is noticeable by comparing the test of X in table 2 with table 1, which represents a test of the same capacitor about an hour earlier.

Standards of grounded capacitance, often called two-terminal capacitors, are characterized by having one of the capacitor electrodes connected to the case, in contrast with standards of direct capacitance (three-terminal capacitors) having both capacitive electrodes insulated from the case. The direct capacitance, C_D, between the two active electrodes, as shown in figure 3, is definite to the extent that the separate terminals and associated leads are shielded from each other. Adequate shielding that does not interfere with the direct capacitance is relatively easily obtained, and excellent accuracy in direct capacitance measurements is possible to a fraction of a micropicofarad (10^{-18} f).

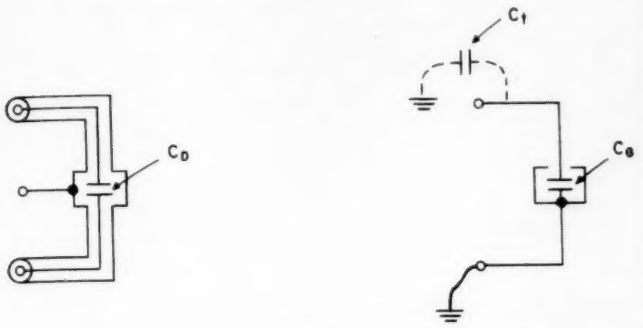

FIGURE 3. *The direct (three-terminal) capacitance,* C_D, *is made definite by complete shielding. The grounded (two-terminal) capacitance,* C_G, *is indefinite because of variations in the stray capacity.*

The grounded capacitance, C_G, shown in figure 3, is more difficult to define in a precise manner, because the capacitance between the ungrounded terminal and all grounded objects, C_t, is indistinguishable from C_G unless a separate "zero-balance" of the measuring apparatus is made with the leads attached but the capacitor disconnected. Even this procedure will not insure good precision unless care is used to connect the capacitor to the measuring apparatus in identically the same way every time. The best precision in practical measurements of grounded capacitance is possible only if the method of connection to the measurement circuit is well defined. An adequately shielded rigid adapter or connector is necessary as an auxiliary part of the capacitor and must be used with it for every measurement. If the capacitor is to be used as a standard for accurate capacitance measurements, the same connector must be used with the capacitor when it is calibrated, and the assembly becomes a standard of, capacitance added to a circuit, or in other words, capacitance difference. Thus, good precision of repeated measurements is simply obtained in any laboratory if the successive measurements are accomplished using rigid wiring and the same connectors every time. The best accuracy in terms of the national reference standards can be obtained only for magnitudes sufficiently large that negligible errors result from differences between the connectors used in the several laboratories involved. Accurate calibration of small fixed capacitors can only be accomplished if mating connectors are submitted.

The accuracy of measurements on fixed standards of grounded capacitance having electrodes terminated in binding posts or unshielded plugs is limited by the variation in the geometrical design of the instrument panels, cables, and connectors to which the standard can be attached. Differences as large as several tenths of a picofarad are possible with present commercially available standards and apparatus with which they may be used. It is understandable that differences of several tenths of a percent are to be expected if a fixed 100-pf standard of this type is measured in several laboratories or on different equipment, while if measurements are performed on 1,000-pf standards the uncertainties at the connectors would be only several hundredths of a percent of the quantity measured. In the step-up procedure described in this paper it is evident that the precision of repeated measurements, the freedom from the effects of residuals in test apparatus obtainable by substitution methods, and the accuracy of measurements at magnitudes closer to optimum, are combined in a manner favorable to the accurate calibration of the capacitance differences of variable capacitors. The method is quite applicable at any frequency although at higher frequencies residuals in components can be troublesome and may require special attention. For example, it may be necessary to apply corrections for errors introduced by residual inductance in the cables connecting the apparatus.

6. Conclusion

Step-calibration methods can be employed for the calibration of variable capacitors. The few necessary items of equipment are generally available in any electrical measurements laboratory. Reference to the national electrical standards is made through the use of a single fixed capacitance standard that can be transported to other standardizing laboratories more easily, and calibrated less expensively than variable capacitors.

7. References

[1] Lord Rayleigh, Phil. Trans. **173,** 661 (1882).
[2] F. Wenner, J. Research NBS **25,** 252 (1940). RP 1323.
[3] F. B. Silsbee and F. J. Gross, J. Research NBS **27,** 269 (1941). RP1419.
[4] J. L. Thomas, NBS Circ. 470 (1948).
[5] L. H. Ford and N. F. Astbury, J. Sci. Instr. **15,** 122 (1938).

BOULDER, COLO.

(Paper 64C1–27)

Publications of the National Bureau of Standards*

Selected Abstracts

The "1958 He^4 scale of temperatures," F. G. Brickwedde, H. van Dijk, M. Durieux, J. R. Clement, and J. K. Logan, *J. Research NBS* **64A,** *No. 1, 1 (1960).*

The generally used practical scale of temperatures between 1° and 5.2° K is the He^4 vapor-pressure scale based on an accepted vapor-pressure equation or table. In Servres (Paris), October 1958, the International Committee on Weights and Measures recommended for international use the "1958 He^4 Scale" based on a vapor-pressure table arrived at through international cooperation and agreement. This table resulted from a consideration of all reliable He^4 vapor-pressure data obtained using gas thermometers, and paramagnetic susceptibility and carbon resistor thermometers. The theoretical vapor-pressure equation from statistical thermodynamics was used with thermodynamic data on liquid He^4 and the vapor equation of state to insure satisfactory agreement of the vapor-pressure table with reliable thermodynamic data.

Analytic comparison of suggested configurations for automatic mail sorting equipment, B. K. Bender and A. J. Goldman, *J. Research NBS* **63B,** *No. 2, 83 (1959).*

Analytic methods are developed to aid in determining the equipment configuration which achieves sorting of outgoing mail at a given (required) rate at least cost. The techniques are applied to a specific numerical problem; several of the suggested configurations are quickly eliminated, and a "hybrid" of two of the proposed configurations is found which comes within 4 percent of optimum (if a certain pair of parameters is chosen correctly).

Limit of spatial resolution of refractometer cavities, W. J. Hartman, *J. Research NBS* **64D,** *No. 1, 65 (1960).*

Filter factors that determine an upper limit for the wave numbers for which refractometer measurements can be used to calculate the spectrum of refractivity are derived in this paper based on the assumption that refractometers measure a weighted average of the dielectric constant in a volume of air surrounding the center of the refractometer cavity. Two models are used assuming the weighting function has spherical symmetry around the center and one model is used assuming the function is symmetrical about the axis of the cavity but not along the axis. All models result in a simple mathematical form which should be easy to use in further theoretical developments.

Recorder survey: Recording surfaces and marking methods, G. Keinath, *NBS Circ. 601, 41 (1959), 30 cents.*

This Circular surveys the characteristics and comparative advantages of continuous traces, dotted traces, and printed characters, as produced by inking, incision, impression, indentation, deposition, heat, light, electric discharge, electron beam, magnetism, chemical action, or fluid streamlines. Descriptive and reference material is included on three physical components of the recording system—the reservoir of material or energy, the marking point or matrix positioned by the measuring element, and the chart surface which preserves the record.

Precise time synchronization of widely separated clocks, A. H. Morgan, *NBS Tech. Note 22 (PB151381) $1.50.*

In many fields of science, such as in astronautics, missiles, astronomy, etc., which are being intensely investigated, the needs for new orders of magnitude of timing precisions have grown. For instance, the need has been greatly increased for more precise determination of the time of initiation and termination of certain events, which may occur several hundred miles apart. Or, in the location of bodies in space flight, the precise determination of their transit time at known sites is of major importance.
This paper describes known precise methods of setting a group of widely separated clocks to precisely the same time and keeping them in close agreement indefinitely.

Design of single frequency filters, F. F. Fulton, Jr., *NBS Tech. Note 23 (PB151382) 50 cents.*

Efficient procedures are shown for designing filters formed by a number of identical resonant circuits loosely coupled together, and which are required to accept one narrow band of frequencies and reject another narrow band somewhat removed in frequency, without any special requirements on the shape of the attenuation curve in between these regions. The design is based on using a large number of sections.

PILOT—A new multiple computer system, A. L. Leiner, W. A. Notz, J. L. Smith, and A. Weinberger, *J. Assoc. Computing Mach.* **6,** *No. 3, 313 (1959).*

The PILOT data processor is a high-speed multiple computer system, more than 100 times faster than SEAC. It contains three interconnected computers for rapid processing of data, and also contains multiple input-output channels for rapid transfer of data into and out of the system. All of these units operate concurrently in a coordinated fashion. A summary description is given of the overall logical plan of the system, including the principal characteristics of the first computer, the second computer, the third computer, the internal controls, and the external controls.
The system combines internal processing capabilities that are fast and versatile with external communication capabilities that are exceptionally flexible. This combination permits the internal power of the machine to be exploited readily by the outside world—either by other automatic devices or by human operators.

The interlaboratory evaluation of testing methods, J. Mandel and T. W. Lashof, *ASTM Bull. No. 239, 53 (1959).*

The various sources of variability in test methods are examined, and a new general scheme to account for them is proposed. The assumption is made that systematic differences exist between sets of measurements made by the same observer at different times or on different instruments or by different observers in the same or different laboratories and that these systematic differences are linear functions of the magnitude of the measurements. Hence, the proposed scheme is called "the linear model." The linear model leads to a simple design for round-robin tests but requires a new method of statistical analysis, geared to the practical objectives of a round robin. The design, analysis, and interpretation of a round robin in accordance with the linear model are presented, and the procedure is illustrated in

terms of the data obtained in an interlaboratory study of the Bekk smoothness tester for paper. It is believed that this approach will overcome the "frustrations" that are often associated with the interpretation of round-robin test data.

The use of a vacuum microbalance in studies of electron tube materials, G. F. Rouse, *Proc. 4th Natl. Conf. on Tube Tech., Sept. 10 to 12, 1958, sponsored by the Advisory Group on Electron Tubes, p. 262 (New York Univ. Press, New York, N.Y., 1959).*

Several of the physical and chemical processes which occur in an electron tube involve changes of mass. For instance, sublimation from the cathode or breakdown of the coating decrease the cathode mass. Absorption or adsorption of gas by a tube part increases its mass. If change of mass can be measured with sufficient accuracy and the measured change can be correlated with controlled experimental conditions, a better understanding of the factors governing particular processes may be possible. This greater understanding may make it possible to control the processes so as to minimize any harmful effects which might arise from them.
A study based on this idea of measuring change of mass was initiated some time ago, a vacuum microbalance being the test device.

Transistorized velocimeter for measuring speed in the sea, C. E. Tschiegg, *J. Acoust. Soc. Am.* **31,** *No. 7, 1038 (1959).*

An instrument is described which measures the speed of sound in the sea with an accuracy of 1 part in 5,000. Maximum working depth for the instrument is about seven miles.

Gaseous heat conduction at low pressures and temperatures, R. J. Corruccini, *Vacuum* **7–8,** *19 (Pergamon Press Ltd., London, England, 1959).*

Over the large temperature differences that can exist in vacuum insulation of cryogenic devices some of the assumptions on which the formulas for free molecule heat conduction are based are not strictly valid. The consequences of this are discussed and some incorrect usages are pointed out. Working formulas and auxiliary data on mean free paths and accommodation coefficients at cryogenic temperatures are presented.

Microwave reflectometer, G. F. Engen and R. W. Beatty, *IRE Trans. on Microw. Theory Tech.* **MTT–7,** *351 (1959).*

A rigorous analysis of the microwave reflectometer is presented for what is believed to be the first time. By means of this analysis, the correct adjustment of auxiliary tuners is described and the errors resulting from incorrect adjustments are treated in a quantitative manner.

Problems of the experimenter, W. J. Youden' *Natl. Conv. Trans. Am. Soc. Qual. Control, p. 41 (1959).*

During the last forty years, several major types of designed experiments have been introduced. The paper reviews these types briefly and points out that increasing the number of variables or the number of permitted comparisons involves some loss of efficiency in the evaluation of experimental results.

Measurements made by matching with known standards, W. J. Youden, W. S. Connor, and N. C. Severo, *Technometrics* **1,** *No. 3, 101 (1959).*

Quick estimates of an unknown quantity are often made by matching the unknown against a graded series of known standards. This paper discusses the problem of choosing the proper size and number of intervals in establishing a standard. Methods for determining the standard deviation of the matching process are described.

A direct-reading viscometer, M. R. Shafer, *Instr. and Control Systems* **32,** *No. 7, 1044 (1959).*

Prototype instruments for determining directly the kinematic viscosity of liquids have been developed using the restrictions-in-series principle. Although not an absolute method, a simple calibration with liquids of known viscosities permits the subsequent measurement of the viscosities of other liquids by reading a single manometric column; no corrections or other calculations are required. Theory, construction, and operation of instruments having the range 0.5 to 5.0 centistokes are discussed.

Other NBS Publications

Journal of Research, Section A. Physics and Chemistry, Volume 63A, No. 3, November–December 1959. 70 cents.

Multiple ionization of rare gases by electron impact. M. Krauss, R. M. Reese, and V. H. Dibeler.
Light scattering by commercial sugar solutions. Carl J. Rieger and Frank G. Carpenter.
Analysis of the first spectrum of ruthenium (Ru I). K. G. Kessler.
Supplementary Zeeman data for the first spectrum of ruthenium (Ru I). J. Rand McNally, Jr., and Karl G. Kessler.
Low even configurations in the first spectrum of ruthenium (Ru I), part 2. R. E. Trees.
Thermal degradation of polymers at high temperatures. Samuel L. Madorsky and Sidney Straus.
Influence of impurities on the pyrolysis of polyamides. Sidney Straus and Leo A. Wall.
A preliminary list of levels and g-values for the first spectrum of thorium (Th I). Romuald Zalubas.
OH in the solar spectrum. Charlotte E. Moore and Herbert P. Broida.
Use of Chebychev polynomials in thin film computations. Klaus D. Mielenz.

Journal of Research, Section A. Physics and Chemistry, Volume 64A, No. 1, January–February 1960. 70 cents.

The "1958 He^4 scale of temperatures." F. G. Brickwedde, H. van Dijk, M. Durieux, J. R. Clement, and J. K. Logan. (See above abstracts.)
Energy levels and spectrum of neutral helium (^4He I). William C. Martin.
Vibration-rotation structure in absorption bands for the calibration of spectrometers from 2 to 16 microns. Earle K. Plyler, Alfred Danti, L. R. Blaine, and E. D. Tidwell.
Combustion calorimetry with fluorine: Constant pressure flame calorimetry. G. T. Armstrong and R. S. Jessup.
Pits in metals caused by collision with liquid drops and rigid steel spheres. Olive G. Engel.
Theory of formation of polymer crystals with folded chains in dilute solution. John I. Lauritzen, Jr., and John D. Hoffman.
Studies of beryllium chromite and other beryllia compounds with R_2O_3 oxides. C. E. Weir and A. Van Valkenburg.
The uranium-platinum system. J. J. Park and D. P. Fickle.
Nitriding phenomena in titanium and the 6Al-4V titanium alloy. J. R. Cuthill, W. D. Hayes, and R. E. Seebold.
Stability of silver and Pyrex in perchloric acid-silver perchlorate solutions and in conductivity water. D. Norman Craig, Catherine A. Law, and Walter J. Hamer.
Note on the preparation of sodium amalgam in the form of pellets. H. S. Isbell, H. L. Frush, and N. B. Holt.

Journal of Research, Section B. Mathematics and Mathematical Physics, Volume 63B, No. 2, October–December 1959. 75 cents.

Applications of a theorem on partitioned matrices. E. V. Haynsworth.
Capacity requirement of a mail sorting device: II. A. J. Goldman.
Analytic comparison of suggested configurations for automatic mail sorting equipment. B. K. Bender and A. J. Goldman. (See above abstracts.)
New method of solution for unretarded satellite orbits. John P. Vinti.
Effect of sudden water release on the reservoir free outflow hydrograph. Vujica M. Yevdjevich.
Uniform asymptotic expansions for Weber parabolic cylinder functions of large orders. F. W. J. Olver.

Journal of Research, Section D. Radio Propagation, Volume 63D, No. 3, November–December 1959. 70 cents.

Radio-refractive-index climate near the ground. B. R. Bean and J. D. Horn.
Path antenna gain in an exponential atmosphere. W. J. Hartman and R. E. Wilkerson.
Effect of atmospheric horizontal inhomogeneity upon ray tracing. B. R. Bean and B. A. Cahoon.
Correlation of solar noise fluctuations in harmonically related bands. L. R. O. Storey.
A monochromatic low-latitude aurora. F. E. Roach and E. Marovich.
Pattern synthesis for slotted-cylinder antennas. James R. Wait and James Householder.
Central Radio Propagation Laboratory exponential reference atmosphere. B. R. Bean and G. D. Thayer.
Excitation mechanisms of the oxygen 5577 emission in the upper atmosphere. E. Tandberg-Hanssen and F. E. Roach.
Method for measuring local electron density from an artificial satellite. L. R. O. Storey.

Journal of Research, Section D. Radio Propagation, Volume 64D, No. 1, January–February 1960. 70 cents.

Effect of antenna size on gain, bandwidth, and efficiency. R. G. Harrington.
Surface-wave resonance effect in a reactive cylindrical structure excited by an azial line source. A. L. Cullen.
Basic experimental studies of the magnetic field from electromagnetic sources immersed in a semi-infinite conducting medium. Martin B. Kraichman.
A very-low-frequency antenna for investigating the ionosphere with horizontally polarized radio waves. R. S. Macmillan, W. V. T. Rusch, and R. M. Golden.
Effects of high-altitude nuclear explosions on radio noise. C. A. Samson.
Measured frequency spectra of vlf atmospherics. Tatsuzo Obayashi.
Determination of the amplitude-probability distribution of atmospheric radio noise from statistical moments. W. G. Crichlow, C. J. Roubique, A. D. Spaulding, and W. M. Beery.
Measurements of coastal deviation of high-frequency radio waves. C. W. McLeish.
An exact earth-flattening procedure in propagation around a sphere. Benjamin Y.-C. Koo and Martin Katzin.
Limit of spatial resolution of refractometer cavities. William J. Hartman. (See above abstracts.)
Conference on arctic communication.
Tropospheric scatter propagation and atmospheric circulations. William F. Moler and D. B. Holden.
Layered earth propagation in the vicinity of Point Barrow, Alaska. Glenn M. Stanley.
Announcement of systematic ionospheric electron density data.

Tables of the bivariate normal distribution function and related functions, NBS Applied Math. Series 50 (1959) $3.25.
Energy dissipation by fast electrons, L. V. Spencer, NBS Monograph 1 (1959) 45 cents.
Thermodynamic properties of helium at low temperatures and high pressures, D. B. Mann and R. B. Stewart, NBS Tech. Note 8 (PB151367) $1.25.
Calculated behavior of a fast neutron spectrometer based on the total absorption principle, J. E. Leiss, NBS Tech. Note 10 (PB151369) $1.00.
Penetration of gamma rays from isotropic sources through aluminum and concrete, M. J. Berger and L. V. Spencer, NBS Tech. Note 11 (PB151370) 50 cents.
Transmission loss in radio propagation—II, K. A. Norton, NBS Tech. Note 12 (PB151371) $3.00.
Technical considerations leading to an optimum allocation of radio frequencies in the band 25 to 60 Mc, K. A. Norton, NBS Tech. Note 13 (PB151372) $2.50.
Analysis of ionospheric vertical soundings for electron density profile data. 1. Facilities for convenient manual reduction of ionograms, J. W. Wright and R. B. Norton, NBS Tech. Note 14 (PB151373) 50 cents.
Prediction of the cumulative distribution with time of ground wave and tropospheric wave transmission loss. Part 1. The prediction formula, P. L. Rice, A. G. Longley, and K. A. Norton, NBS Tech. Note 15 (PB151374) $1.50.
Analysis of ionospheric vertical soundings for electron density profile data. II. Extrapolation of observed electron density profiles above h_{max}F2, J. W. Wright, NBS Tech. Note 19 (PB151378) 50 cents.
The role of Government research laboratories, A. V. Astin, Elec. Engr. **78,** No. 7, 738 (1959).
The ampere, F. B. Silsbee, Proc. IRE **47**, No. 5, 643 (1959).
On the theory of reflection from a wire grid parallel to an interface between homogeneous media (II), J. R. Wait, Appl. Sci. Research **7,**, 355 (1959).
The basis of our measuring system, A. G. McNish, Proc. IRE, **47,** No. 5, 636 (1959).
Reflectors for a microwave Fabry-Perot interferometer, W. Culshaw, IRE Trans. on Microw. Theory Tech. **MTT–7,** No. 2, 221 (1959).
The research frontier, I. C. Schoonover, Saturday Rev. p. 58 (May 2, 1959).
The nature, cause and effect of the porosity in electrodeposits, III. Microscopic detection of porosity, F. Ogburn and D. W. Ernst, Plating **46,** 831 (1959).
Paper test data from pendulum and inertialess testers, R. J. Capott, S. B. Newman, and J. Mandel, TAPPI **42,** No. 6, 480 (1959).
Convexity of the field of a linear transformation, A. J. Goldman and M. Marcus, Can. Math. Bull. **2,** No. 1, 15 (1959).
Factors affecting the accuracy of distortion measurements made on the nodal slide optical bench, F. E. Washer and W. R. Darling, J. Opt. Soc. Am. **49,** No. 6, 517 (1959).

Mechanism of contraction in the muscle fiber-ATP system, L. Mandelkern, A. S. Posner, A. F. Diorio, and K. Laki, Proc. Natl. Acad. Sci. **45,** No. 6, 814 (1959).

Microwave spectrum of methyl germane, V. W. Laurie, J. Chem. Phys. **30,** No. 5, 1210 (1959).

IGY instruction manual. Part 1: World days and Communications, A. H. Shapley, Annals of IGY **7,** Pt. 1, 1 (Pergamon Press, New York, N.Y., 1959).

Measurement of ozone in terms of its optical absorption, R. Stair, Advances in Chem. Ser., No. 21, 269 (1959).

On the perturbation of the vibrational equilibrium distribution of reactant molecules by chemical reactions, K. E. Shuler, 7th Symp. (Intern.) on Combustion, London and Oxford, Aug. 28 to Sept. 3, 1958, Combustion Inst., p. 87 (Butterworths Sci. Publ., London, England, 1958).

The calculation of the field in a homogeneous conductor with a wavy interface, J. R. Wait, Proc. IRE **47,** 1155 (1959).

Rack for standard resistors, P. H. Lowrie, Jr., Rev. Sci. Instr. **30,** No. 4, 291 (1959).

Lower bounds for eigenvalues with application to the helium atom, N. W. Bazley, Proc. Natl. Acad. Sci. **45,** No. 6, 850 (1959).

Graphical diagnosis of interlaboratory test results W. J. Youden, Ind. Qual. Control **XV,** No. 11, 1 (1959).

Spectroscopic evidence for triatomic nitrogen in solids at very low temperature, M. Peyron, E. M. Horl, H. W. Brown, and H. P. Broida, J. Chem. Phys. **30,** No. 5, 1304 (1959).

The evaluation of small color differences: Part I. Visual observations, J. C. Richmond and W. N. Harrison, Am. Ceram. Bul. **38,** No. 6, 292 (1959).

Properties of rutile (titanium dioxide), F. A. Grant, Rev. Mod. Phys. **31,** 646 (1959).

Analysis of vibrational relaxation data in shock wave experiments, K. E. Shuler, J. Chem. Phys. **30,** No. 6, 1631 (1959).

Radioactivity standardization in the United States, W. B. Mann and H. H. Seliger, 2d U.N. Intern. Conf. on the Peaceful Uses of Atomic Energy, Vol. 21, Health and Safety: Dosimetry and Standards, P/750 USA, p. 90 (1959).

Program of the International Commission on radiological units and measurements, L. S. Taylor, L. H. Gray, and H. O. Wycoff, 2d U.N. Intern. Conf. on the Peaceful Uses of Atomic Energy, Vol. 21, Health and Safety: Dosimetry and Standards, P/2243 WHO, p. 81 (1959).

The changing character of chemical research in government, E. Wichers, The Chemist **XXXVI,** No. 7, 260 (1959).

Study of the setting of plaster, K. D. Jorgensen and A. S. Posner, J. Dental Research **38,** No. 3, 491 (1959).

Radiation attenuation data, H. O. Wyckoff, Radiation Hygiene Handbook, ed. by H. Blatz, Sect. 8, p. 1 (McGraw-Hill Book Co., Inc., New York, N.Y., 1959).

Optimum antenna height for ionospheric scatter propagation, R. G. Merrill, IRE Conv. Record **7,** Pt. 1, 10 (1959).

Corrosion of type 310 stainless steel by synthetic fuel oil ash, H. L. Logan, Corrosion **15,** 443t (1959).

Physical research, Part 2, G. C. Paffenbarger and W. Souder, J. Am. Dental Assoc. **58,** 98 (1959).

Effects of gamma radiation on collagen, J. Cassel, J. Am. Leather Chemists' Assoc. **LIV,** No. 8, 432 (1959).

Standards for neutron flux measurement and neutron dosimetry, R. S. Caswell, E. R. Mosburg, Jr., and J. Chin, 2d U. N. Intern. Conf. on the Peaceful Uses of Atomic Energy, Vol. 21, Health and Safety; Dosimetry and Standards, P/752 USA, p. 92 (1959).

Note on bivariate linear interpolation for analytic functions, W. Gautschi, Math. Tables and Other Aids to Computation **13,** No. 66, 91 (1959).

Absorption of radiation by a cylindrical sample of a strong absorber, P. H. Fang and I. A. Stegun, Letter to Editor, J. Chem. Phys. **31,** 267 (1959).

Branched-chain higher sugars. I. A 9-aldo-4-*C*-formyl-nonose derivative, R. Schaffer and H. S. Isbell, J. Am. Chem. Soc. **81,** 2178 (1959).

The structure of electrolytic solutions, W. J. Hamer (John Wiley & Sons, Inc., New York, N.Y., 1959).

Width of cracks in concrete at the surface of reinforcing steel evaluated by means of tensile bond specimens, D. Watstein and R. G. Mathey, J. Am. Concrete Inst. **31,** No. 1, 47 (1959).

Exposure standards and radiation protection regulations, L. S. Taylor, Radiation Hygiene Handbook, Ed. by H. Blatz, Sect. 3, p. 2 (McGraw-Hill Book Co., Inc., New York, N.Y., 1959).

Geometerical anisotropy of magnetic materials in wave guides and cavities, L. A. Steinert, J. Appl. Phys. **30,** 1109 (1959).

Magnetic interaction of H_3, V. Griffing, J. L. Jackson and B. J. Ransil, J. Chem. Phys. **30,** No. 4, 1066 (1959).

The nature, cause and effect of the porosity in electrodeposits, IV. Influence of gas bubbles on the formation of pores, F. Ogburn and D. W. Ernst, Plating **46,** 957 (1959).

A study of limb flares and associated events, C. Warwick and M. Wood, Astrophys. J. **129,** No. 3, 801 (1959).

Low even configurations in the first spectrum of ruthenium (Ru I), R. E. Trees, J. Opt. Soc. Am. **49,** 838 (1959).

Magnetic study of the frozen products from the nitrogen microwave discharge, B. J. Fontana, J. Chem. Phys. **31,** No. 1, 148 (1959).

Spectrum of thin target bremsstrahlung bounded by a forward circular cone, J. H. Hubbell **30,** 981 (1959).

Negative atomic ions, H. R. Johnson and F. Rohrlich, J. Chem. Phys. **30,** 1068 (1959).

Inclusion theorems for congruence subgroups, M. Newman and I. Reiner, Trans. Am. Math. Soc. **91,** No. 3, 369 (1959).

Factors affecting modulation techniques for vhf scatter systems, J. W. Koch, IRE Trans. Commun. Syst. **CS–7,** No. 2, 77 (1959).

The very low-frequency emissions generated in the earth's exosphere, R. M. Gallet, Proc. IRE **47,** No. 2, 211 (1959).

Reaction of hydrogen atoms with solid oxygen at 20° K, R. Klein and M. D. Scheer, J. Chem. Phys. **31,** 278 (1959).

Application of the Williams-Landel-Ferry-equation to silicate glasses, A. B. Bestul, Glastech, Ber. (Frankfurt, Germany) **32 K,** No. VI, 59 (1959).

Calculated patterns of slotted elliptic-cylinder antennae, J. R. Wait and W. E. Mientka, Appl. Sci. Research **B 7,** 449 (1959).

Glow discharge spectra of copper and indium above aqueous solutions, D. E. Couch and A. Brenner, Tech. Notes, J. Electrochem. Soc. **106,** 628 (1959).

Free radical chemistry, J. W. Moyer and A. M. Bass, Chem. and Eng. News, p. 51 (Aug. 24, 1959).

Discussion of the papers of Messrs. Satterthwaite and Budne, W. J. Youden, Technometrics **1,** No. 2, 157 (1959).

New approach in the theory of satellite orbits, J. P. Vinti, Phys. Rev. Letters **3,** No. 1 (1959).

Production of embossing plates from texture patterns by electroforming methods, J. P. Young and V. A. Lamb, Plating **46,** 1033 (1959).

Method of evaluating the clinical effect of warping a denture: Report of a case, J. B. Woelfel and G. C. Paffenbarger, J. Am. Dental Assoc. **59,** 250 (1959).

The sound transmission loss of some building construction, R. V. Waterhouse, R. D. Berendt, and R. K. Cook, Noise Control **5,** No. 4, 40 (1959).

Cryogenic insulation, R. H. Kropschot, Am. Soc. Heating, Refrig. and Air Conditioning Engrs. **1,** No. 9, 48 (1959).

End plate modification of X-band TEO11 cavity resonators, M. S. Thompson, F. E. Freethey, and D. M. Waters, IRE Trans. on Microw. Theory Tech. **MTT–7,** 388 (1959).

Evolution of amplified waves leading to transition in a boundary layer with zero pressure gradient, P. S. Klebanoff and K. T. Tidstrom, NASA Tech. Note D–195, 1 (1959).

Multiple ionization of sodium vapor by electron impact, V. H. Dibeler and R. M. Reese, J. Chem. Phys. **31,** No. 1, 282 (1959).

Penetration and diffusion of X-rays, U. Fano, L. V. Spencer, and M. J. Berger, Encyclopedia of Phys. **38,** No. 2, 660 (1959).

Vibrational intensity distributions in the nitrogen afterglow, U. H. Kurzweg and H. P. Broida, J. Mol. Spect. **3,** No. 4, 388 (1959).

Some characteristics of VLF propagation using atmospheric waveforms, W. L. Taylor and L. J. Lange, Recent Advances in Atmospheric Elec.; (Proc. 2nd Conf. on Atmospheric Elec., Portsmouth, N.H., May 20 to 23, 1958, p. 609 (Pergamon Press, Inc., New York, N.Y., 1958).

A new aid for the rapid determination of absorption corrections by Albrecht's method, D. K. Smith, Acta Cryst. (Copenhagen, Denmark) **12,** Pt. 6, 479 (1959).

Influence of crystallographic orientation on the pitting of iron in distilled water, J. Kruger, J. Electrochem. Soc. **106,** No. 8, 736 (1959).

Recent advances in cryogenic engineering, R. B. Jacobs, Am. Rocket Soc. ARS J. **29,** 245 (1959).

The thermal E.M.F. of several thermometric alloys, R. L. Powell and M. D. Bunch, Suppl. au Bull. de l'Inst. Intern. du Froid (Delft, Holland) Comm. **1,** 129 (1958).

Electrical discharge induced luminescence of solids at low temperatures, L. J. Schoen and R. E. Rebbert, J. Mol. Spect. **3,** No. 4, 147 (1959).

The nature, cause and effect of the porosity in electrodeposits. V. An evaluation of the sensitivity of the ferroxyl test, F. Ogburn, D. W. Ernst, and W. H. Roberts, Plating **46,** 1052 (1959).

Evacuated powder insulation for low temperatures, M. M. Fulk, Progress in Cryogenics—1, 65 (Heywood & Co., Ltd., London, England, 1959).

The following papers are published in the Proc. 5th Tech. Session on Bone Char 1957 (Bone Char Research Project, Inc., Charlestown, Mass., 1959):

Introductory remarks, A. V. Astin, p. 1.
Analysis of liquid sugars, E. J. McDonald, p. 77.
Development of a new test for the abrasion hardness of bone char, F. G. Carpenter, p. 99.
Effects of controlled decarbonizatien on the performance of service synthad, F. W. Schwer, W. V. Loebenstein, and E. P. Barrett, p. 145.
Some mechanisms of color and ash removal by bone char, A. Gee, p. 163.
Survey of variations in use for conducting laboratory-scale column filteration tests, V. R. Deitz, p. 237.
Comparison of column decolorization experiments with theory, W. V. Loebenstein, p. 253.
Sugar retention by char, F. G. Carpenter, p. 279.
Removal of organic anions by bone char, V. R. Deitz and H. M. Rootare, p. 297.

**Publications for which a price is indicated (except for Technical Notes) are available only from the Superintendent of Documents, U.S. Government Printing Office, Washington 25, D.C. (foreign postage, one-fourth additional). Technical Notes are available only from the Office of Technical Services, U.S. Department of Commerce, Washington 25, D.C. (Order by PB number.) Reprints from outside journals and the NBS Journal of Research may often be obtained directly from the author.*

UNITED STATES
GOVERNMENT PRINTING OFFICE
DIVISION OF PUBLIC DOCUMENTS
WASHINGTON 25, D.C.

OFFICIAL BUSINESS

PENALTY FOR PRIVATE USE TO AVOID
PAYMENT OF POSTAGE, $300
(GPO)

National Bureau of Standards, Journal of Research Vol. 64C, No. 1 January–March 1960
C. Engineering and Instrumentation

Contents

	Page
Power loss and operating temperature of tires. R. D. Stiehler, M. N. Steel, G. G. Richey, J. Mandel, and R. H. Hobbs.	1
Effects of antioxidants on asphalt durability. Burton D. Beitchman.	13
Temperature stratification in a nonventing liquid helium Dewar. L. E. Scott, R. F. Robbins, D. B. Mann, and B. W. Birmingham.	19
Expansion engines for hydrogen liquefiers. Edmund H. Brown.	25
A statistical chain-ratio method for estimating relative volumes of mail to given destinations. Norman C. Severo and Arthur E. Newman.	37
Standard free-air chamber for the measurement of low energy X-rays (20 to 100 kilovolts-constant-potential). Victor H. Ritz.	49
Transmittance of materials in the far infrared. Earle K. Plyler and L. R. Blaine.	55
Equipment and method for photoelectric determination of image contrast suitable for using square wave targets. Fred W. Rosberry.	57
Formation of silver sulfide in the photographic image during fixation. Chester I. Pope.	65
Capacitor calibration by step-up methods. Thomas L. Zapf.	75
Publications of the National Bureau of Standards.	81

For sale by the Superintendent of Documents, U.S. Government Printing Office, Washington 25, D.C. Price 75 cents (single copy)
Subscription price: $2.25 a year; 50 cents additional for foreign mailing.

UNITED STATES GOVERNMENT PRINTING OFFICE, WASHINGTON : 1960